Optical Antennas for Single Emitters

Tim Hugo Taminiau

ICFO - Institut de Ciències Fotòniques
Universitat Politècnica de Catalunya
Barcelona, 2011

Optical Antennas for Single Emitters

Tim Hugo Taminiau

under the supervision of

Professor Niek F. van Hulst

submitted this thesis in partial fulfillment

of the requirements for the degree of

Doctor

by the

Universitat Politècnica de Catalunya

Barcelona, 2011

To my parents.

Acknowledgements

Creating this manuscript and its contents was hard. I am grateful to all those that have supported me personally and scientifically during these years.

I feel privileged to have studied under Niek van Hulst. Working with Niek I experienced a rare combination of freedom, responsibility, and scientific and personal advice. Niek not only provides extended scientific knowledge, but is also always willing to discuss and explain the many other aspects of the scientific community. I cannot imagine a better environment for a PhD-student to develop him- or herself.

I cannot thank my parents, Ied and Boudewijn, enough. They have supported me unconditionally through all my studies and the 17 years before that. I can only hope that the trips to sunny Castelldefels have provided some compensation. I am equally grateful for the support of my sisters, Lotte and Kim, and my brother Job, to whom I hope to show the same type of support during his time in grad school.

I believe that every PhD-student needs a mentor. I have been lucky enough to have had three. First, Fernando Stefani who introduced me to many aspects of scientific life. Second, Richard Hildner who advised me often during the second phase of my PhD. Third, Rashid Zia who was a great source of advise and motivation at the final stages of my studies.

It was a pleasure to work, discuss and socialize together with all of the Van Hulst group: Florian, Daan, Alberto, Koen, Jacob, Richard, Fernando, Lars, Aude, Martin, Riccardo, Dominique, Marta, Pablo, Salvatore, Pavan, and Gabriel, as well as with the Zia group: Sinan and Yana.

I am grateful to Robert Moerland, Marjolein Koopman, Herman Offerhaus, Maria Garcia-Parajo, Frans Segerink and Jeroen Korterik for their support during my master project; to Jasper Overman for initial measurements that turned out to be very valuable; to Petru Ghenuche, Mark Kreuzer, Giorgio Volpe and Romain Quidant for fruitful collaborations.

I thank Kobus Kuipers, Lukas Novotny and Harry Atwater for the advice and inspiration they provided. I also thank Harry Atwater and the Atwater group for hosting me, and for a great time during which I learned a lot.

I am heavily indebted to Ronald Hanson, who has been very supportive and patient during the finalization of this thesis. Without him this thesis would not have been completed.

Laura Grau has been the driving force behind many evenings full of diversion from work. I thank her, Maurizio, Nico, Mario, and Artur for all the fun and relaxing times.

Finally, I am absolutely certain that I could not have done any of this without Clara.

Scientific contributions

Science is teamwork. I am indebted to the following people who made invaluable scientific contributions to this thesis.

All the work in this thesis was supervised and guided by Niek van Hulst. He contributed to all aspects of this work, from the early conception to the final presentation.

Frans Segerink played a major role in the fabrication of the monopole antennas used in chapters 2 and 3. Robert Moerland and Kobus Kuipers were instrumental in many aspects of the experiments in chapter 2 and their interpretation.

The theoretical analysis and calculations in chapters 3 and 4 greatly benefitted from the extended knowledge and programming skills of Fernando Stefani, who helped develop several of the key concepts. The experimental work reported in chapter 4 was headed by Alberto Curto, the antenna fabrication is a collaboration with Giorgio Volpe and Mark Kreuzer, and the project greatly benefitted from the co-supervision of Romain Quidant.

Finally, chapter 5 builds on theoretical concepts initially developed together with Fernando Stefani.

Tim Hugo Taminiau, 13 October 2011, Delft

When he [Kepler] found that his long cherished beliefs did not agree with the most precise observations, he accepted the uncomfortable facts, he preferred the hard truth to his dearest illusions.
That is the heart of science.

Cosmos - Carl Sagan

Abstract

The interaction of light with matter is a central topic in both fundamental science and applied technology. At the heart of this interaction lies the absorption or emission of a photon by an electronic transition in for example an atom, molecule or semiconductor. Because such quantum emitters are generally much smaller than the wavelength of light, they interact slowly and omnidirectionally with light, limiting their absorption and emission.

At radio frequencies similar issues were encountered and addressed long ago. Electrical circuits radiate little because they are much smaller than the corresponding wavelength. To enable wireless communication, they are connected to antennas that have dimensions in the order of the wavelength. These antennas are designed to effectively convert electrical signals into radiation and vice versa. The same concept can be applied in optics.

The central idea of this thesis is that the interaction of a quantum emitter with light can be improved by near-field coupling it to the resonant plasmon modes of a metal nano-particle, which then acts as an optical antenna. In this way, excitation and emission rates can be enhanced, and the angular, polarization, and spectral dependence controlled. Chapter 1 of this thesis outlines these concepts and introduces optical antennas for single emitters.

The experimental demonstration of optical antennas requires the near-field coupling of a single emitter to a resonant optical antenna. We fabricated optical monopole antennas on scanning probes, so that they can be precisely positioned near single fluorescent molecules. In this way we directly mapped the changes in the excitation and emission of a single quantum emitter as it is scanned near the antenna.

Chapter 2 presents the results for the excitation part of the interaction. The enhanced excitation field at the antenna is highly confined (within 25 nm); the emitter only interacts with the antenna mode over this short distance. The antenna resonances were probed directly in the near-field and show that the antenna is indeed an optical analog of a monopole antenna.

The experiments in Chapter 3 demonstrate how the antenna controls the emission. If the emitter is placed at the right position and if the antenna is tuned to resonance, the angular emission of the coupled system is determined by the antenna mode, regardless of the orientation of the emitter. In Chapter 4, we exploit that fact. We demonstrate, theoretically and experimentally, that the radiation from a single emitter coupled to a multi-element optical Yagi-Uda antenna is highly directed. We show that by reciprocity such a high directivity both enhances the excitation field and the collection efficiency.

An intuitive way to understand optical antennas is as cavities for surface plasmon polaritons. In chapter 5, I present an extended description of the

interaction of dipolar emitters with radiation through nano-rod antenna modes, by treating the antenna as a cavity. The results demonstrate how the properties of the antenna modes evolve from macroscopic perfectly conducting antennas to nanoscale plasmonic antennas, and highlight the similarities and differences between optical and conventional antennas.

The results presented in this thesis show that optical antennas provide a new way to link single emitters to light. By designing the antenna the absorption and emission properties of the emitter can be tailored. More generally, optical antennas enhance and control light-matter interaction on the nano-scale, making them promising tools for applications in topics as diverse as high resolution near-field scanning optical microscopy, non-linear optics and spectroscopy, and photovoltaic devices.

List of publications

This thesis is based on the following publications:

T. H. Taminiau, F. D. Stefani, and N. F. van Hulst. Optical Nanorod Antennas Modeled as Cavities for Dipolar Emitters: Evolution of Sub- and Super-Radiant Modes. *Nano Lett.* 11, 1020 (2011).

A. G. Curto, G. Volpe, **T. H. Taminiau**, M. P. Kreuzer, R. Quidant, and N. F. van Hulst. Unidirectional Emission of a Quantum Dot Coupled to a Nanoantenna. *Science* 329, 930 (2010).

T. H. Taminiau, F. D. Stefani, and N. F. van Hulst. Single emitters coupled to plasmonic nano-antennas: angular emission and collection efficiency. *New J. Phys.* 10, 105005 (2008).

T. H. Taminiau, F. D. Stefani, and N. F. van Hulst. Enhanced Directional Excitation and Emission of Single Emitters by a Nano-Optical Yagi-Uda Antenna. *Opt. Express* 16, 10858 (2008).

T. H. Taminiau, F. D. Stefani, F. B. Segerink and N. F. van Hulst. Optical Antennas Direct Single Molecule Emission. *Nature Photon.* 2, 234 (2008).

T. H. Taminiau, R. J. Moerland, F. B. Segerink, L. Kuipers and N. F. van Hulst. $\lambda/4$ Resonance of an Optical Monopole Antenna Probed by Single Molecule Fluorescence. *Nano Lett.* 7, 28 (2007).

T. H. Taminiau, F. B. Segerink, R. J. Moerland, L. Kuipers and N. F. van Hulst. Near-Field Driving of a Optical Monopole Antenna. *J. Opt. A: Pure Appl.* Opt. 9, S315 (2007).

T. H. Taminiau, F. B. Segerink, N. F. van Hulst. A Monopole Antenna at Optical Frequencies: Single-Molecule Near-Field Measurements. *IEEE Trans. Antennas Propag.* 55, 3010 (2007).

Other publications by the author:

D. Brinks, F. D. Stefani, F. Kulzer, R. Hildner, **T. H. Taminiau**, Y. Avlasevich, K. Mullen, and N. F. van Hulst. Visualizing and controlling vibrational wave packets of single molecules. *Nature* 465, 905 (2010).

P. Ghenuche, S. Cherukulappurath, **T. H. Taminiau**, N. F. van Hulst and R. Quidant. Spectroscopic Mode Mapping of Resonant Plasmon Nanoantennas. *Phys. Rev. Lett.* 101, 116805 (2008).

R. J. Moerland, **T. H. Taminiau**, L. Novotny, N. F. van Hulst and L. Kuipers. Reversible Polarization Control of Single Photon Emission. *Nano Lett.* 8, 606 (2008).

Contents

CHAPTER 1

Optical antennas and single emitters

The central topics of this thesis are optical antennas and how such antennas can be used to control and improve the interaction of single quantum emitters with light. The key idea is that the plasmon resonances of a metal nano-particle create a strong local field at the particle. If an emitter is placed in this field its absorption and emission of radiation are enhanced. The function of the particle is then analogous to an antenna.

This chapter introduces optical antennas, single emitters, and the concepts required in the following chapters. Section 1.1 treats the antennas. It first presents the definition of optical antennas used here. It then highlights the main properties of optical antennas, and the experimental challenges they present, by describing nanorod antennas as cavities for surface plasmon polaritons.

Although the emitters considered here are intrinsically quantum objects, the effect of optical antennas on their absorption and emission can be described by classical electrodynamics. Section 1.2 summarizes the ways in which optical antennas can improve the interaction of quantum emitters with light, and overviews the equations for the excitation rates, emission rates and fluorescence that describe this interaction. Additionally it introduces several convenient definitions from traditional antenna theory, and adapts them for optical antennas and single emitters.

Finally, enhancing the interaction of nano-scale objects with light using optical antennas is a surprisingly general and useful concept. Section 1.3 gives an overview of some of the applications of optical antennas.

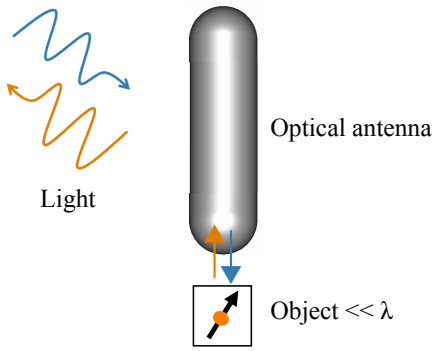

Figure 1.1: **The main concept of optical antennas.** An object that is much smaller than the wavelength of light, and that therefore interacts slowly with light by itself, is near-field coupled to a larger antenna. This coupling improves the interaction of the object with propagating radiation, both in emission and absorption.

1.1 Introduction to optical antennas

Optical antennas link objects to light. The main idea is illustrated in figure 1.1. Consider a quantum object, such as a molecule, quantum dot or atom. Although these objects both emit and absorb light, I will simply call them *single emitters*. Because the emitter has dimensions much smaller than the wavelength of light it interacts slowly and omnidirectionally with radiation. For example, the typical timescale for an atomic electric dipole transition to emit a photon is on the order of nanoseconds, and the photon is emitted in an undirected dipolar angular pattern. This slow undirected interaction places several limits on the absorption and emission by the emitter.

First, the long radiative lifetime limits the maximum amount of photons that can be emitted per second, i.e. the maximum brightness. Second, if faster competing loss channels and/or dephasing are present, as is often the case for condensed matter at room temperature, a slow interaction becomes a weak interaction. The emitter then absorbs only a small fraction of the incident light, and radiates its energy with a low efficiency. Third, the undirected nature of the interaction makes it challenging to efficiently collect the emission and further reduces the probability of absorption under illumination.

The interaction of the emitter with light can be improved by near-field coupling it to a second larger - but still small - object: an antenna. The emitter now mainly absorbs and emits light through the modes of the antenna. By suitably designing the antenna, the absorption and emission rates can be enhanced. Furthermore the angular, polarization and spectral dependence of both the emission and absorption can be controlled.

Such optical antennas are not a new concept. The use of local fields at sub-wavelength structures to enhance light-matter interaction goes back at least to near-field optical microscopy [1–3] and surface enhanced Raman scattering (SERS) [4–6]. Recently, however, nano-optics and in particular metal nano-particles have been systematically investigated in the context of antenna theory

[7–15]. These efforts are for an important part driven by improvements in nano-fabrication that allow studying individual nano-structures and single emitters. This treatment of nano-optics as an antenna problem has led to several new insights and design strategies to enhance absorption and emission with optical antennas.

This section presents the definition of optical antennas that is used in this thesis, and introduces the main properties of optical antennas. It outlines how optical antennas can intuitively be understood as cavities for surface plasmon polaritons. These cavities are unique in two ways. First, the wavelength of the plasmon in the cavity can be much shorter than the wavelength in the surrounding medium. Second, the modal fields are highly confined.

The objective of this section, and the remainder of this chapter, is not to give an exhaustive review, but to establish some of the key properties of optical antennas, and the type of opportunities and experimental challenges presented by these properties. Several excellent reviews are available for those seeking more detail [13, 16–18].

A definition for optical antennas

I will use the following definition for optical antennas throughout this thesis. An optical antenna is [19]:

A device designed to improve the interaction
of an object with light through a near-field coupling.

This definition emphasizes two aspects of optical antennas. The fact that the antenna is a tool to improve the interaction of a second object with propagating radiation, and the fact that this is achieved by means of a near-field coupling of the object to the antenna.

The above definition has some overlap with optical cavities or resonators. Indeed optical antennas have conceptually much in common with micro- and photonic crystal cavities [14, 20, 21], and no clear distinction can be made. Nevertheless, compared to traditional cavities, optical antennas tend to be small and tend to use conducting materials, allowing very localized modes and high field enhancements with large bandwidths. The last part of this section will consider optical antennas as cavities for surface plasmons, in order to introduce two important properties of optical antennas.

Optical antennas as cavities

There are several theoretical approaches available to understand nano-particle optical antennas, and how they differ from conventional antennas. The powerful Mie solutions can be used for ellipsoids [22, 23], whereas extensive numerical studies are performed for other shapes [24]. Perhaps more intuitively, optical antennas have been described as resonators or (Fabry-Pérot) cavities for surface plasmons [21, 25–34].

Consider a surface plasmon polariton, i.e. a bound wave, traveling along an elongated metal nano-rod antenna. The waves are reflected at the antenna ends so that resonant cavity modes are formed, figure 1.2. These resonant modes occur when the antenna length is close to a multiple of half the plasmon

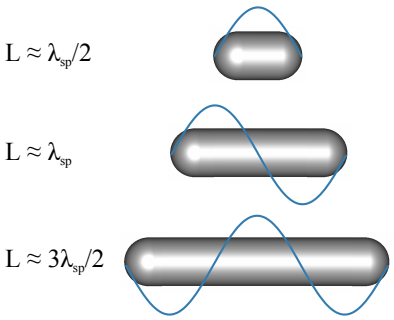

Figure 1.2: **Optical antennas as cavities for surface plasmons**. An intuitive way to understand optical antennas is as resonators for surface plasmons that travel along the antenna and are reflected at the antenna ends. Resonant modes form for antenna lengths that are close to a multiple of half the surface plasmon wavelength λ_{sp}. Most of this thesis considers the dipolar antenna resonance with $L \approx \lambda_{sp}/2$. The higher order modes are revisited in detail in chapter 5.

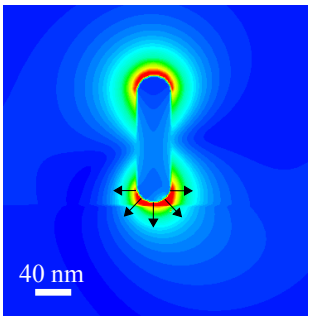

Figure 1.3: **The antenna modal field is highly localized**. An example of an instantaneous electric field (absolute value) near a dipolar optical antenna with a radius of 20 nm [11]. The field is concentrated at the antenna ends, and is localized within approximately 20 nm. The arrows are a sketch of the electric field orientation. The antenna is 150 nm long and the vacuum wavelength of the radiation is 570 nm.

wavelength λ_{sp}. This relation is only approximate because the reflection at the ends introduces an additional phase shift [15, 32, 35, 36].

Two of the key characteristics of such cavities for surface plasmons are that the electromagnetic field is highly confined at the antenna, and that the wavelength of the surface plasmon along the antenna is shorter than the vacuum wavelength.

Figure 1.3 shows an example of the electric field at an optical dipole antenna ($L \approx \lambda_{sp}/2$). The modal field of the antenna is localized in a volume with dimensions smaller than the wavelength of the light used, and is concentrated at the antenna ends. This confined field allows the antenna to enhance

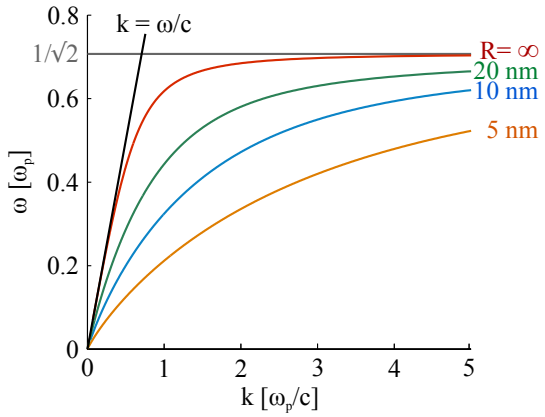

Figure 1.4: **The wavelength along the antenna is shorter than the vacuum wavelength.** Dispersion diagrams for infinitely-long cylindrical rods of different radii R. The magnitude of the surface plasmon wave vector, $k(\omega)$, along the rod is always larger than the magnitude of the wave-vector in the surrounding medium (ω/c), and increases with decreasing radius. ω is the angular frequency and c is the vacuum speed of light. The infinite radius corresponds to the planar surface plasmon. The dielectric function of the cylinder is described as a simple Drude dispersion $\epsilon = \epsilon_0(1-\omega_p^2/\omega^2)$, with $\omega_p = 2\pi \cdot 2.32 \cdot 10^{15}$ rad/s. The dielectric constant of the environment is ϵ_0.

the interaction of an emitter with radiation. In addition it provides a high spatial selectivity; only emitters that are placed very close to the antenna interact with the antenna mode. The near-field nature of the coupling also poses an experimental challenge; the emitter has to be positioned with nanometer accuracy at the antenna. In chapters 2 and 3, we present experiments that overcome this challenge by precisely scanning probe-based optical monopole antennas near single fluorescent molecules. In this way we directly probe the locally enhanced field at the antenna.

The second distinguishing feature of these cavities is that the wavelength of the surface plasmon along the cavity can be much shorter than the wavelength in the surrounding medium. As an example, figure 1.4 shows calculated dispersion relations for the waveguide modes of infinitely-long cylindrical rods of different radii, for which semi-analytical solution are available [15, 37, 38]. The plasmon wave vector ($k = 2\pi/\lambda_{sp}$) is always larger than the wave vector in free space ($k_0 = \omega/c$) as expected for a bound wave. Moreover, the wave vector increases with decreasing radius, and can take very large values for small radii.

This short surface plasmon wavelength has two important consequences. First, it implies that the antenna resonances for optical antennas will occur for lengths a fraction of the wavelength of the light used. Because, these resonances enhance the local field, the antenna is ideally tuned to resonance with the excitation and/or emission of the emitter. The small dimensions required present a fabrication challenge. Second, the short plasmon wavelength along the antenna results in lower radiative damping rates, while the lossy nature of surface plasmons introduces additional dissipation. The effect that these

properties have on the characteristics of the modes of optical antennas will be discussed in detail in Chapter 5, which presents an extended description of optical antennas based on the cavity model outlined here.

In summary, optical antennas can conceptually be understood as cavities with two distinguishing features: the wavelength along the cavity is shorter than the wavelength in the surrounding medium and the cavity mode is strongly confined. The combination of the resonances and the field confinement creates strong local fields. The next section explores how the absorbtion and emission properties of a single quantum emitter are altered when it is placed in that local field.

1.2 Single emitters

This thesis treats the interaction of single emitters, for example atoms, molecules or quantum dots, with optical antennas. Even though these emitters are inherently quantum objects the changes in their emission and absorption properties near an optical antenna can be understood entirely classically, by using macroscopic classical electrodynamics and describing the two-level system of the emitter as a harmonically oscillating electric dipole moment. The antenna modifies both the electric field radiated by the emitter, and the electric field formed at the emitter position under external illumination. In this way, optical antennas can improve the absorption and emission of single emitters in a variety of ways, and much experimental progress has been made over the last years.

First, the total transition rates of the emitter can be enhanced, both in emission and in excitation. In excitation, the locally enhanced field at the antenna increases the excitation rate of an emitter by external illumination [10, 35, 39–42]. In emission, optical antennas can enhance the total radiative transition rate [10, 41, 43–47], as well as the (usually detrimental) dissipative, or non-radiative, rate [10, 39, 48]. Second, both in excitation and emission the spectral dependence [22, 49, 50], the polarization dependence [11, 51, 52], and the angular dependence [10–12, 41, 53–55] can be controlled.

If the antenna-emitter system is designed well, the combination of the above effects can enhance the total amount of photons absorbed, emitted and/or detected.

This section presents the theoretical relations that describe the changes in the excitation properties, the emission properties, and the resulting fluorescence. Additionally it introduces several concepts from antenna theory to conveniently summarize the properties of the emitter-antenna system. Finally, it outlines the main advantages of using single emitters, compared to ensembles, when studying the properties of optical antennas.

The theory outlined in this section is used throughout this thesis to interpret the experimentally observed single-emitter fluorescence and to compare the results to numerical calculations of the electromagnetic field.

Excitation rates

The experiments in this thesis consider emitters in the solid state at room temperature. Therefore I will limit the discussion to systems with fast electronic

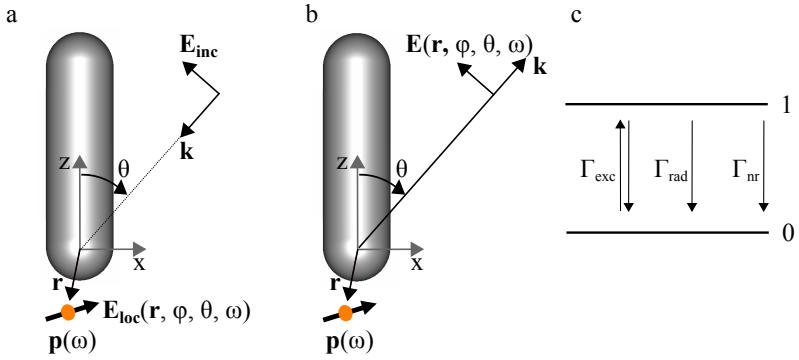

Figure 1.5: **Definition of parameters** (a) The excitation process is determined by the local electric field $\mathbf{E}_{loc}(\mathbf{r}, \phi, \theta, \omega)$ at the position of the dipole moment $\mathbf{p}(\omega)$ for a plane wave incident under angle (ϕ, θ) and with amplitude $\mathbf{E}_{inc}$. ϕ is the azimuth. Note that any illumination can be described as a superposition of such waves plane waves. (b) The emission process is defined by the emitted far field $\mathbf{E}(\mathbf{r}, \phi, \theta, \omega)$ by the dipole moment $\mathbf{p}(\omega)$. (c) Definition of the transition rates between the ground state (0) and the excited state (1). The excitation rate Γ_{exc} follows from the calculation defined in (a). The radiative Γ_{rad} and non-radiative Γ_{nr} emission rates follow from the situation sketched in (b). The interplay of these rates determines the fluorescence emitted by the emitter. Note that the relevant quantities generally depend on the emitter position $\mathbf{r}$, the angle involved (ϕ, θ) and the frequency ω. For conciseness I will frequently drop some of these labels.

dephasing due to interactions with the environment. The interaction of such emitters with light is accurately described by rate equations.

Consider the situation shown in figure 1.5a. The emitter and its local environment are illuminated by a plane wave with complex amplitude $\mathbf{E}_{inc}$ and angular frequency ω. The excitation rate Γ_{exc} is proportional to the projection of the resulting local electric field at the emitter position, $\mathbf{E}_{loc}(\mathbf{r}, \phi, \theta, \omega)$, on the emitter dipole moment $\mathbf{p}(\omega)$. We assume that the scattering and absorption by the emitter is negligible compared to the scattering and absorption by the antenna. Therefore, the field $\mathbf{E}_{loc}(\mathbf{r}, \phi, \theta, \omega)$ is unaffected by the presence of the emitter, and can be calculated separately. This assumption also implies that the interaction between the antenna and the emitter is in the weak coupling regime.

The magnitude of the emitter dipole moment $\mathbf{p}(\omega)$ requires a quantum mechanical treatment and is unknown in most experiments. Therefore, all transition rates will be given relative to the transition rates for the same dipole in a reference situation. For the excitation rate we thus have:

$$\frac{\Gamma_{exc}}{\Gamma_{exc,0}} = \frac{|\hat{\mathbf{p}} \cdot \mathbf{E}_{loc}(\mathbf{r}, \phi, \theta, \omega)|^2}{|\hat{\mathbf{p}}_0 \cdot \mathbf{E}_{loc,0}(\mathbf{r_0}, \phi_0, \theta_0, \omega)|^2}, \tag{1.1}$$

in which $\hat{\mathbf{p}} = \mathbf{p}/\|\mathbf{p}\|$ is the unit vector in the direction of the orientation of the dipole moment.

The subscript 0 indicates the reference situation. The reference situation can be chosen freely, for example as the emitter without antenna or as the same system illuminated from a different direction (ϕ, θ). The only requirements are that the emitter dipole moment in both cases has the same magnitude, $\|\mathbf{p}_0\| = \|\mathbf{p}\|$, and that any changes in the environment alter exclusively the macroscopic electromagnetic fields at the emitter.

Equation 1.1 describes how the excitation rate of a single emitter can be enhanced. The antenna locally enhances the electric field at the emitter, increasing the rate of absorbtion. This enhancement depends critically on the emitter position and orientation, figure 1.3, and on the resonances of the antenna. Chapter 2 describes experiments that characterize the locally enhanced field at the antenna and the resonances of the antenna using single fluorescent molecules.

Emission rates

The emission properties of the quantum emitter in its environment are determined by the far-field emitted by a classical electric dipole placed at position $\mathbf{r}$, figure 1.5b:

$$\mathbf{E}(\mathbf{r}, \phi, \theta, \omega) = \begin{bmatrix} E_\phi(\mathbf{r}, \phi, \theta, \omega) \\ E_\theta(\mathbf{r}, \phi, \theta, \omega) \end{bmatrix}, \tag{1.2}$$

in which E_ϕ and E_θ are the complex amplitudes of the two polarization components. I will call $\mathbf{E}(\mathbf{r}, \phi, \theta, \omega)$ the angular emission. It directly describes all the (classical) emission properties of the emitter, except for the absolute total emission rate, which depends on the unknown emitter transition dipole moment. It gives the angular distribution of the emission, including the phase, polarization and spectrum for each angle.

The angular power emitted by the dipole into each polarization component is given by:

$$P_\phi(\mathbf{r}, \phi, \theta, \omega) = \frac{|E_\phi(\mathbf{r}, \phi, \theta, \omega)|^2}{2Z_0}, \quad P_\theta(\mathbf{r}, \phi, \theta, \omega) = \frac{|E_\theta(\mathbf{r}, \phi, \theta, \omega)|^2}{2Z_0}, \tag{1.3}$$

in which Z_0 is the impedance of the surrounding medium. The total angular emitted power is:

$$P(\mathbf{r}, \phi, \theta, \omega) = P_\phi(\mathbf{r}, \phi, \theta, \omega) + P_\theta(\mathbf{r}, \phi, \theta, \omega). \tag{1.4}$$

The radiative transition rate Γ_{rad} of the emitter is proportional to the total emitted power by the classical dipole P, which at a given frequency is given by:

$$P(\mathbf{r}) = \int_\pi \int_{2\pi} P(\mathbf{r}, \phi, \theta) \sin\theta d\phi d\theta. \tag{1.5}$$

Compared to a reference situation labeled 0, we thus obtain:

$$\frac{\Gamma_{rad}}{\Gamma_{rad,0}} = \frac{P(\mathbf{r})}{P_0(\mathbf{r_0})}. \tag{1.6}$$

The collection efficiency η_{coll} gives the fraction of the far-field emission that is collected by the collection optics:

$$\eta_{coll}(\mathbf{r}) = \frac{\int\int P(\mathbf{r}, \phi, \theta) \sin\theta d\phi d\theta}{P(\mathbf{r})}. \tag{1.7}$$

The limits of the integrals are set by the solid angle corresponding to the collection optics.

Chapter 3 studies how the angular emission, including the polarization, of single fluorescent molecules changes as they are coupled to an optical antenna, and how these changes in angular emission can affect the collection efficiency.

Dissipation rates

Not all transition events result in the emission of a photon into the far-field. Part of the energy is dissipated in the antenna and other lossy dielectrics in the emitters environment, leading to a dissipation rate Γ_{diss}. This rate is proportional to the dissipated power, P_{diss}, so that

$$\frac{\Gamma_{diss}}{\Gamma_{rad,0}} = \frac{P_{diss}(\mathbf{r})}{P_0(\mathbf{r_0})}. \tag{1.8}$$

The dissipation rate together with the intrinsic loss rate of the emitter, Γ_{int}, defines a quantum efficiency for the emission process:

$$\eta_q = \frac{\Gamma_{rad}}{\Gamma_{rad} + \Gamma_{nr}}, \tag{1.9}$$

in which $\Gamma_{nr} = \Gamma_{diss} + \Gamma_{int}$ is the total non-radiative loss rate. The quantum efficiency η_q gives the amount of photons emitted into the far field for each photon absorbed. Finally, the (excited state) lifetime is given by the inverse of the total decay rate, $\Gamma_{tot} = \Gamma_{rad} + \Gamma_{nr}$.

Directivity and gain

Although equations 1.2-1.4 describe the complete angular emission pattern, it is interesting to quantify how directed the emission is. The angular directivity $D(\phi, \theta)$ describes how effectively the power is concentrated into a particular direction, i.e. a very small solid angle or approximately a plane wave. $D(\phi, \theta)$ is defined as the power emitted into direction (ϕ, θ) compared to the power averaged over all directions:

$$D(\phi, \theta) = \frac{4\pi P(\phi, \theta)}{P}. \tag{1.10}$$

For example, $D(\phi, \theta) = 1$ for a hypothetical isotropic emitter, and the maximum of the angular directivity for a dipolar emitter in an isotropic homogeneous environment is 1.5.

For plane waves, or a very small solid angle, the collection efficiency η_{coll} is directly proportional to the directivity:

$$\frac{\eta_{coll}}{\eta_{coll,0}} = \frac{D(\phi, \theta)}{D_0(\phi, \theta)}. \tag{1.11}$$

An increased directivity can therefore provide an enhanced collection efficiency. However, since an increased directivity in general requires larger antennas, it often comes at the price of increased losses. The antenna gain $G(\phi, \theta)$ quantifies how much the total efficiency is increased, compared to an isotropic emitter with $\eta_{q,0} = 1$:

$$G(\phi, \theta) = \eta_q D(\phi, \theta). \tag{1.12}$$

For single optical emitters it is rare to detect the emission of (approximately) plane waves. The concept of gain can be generalized to larger solid angles using equation 1.7, so that the gain G in the general case becomes:

$$\frac{G}{G_0} = \frac{\eta_q}{\eta_{q,0}} \frac{\eta_{coll}}{\eta_{coll,0}}. \tag{1.13}$$

Both these definitions for the gain quantify how much the antenna improves the emission by redirecting the emission into the correct angles. These concepts will be treated in more detail in chapter 4, which discusses the highly directed emission from multi-element optical Yagi-Uda antennas. The directivity and gain are crucial parameters for such antennas.

Fluorescence intensity

The rates discussed up to now are transition rates. The detected signal is the fluorescence intensity I (in units of photons per second), which is proportional to the radiative transition rate Γ_{rad} times the excited state population. The intensity is therefore given by the interplay of all the different rates. For a two level system in the steady state we have

$$I = \eta_d \eta_c \Gamma_{rad} \frac{\Gamma_{exc}}{2\Gamma_{exc} + \Gamma_{rad} + \Gamma_{nr}}, \tag{1.14}$$

in which η_d is the detection efficiency, which is a simple constant and plays no direct role in the relative intensity measurements considered here.

Importantly, the fluorescence intensity depends on properties associated with the excitation process (Γ_{exc}), as well as on those associated with the emission process (Γ_{rad}, Γ_{nr} and η_c). As a result, the intensity is generally difficult to interpret, and requires a complete analysis of the collection system, as well as excitation power dependent measurements [56]. Note that this is not the case, for example, for parameters like the lifetime, the angular emission pattern (equation 1.4) or the emission polarization (equation 1.2), which are all completely independent of the how the emitter is excited. This independence makes these parameters powerful tools to study the effects of optical antennas on single emitters.

Equation 1.14 can be further simplified in several limiting cases: low excitation powers, high excitation powers, and negligible intrinsic quantum efficiencies.

Low excitation power

For low excitation powers ($\Gamma_{rad} >> \Gamma_{exc}$) the excitation rate Γ_{exc} is the limiting factor in the fluorescence cycle, and equation 1.14 gives

$$\frac{I}{I_0} \approx \frac{\Gamma_{exc}}{\Gamma_{exc0}} \frac{\eta_c}{\eta_{c0}} \frac{\eta_q}{\eta_{q0}} \tag{1.15}$$

Provided that the antenna is designed so that the collection efficiency η_c and the quantum efficiency η_q, i.e. the gain G, do not change strongly, the intensity

enhancement at low powers is mostly governed by the enhancement of the excitation field. All experimental results in this thesis fall in this low excitation power regime.

High excitation power

For high excitation powers, $\Gamma_{exc} >> \Gamma_{rad} + \Gamma_{nr}$, the excitation transition is saturated and the fluorescence is limited by the emission rate Γ_{rad}:

$$\frac{I}{I_0} \approx \frac{\eta_c \Gamma_{rad}}{\eta_{c0} \Gamma_{rad0}}. \tag{1.16}$$

In this regime the fluorescence intensity is determined by the total radiative mode density within the angles of the collection optics. Equation 1.16 gives the maximum number of photons per second that can be obtained from the emitter, which is an important figure for an optical antenna-emitter system.

Negligible intrinsic quantum efficiency

If the emitter is intrinsically very inefficient, $\Gamma_{int} >> \Gamma_{diss} + \Gamma_{rad} + \Gamma_{exc}$, so that $\eta_q \approx 0$, and we obtain:

$$\frac{I}{I_0} \approx \frac{\Gamma_{exc}}{\Gamma_{exc0}} \frac{\eta_c \Gamma_{rad}}{\eta_{c0} \Gamma_{rad0}}. \tag{1.17}$$

The fluorescence is limited by both the excitation rate and the emission rate. Because the excitation and emission processes can be related by reciprocity, as will be discussed in chapter 4, equation 1.17 often implies an approximately Γ_{exc}^2, or $|\mathbf{E}(\mathbf{r})|^4$, enhancement of the fluorescent intensity. The strongest enhancements of the fluorescence intensity are thus obtained for emitters with intrinsically low quantum efficiencies.

For the antennas, the enhancement of Γ_{rad} is the result of an increased spontaneous emission, i.e. stimulated emission by the vacuum fluctuations. Similarly, the emission rate can be enhanced by stimulated emission by a second laser beam at the emission wavelength. The resulting enhanced emission has been used as a microscopy technique for low quantum efficiency emitters. The quadratic response then provides three dimensional imaging capabilities [57].

Why single emitters?

Other than the intellectual satisfaction of being able to control light-matter interaction on the single molecule level, there are several aspects that make the problem of a single emitter coupled to a single optical antenna of particular interest. The next section will list some applications of optical antennas for single emitters. Here I will first discuss two advantages of using single emitters to study the properties of optical antennas.

First, a single emitter with a fixed dipole moment is a nano-scale vectorial detector for the local optical electric field. The spatial distributions of the modal fields at optical antennas can thus be obtained with nano-scale resolution. This property of single emitters allows studying the spatial confinement of the enhanced fields at the antenna, which is one of the crucial properties of optical antennas (see figure 1.3). Chapter 2 demonstrates this concept by

using single molecules to map the nano-scale spatial distribution of the field at optical antennas placed on scanning probes.

Second, by observing a single molecule at the time, measurements of the properties of the antenna-emitter system are greatly simplified because the excitation and emission properties can be considered separately. This is not the case for ensembles of emitters, as will be discussed in detail below.

When observing a single emitter, several properties of the antenna-emitter system are independent of the absolute fluorescence intensity. These properties include the lifetime and the angular emission and excitation, which encompass the polarization and spectral degrees of freedom. These intrinsic proprieties are well-defined and are independent of the details of the measurement. For example, the lifetime observed does not depend on how the emitter was excited nor on what directions, polarizations or spectral components are being detected. As another example, the angular emission observed is independent of how the system was illuminated. This concept plays a crucial role in Chapter 3 in which we study the changes in the angular emission of a single molecule as it is coupled to an optical antenna, using only a qualitative understanding of the excitation field.

In contrast, for ensemble measurements the obtained values are averages weighed by the intensity for each emitter. In an inhomogeneous environment, which is the only type of environment that this thesis and optical antennas are concerned with, we do not know *a priori* which emitters are observed. The contribution of each emitter depends on its intensity and thus on an intricate combination of both the experimental excitation and detection, equation 1.14.

In other words, *the* lifetime and *the* angular emission/excitation of an ensemble of emitters in an inhomogeneous environment do not exist, i.e. they are not uniquely defined. For the angular emission, for example, the measured pattern now depends on how the system was illuminated because a different subset of emitters will be excited for different illuminations. Note that for the lifetime the above statement does not refer to the fact that the emission dynamics of an ensemble can deviate from a single exponential decay. Instead, it conveys that the time-resolved emission - whatever it might look like - is a complicated function of all the properties of the illumination and detection schemes.

In conclusion, measurements that observe a single emitter typically are easier to interpret, need less assumptions, and give more information than ensemble experiments. Single emitter experiments thus provide a direct way to study the functionality of optical antennas.

1.3 Applications of optical antennas

The distinguishing property of optical antennas is the strongly localized enhanced field at the antenna. If an object or emitter is placed in those locally enhanced fields, its interaction with radiation is enhanced. Any application of optical antennas is likely to be based on these enhanced localized fields: optical antennas are particularly useful in applications for which the object is inherently small or for which there is an independent reason that makes it beneficial for the object to be small.

This section outlines several examples of such applications. The list is not complete and various applications of optical antennas such as nanoscale trapping [58] and controlling thermal radiation [59] are not discussed. Several excellent recent reviews offer a more detailed discussion of the many applications of optical antennas [13, 17, 18].

Non-linear effects

If the response of the object is non-linear, then an intense field over a small volume gives a stronger interaction than a weak field spread out over a large volume. Optical antennas can thus greatly enhance the generation of non-linear signals that originate either from the non-linearities of the antenna itself or from a material brought in close proximity to the antenna. Strong enhancements of two photon-excited photoluminescence [9, 60, 61], white light continuum generation [9], second harmonic generation [62], four-wave mixing [63], and high harmonic generation [64], have been demonstrated.

Although the fluorescence emission considered in section 1.2 is a linear process, a low intrinsic quantum efficiency of the emitters results in effectively quadratic enhancement of the fluorescence with optical antennas, equation 1.17. For such weak emitters strong fluorescence enhancements have been demonstrated [40], and have allowed the observation of single molecules coupled to antennas even within an ensemble background [42].

The process of surface enhanced Raman scattering can be described by equation 1.17 as well, although the underlying principle appears to be different [65]. Optical antennas can thus play in important role in Raman spectroscopy [66–68].

Single emitters

Observing a single emitter at the time, and enhancing its emission, is an application by itself. Two examples of its usefulness are single emitter spectroscopy to overcome intrinsic inhomogeneities and using single emitters as single photon sources.

Many types of emitters are too weak to study on the level of a single emitter, so that spectroscopy can be done only averaged over ensembles, which suffer from intrinsic inhomogeneities. These inhomogeneities are present even when the macroscopic electromagnetic environment is considered to be homogeneous, for example because the local microscopic environment of the emitters varies or because the emitters exist in various conformations.

Optical antennas can enhance the fluorescence of such emitters, making it possible to use the tool box of single molecule spectroscopy [69]. In this way the intrinsic inhomogeneities in ensembles of emitters can be studied and overcome, and the dynamics visualized without the need for synchronization [70].

In addition, single emitters emit single photons. Optical antennas can enhance, direct and control such single photon sources and are therefore potentially interesting for quantum information applications [71].

Semiconductor and photovoltaic devices

Optical antennas can focus energy down to small volumes in semiconductor devices. Smaller active device areas can improve carrier extraction and device speed. For example, optical antennas have been used to create an effective nanoscale Germanium photo-detector for radiation with a wavelength of 1.3 μm [72]. In photovoltaic devices the locally improved absorbtion using optical antennas could lead to thinner solar cells designs, potentially allowing the use of poorer quality or less scarce materials [73].

Near-field microscopy

In near-field scanning optical microscopy the goal is to interact with only a small, sub-diffraction-limited volume of a sample [3, 74, 75]. If an optical antenna is controllably scanned over the sample, small volumes of the sample can be addressed sequentially, and a high resolution optical image constructed. In this way deep sub-wavelength resolution optical microscopy has been demonstrated with optical antennas [35, 76–79], including on cell membranes [80, 81]. Chapter 2 gives an example of high resolution optical microscopy with optical monopole antennas.

Conclusion

Optical antennas provide a new tool to link quantum emitters to light. They allow enhancing absorption and emission rates, as well as the control of the angular emission, the polarization and spectrum. This versatility makes optical antennas a promising technique for any application where a strong interaction of a nano-scale object or emitter with light is required.

Such optical antennas can be qualitatively understood as cavities for surface plasmons, with highly confined modes, whereas the changes of the emission and absorption of a quantum emitter coupled to an antenna can be quantitatively described by classical electrodynamics.

The remaining chapters use, expand, and experimentally demonstrate the ideas outlined here. Chapter 2 exploits antennas on scanning probes, and single fluorescent molecules, to probe the confined antenna field. Chapter 3 demonstrates the control of the angular emission of a single emitter with optical antennas. Chapter 4 presents optical Yagi-Uda antennas with high directivities and gains. Finally, Chapter 5 revisits and extends the cavity description of optical antennas to derive a full model for the interaction of dipolar emitters with radiation through optical antenna modes.

CHAPTER 2

Monopole antenna: Single-molecule excitation

To experimentally investigate the interaction of single emitters with light through optical antennas modes, a single emitter needs to be controllably positioned near a nano-size antenna. We employed fluorescent molecules as single emitters, and scanned them near probe-based nanorod antennas in a near-field scanning optical microscope. This chapter introduces the antenna, and describes the experimental characterization of the *excitation* part of the interaction.

The key element of the experiment is that the fluorescence intensity of single molecules is an approximate measure of the local excitation field vector. By scanning molecules close to the antenna one maps the excitation field, and directly probes the antenna characteristics in the near field.

We show that the antenna mode is driven only if a local field component along the antenna axis is applied. This driving condition is similar to the far-field polarization selectivity of linear wire antennas. The antenna resonances are tuned by varying the antenna length. We find that these resonances are characteristic for traditional monopole antennas, but happen at shorter lengths because of the reduced wavelength of the surface plasmon and an additional phase shift upon reflection at the antenna ends. The resonantly enhanced field at the antenna apex, which forms for the right driving conditions, is highly confined in space (within $\sim$ 25 nm). The molecule only interacts with the antenna mode over this short distance.

The results for the driving and the resonances reveal that the antenna is an optical version of a conventional monopole antenna, which provides an accurate shorthand description for the nano-antenna. The next chapter, chapter 3, uses this intuitive description, and the characterization of the excitation field, to study the *emission* of single molecules coupled to the antenna.

This chapter contains three sections. Section 2.1 introduces single fluorescence molecules as local excitation-field probes. Section 2.2 describes the optical monopole antennas and their fabrication. Section 2.3 characterizes the excitation field at the optical monopole antennas by scanning single fluorescent molecules close to the antennas.

2.1 Single molecules as near-field probes

Single fluorescent molecules are exceptional probes of local electromagnetic field distributions [52, 74, 75, 82–84]. Their small size ($\sim 1nm$) and single fixed absorption dipole allows the orientation-sensitive probing of strongly confined fields with a high resolution. By scanning a single molecule through a local field distribution, a fluorescence map is obtained. Under certain conditions this fluorescence map is a measure of the amplitude of the local excitation-field vector.

This section first summarizes the equations and conditions for probing local excitation fields with fluorescent molecules. Next, it introduces near-field scanning optical microscopy as a suitable experimental technique to map confined fields at nano structures with single fluorescent molecules.

Mapping excitation fields with single-molecule fluorescence

According to equation 1.15, the detected fluorescence I from a molecule placed in a weak excitation field $\mathbf{E}_{loc}$ is proportional to the molecular excitation rate Γ_{exc}, the quantum efficiency of the emission η_q, and the collection efficiency of the detection system η_c:

$$I = \Gamma_{exc}\eta_c\eta_q. \tag{2.1}$$

Because the quantum and collection efficiency generally depend on the local environment of the molecule, and thus its position, the fluorescence intensity I is a complicated function of the excitation and emission properties [39, 41, 77]. In particular, for strong variations of η_q and η_c the variations in the fluorescence signal do not describe the excitation rate. In our experiments, however, both η_q and η_c vary little and slowly compared to Γ_{ex}.

There are no strong reductions of the quantum efficiency η_q (quenching) because our antenna is fairly efficient, and because the distance of the molecule to the antenna is no less than $\sim$ 10 nm. There is no enhancement of η_q, because the molecules used have a high intrinsic quantum efficiency (≈ 1). Additionally, the collection efficiency η_c varies little because we use a large numerical aperture ($NA = 1.3$), which collects most of the emission for all molecular positions and orientations, as I will demonstrate in chapter 3. Under these conditions, the detected fluorescence intensity I depends mainly on the excitation field. Assuming that the field confinement does not jeopardize the dipole approximation, I thus approximately satisfies

$$I \propto \Gamma_{exc} \propto |\hat{\mathbf{p}} \cdot \mathbf{E}_{loc}|^2. \tag{2.2}$$

By scanning a molecule through the excitation field, the fluorescence intensity thus maps the projection of the amplitude of the local excitation field onto the molecular absorption dipole moment.

Experimental: near-field scanning optical microscopy

To scan single molecules near antennas and to collect the resulting fluorescence, we used a near-field optical microscope (NSOM), figure 2.1. NSOM is well-developed scanning probe technique, in which a localized optical field at a

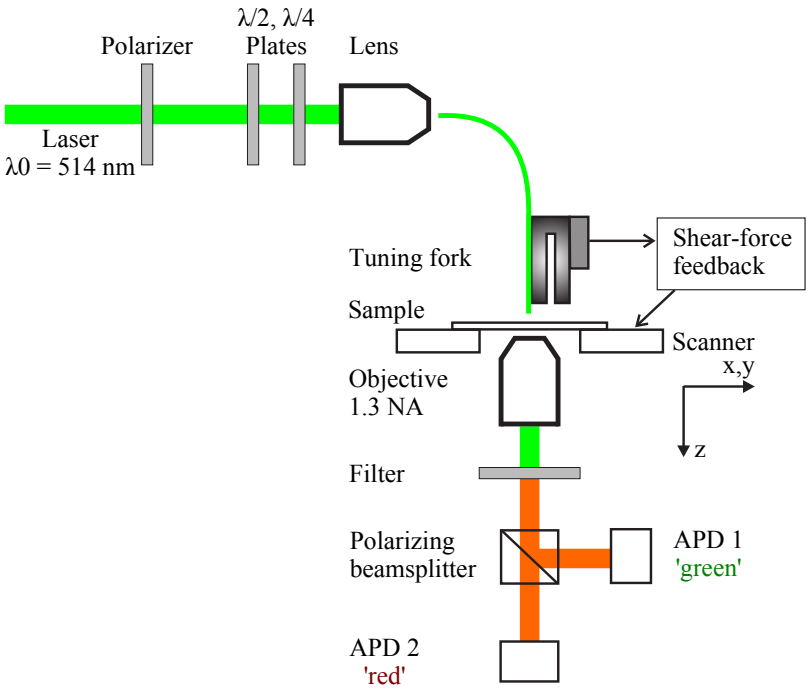

Figure 2.1: **Near-field scanning optical microscope.** To map the local field at nano-antennas, a sample of single fluorescent molecules is XY-raster scanned by shear-force feedback under antennas that are fabricated on fiber probes. All experiments were performed at room temperature. The antenna is illuminated by coupling light ($\lambda_0 = 514$ nm) into the optical fiber. The resulting fluorescence ($\lambda \approx 570$ nm) is recorded for each sample position. The fluorescence signal is split in two polarization directions onto two avalanche photodiodes (APD), so that both the fluorescence intensity and polarization are characterized.

probe is used for sub-diffraction-limited imaging of a sample [84]. Vice versa, if the properties of the sample are well-known, information about the local field at the probe can be obtained instead. We exploit samples containing isolated fluorescent molecules to map the local field at nano-antennas that are fabricated on the end of optical-fiber probes.

We prepared samples of single fluorescent molecules immobilized in a 20 nm thick polymer layer on a glass substrate. First, 0.5% poly(methylmethacrylate) (PMMA) was dissolved in toluene, and $DiIC_{18}$ (1, 1′-dioctadecyl-3, 3, 3′, 3-tetramethyl-indo-carbo-cyanine-perchlorate) molecules were added to a 10^{-8} molar concentration. Next, the solution was spin coated onto glass substrates, which were cleaned by plasma etching. Finally, the samples were dried at ambient conditions. The resulting samples contain spatially isolated molecules with random, but fixed, orientations and positions.

The probe-based antenna is illuminated through the optical fiber, figure 2.1. A laser beam (Ar^+, $\lambda = 514$ nm) of controlled polarization is coupled into the fiber. The single-molecule sample is scanned under the probe, while the probe-

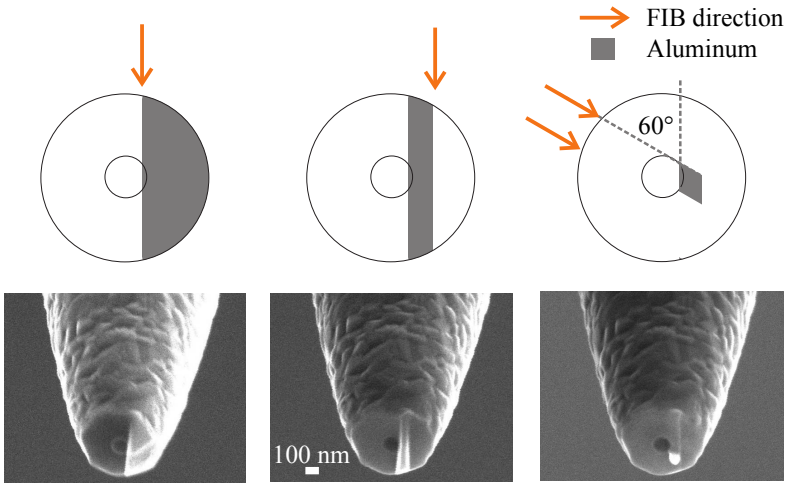

Figure 2.2: **Sculpturing nanoantennas by focused ion beam milling.** The antennas are fabricated by ion beam milling under two different angles. Two intermediate steps and the final result are shown. The 60° angle is a limitation of the ion-beam apparatus. The fabrication scheme predicts a rhomboid antenna footprint, but the actual antennas appear rounded, probably because the antenna dimensions are close to the precision limits of the focused ion beam.

sample distance is kept constant by shear-force feedback [85]. The resulting fluorescence is collected from below by an oil-immersion objective with a 1.3 numerical aperture. The laser light is filtered out, and the fluorescence is split in two orthogonal polarization components. Each polarization component is detected by a separate avalanche photodiode, so that information about both the intensity and the polarization of the fluorescence emission is obtained. [86]

2.2 The optical monopole antenna

The antenna is an aluminum nanorod fabricated on a scanning probe, so that it can be precisely scanned near samples containing single molecules. The antenna resonances can be tuned by controlling the antenna length. This section introduces the antenna and its fabrication by focussed-ion-beam milling, and discusses the antenna design.

Fabrication

We fabricated probe-based nano-antennas following a method for aperture probes by Veerman et al. [87]. Glass probes with sharp tips ($\sim$ 100 nm) were created by heat pulling single-mode optical fibers ($\lambda = 633$ nm) using a commercial pipet puller (Sutter Instruments P2000). The probes were coated all around with a few-nanometer thick chromium adhesion layer (deposition rate 0.1 nm/s), and with approximately 150 nm of aluminum (1 nm/s) by e-beam evaporation. Finally, a rod shaped antenna was sculptured at the probe tip by focussed ion beam milling under two directions. The process is illustrated in

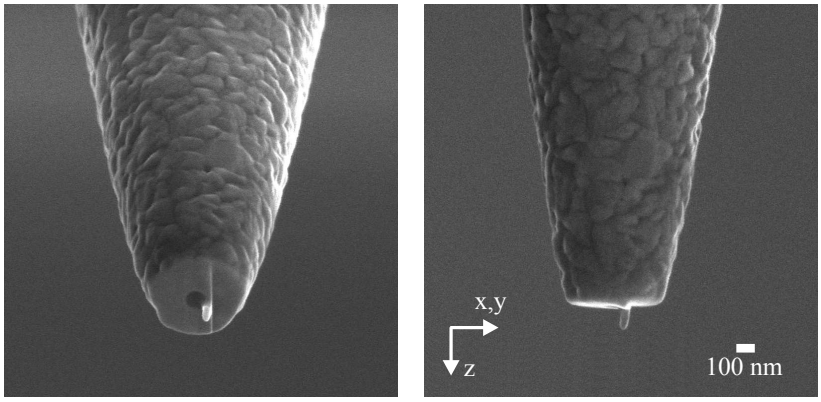

Figure 2.3: **Optical monopole antenna.** The antenna is an elongated aluminum nanorod with a rounded apex. It is positioned on the end face of a coated fiber probe, next to a circular aperture in the aluminum coating that reveals the underlying glass fiber [76, 77]. The antenna diameter is ~ 40 nm, the aperture diameter ~ 100 nm. Left: viewed under 60 degrees. Right: side view.

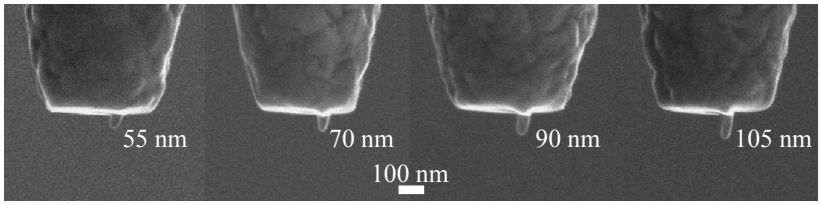

Figure 2.4: **Tuning the antenna resonance by the antenna length.** We controllably fabricated antennas of lengths between 30 and 140 nm, in order to study the antenna resonances.

figure 2.2. The resulting antennas are well-defined elongated nanorods, and are oriented perpendicular to the fiber end face, figure 2.3. The typical antenna diameter is 40 nm. Attempts to create thinner antennas were unsuccessful.

Following the Tip-on-Aperture design of Frey et. al [76, 77], the antenna is positioned next to an aperture (typical diameter $\sim$ 100 nm) in the flat probe end-face (surface roughness less than 10 nm). This aperture reveals the underlying glass fiber. In the experiments the antenna is driven by laser light through the fiber, through the aperture (figure 2.1). Note that without the antenna the probe is simply equivalent to a conventional aperture probe [87].

To tune and investigate the antenna resonances, the antenna length was controllably varied between approximately 30 and 140 nm. Figure 2.4 shows four examples of antennas with different lengths.

Design

Two important design parameters are the material and the position of the antenna. The material largely determines the antenna properties, whereas the

position determines how the antenna is driven by the local field of the aperture.

The antenna is made of aluminum. We chose aluminum because it is suitable for antennas at the absorption wavelength of the molecules used (DiI, $\lambda_{abs} \approx 514$ nm). In addition, aluminum has a small skin depth, which reduces leakage from the fiber probe, and makes it the logical traditional choice for aperture NSOM probes [75, 88].

We anticipate that the antenna is driven by applying a field component along its axis. According to previous studies [74, 75, 89–93], this component is present at the edges of the aperture in the direction of the incoming polarization. We thus expect the antenna to be ideally placed at edge of the aperture. The driving of the antenna by the local aperture field is investigated in detail in the next section.

2.3 The antenna excitation field

To study the properties of the optical monopole antennas (section 2.2), we directly probed the local field at the antennas with single fluorescent molecules in a near-field microscope (section 2.1). This section first presents the obtained experimental maps of the locally-enhanced excitation field. I will then use these maps, and numerical calculations, to separately discuss three properties of the antenna in detail: the highly confined nature of the antenna mode, the driving of the antenna by the local aperture field, and the antenna resonances.

Single molecule mapping of the excitation field

We consider the local excitation field at a 80-nm-long monopole antenna. The antenna is driven by the local field at the aperture [76, 77], which is illuminated from the back through the fiber. The field at the aperture, and thus the driving of the antenna, depends on the polarization of the illuminating light [74, 75, 91]. To control the illumination polarization, the polarization of the laser light was adjusted before being coupled into the fiber, and characterized after emerging from the aperture. Two input polarizations are of special interest: a linear polarization in the direction of the position of the antenna and the polarization perpendicular to that. These polarization directions, and the position of the antenna relative to the aperture, were initially determined by observing the polarization of the far-field transmitted laser light.

For the input polarization in the direction of the antenna, the single molecule fluorescence results contain narrow patterns, as well as weaker larger spots, figure 2.5a. The narrow spots are ~ 25 nm wide (FWHM), figure 2.6. Such narrow features are not expected for a 100 nm aperture, and their width is similar to the radius of curvature of the antenna apex. We attribute these narrow patterns to the response of single molecules to the locally enhanced antenna field; only if a molecule is close to the antenna it interacts with the antenna mode and its fluorescence is enhanced. The larger spots have diameters of ~ 100 nm and originate from the residual aperture field.

When the polarization is rotated by 90 degrees, only large spots were observed, 2.5b. By restoring the polarization, the original image is recovered, 2.5c, indicating that the effects are purely optical. Only for the polarization in the direction of the antenna position, the antenna is driven and a locally enhanced field forms at the antenna apex.

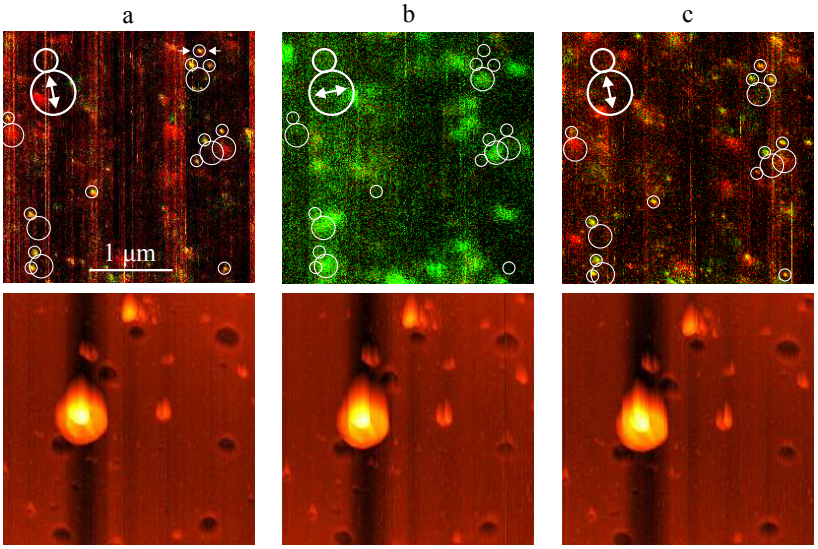

Figure 2.5: **Single molecule fluorescence** for an optical monopole antenna of length 80 ± 5 nm (top row), and simultaneously recorded topography (bottom row). The insets show the position of the antenna (small circle) relative to the aperture (large circle), and the input polarization (arrow). Some examples of the response of single molecules to the antenna field (narrow spots) and the residual aperture field (large spots) are encircled. Only for an incoming polarization in the direction of the position of the antenna, the antenna mode is driven and a highly localized field at the antenna apex is formed. The correlations between the positions of the small and large spots reveal the position of the antenna relative to the aperture. The brightness of the image is linearly proportional to the fluorescence intensity. The color coding contains information of the polarization of the fluorescence: red corresponds to the detector for the vertical polarization, green to the detector for the horizontal polarization (Figure 2.1). Yellow implies equal signal in both polarization channels.

The simultaneously recorded topography confirms that the fluorescence response is not height induced [94], and allows comparing the positions of patterns from different measurements (figure 2.5). Moreover, the height images give information about the antenna probe; surface features that are higher than the antenna length result in a topography signal that contains a convolution of the complete probe. A clearer example, for a different antenna, is shown in figure 2.7. The antenna, the flat end-face and the aperture are clearly visible. The height signal gives an accurate independent *in situ* measurement of the antenna length and allows monitoring of any possible structural changes. Aditionally, the topography gives a second independent way to determine the position of the antenna relative to the aperture.

The positions of several of the narrow patterns are correlated with the position of large spots, so that recurring patterns consisting of a narrow spot to the upper left of a large spot are formed (figure 2.5). These patterns originate from one single molecule. The relative orientation of the narrow and large spots

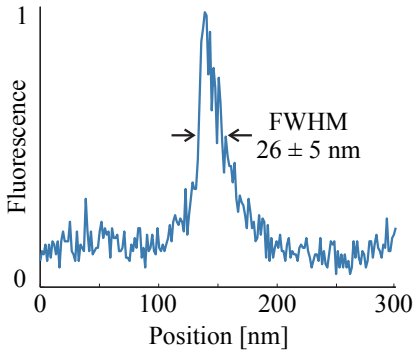

Figure 2.6: **The locally enhanced field at the antenna is strongly confined.** Cross section from the narrow antenna spot marked in figure 2.5a by two arrows. The full width at half maximum (FWHM) is 26 ± 5 nm. Only if the molecule is close to the antenna it interacts with the antenna mode and its fluorescence is enhanced. The orientation of this molecule is approximately along the antenna axis (z).

reveals the antenna position. Evidently, the near-field fluorescence signal gives a third and final independent way to determine the antenna position relative to the aperture.

The relative intensity and emission polarization of the spots for the different incident polarizations contain additional information about the local field at the probe, and about the orientation of each individual molecule. The emission polarization is color coded: the intensity for the detectors corresponding to the vertical and horizontal polarization are colored red and green respectively. Yellow implies equal signal on both detectors.

The large aperture patterns tend to have emission polarizations along the input polarization. As for conventional aperture probes, [75], the aperture field preferentially excites molecules with an absorption dipole oriented along the input polarization (see figure 2.8a) for a calculation). The aperture field thus selects a different set of molecules for each of the two different input polarizations. The local field at the antenna contains field components in all directions (see for example figure 1.3, and figure 2.8 below), and can thus excite molecules with all orientations. This preferential excitation of different orientations of molecules by the aperture field explains why for each narrow spot the corresponding large spot can appear either mostly for vertical or mostly for horizontal input polarization, or can be absent entirely; these molecules are oriented dominantly vertical, horizontal, or out-of-plane respectively.

The changes of color within a single-molecule pattern contain information about the changes of the emission polarization as the molecule is scanned near the antenna. Chapter 3 uses this information in a detailed study of the changes of the angular emission of molecules as they are coupled to the antenna.

To summarize, the above results show that for an input polarization in the direction of the position of the antenna the antenna mode is driven, and a highly localized field (≈ 25 nm) forms at the antenna apex. The rest of this section discusses three main properties of the antennas, and their implications, in more detail: the highly confined antenna field, the driving of the antenna,

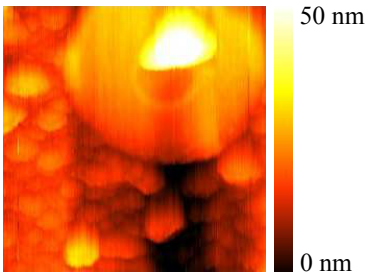

Figure 2.7: The topography contains a wealth of information about the monopole antenna; surface features higher than the antenna length result in a convolution with the probe. The antenna length, 40 nm in this case, and position can be determined and monitored during the actual experiment. The scan area of the image is 570×570 nm.

and the resonant modes of the antenna.

Highly confined antenna fields

Figure 2.6 shows that the fluorescence is only enhanced for small antenna-molecule separations. Because the fluorescence intensity is an approximate measure of the excitation field, equation 2.2, this result experimentally confirms that the antenna mode field is highly confined and locally enhanced. Such confined modes are one of the main properties of optical antennas. This subsection explores two consequences of the field confinement in more detail: near-field optical microscopy and forbidden transitions.

Because the field is locally confined, the scanning probe based antenna is effectively a high-resolution near-field microscope. The 26 nm width of the single-molecule response in figure 2.6 is a measure for the resolution.[1] This width is approximately 1/20th of the wavelength of the light used. Two molecules placed 26 nanometer apart can be distinctly imaged by separately selecting them by placing the antenna over them. The same probe-based antennas have now been used by van Zanten et al. to image molecules on intact cell membranes in physiological conditions with similar resolution [80].

Near-field optical microscopy faces stern competition from far-field microscopy techniques that exploit the molecular photophysics or photochemistry [95–97]. Those techniques are generally easier to apply to biological imaging, and obtain similar resolutions. However, the unique property of optical antennas is that the electromagnetic field is actually strongly confined. As a result, the enhancement and confinement applies to any type of light-matter interaction, for example non-linear processes and Raman scattering.

[1] This measure is approximate because the measurement in figure 2.6 probes only the component of the field along the molecular dipole moment, in this case approximately along the antenna axis. The orientational-averaged response is expected to be slightly broader. Moreover, each molecular orientation will effectively interact with the antenna mode at a different position, which introduces an additional uncertainty on the order of 25 nm in the position of molecules with unknown orientation. The resolution defined here is thus strictly valid only for a sample with all molecules oriented along the antenna axis.

Physically highly confined fields imply strong field gradients; when the field confinement becomes on the order of the size of the emitter, the electric-dipole approximation will break down, and (electric-dipole) forbidden transitions will play an important role in the interaction. For the small molecules used here no strong contributions of higher order transitions are expected. For larger quantum dots (typically $5 - 20$ nm), however, quadrupolar transitions should become very important in the confined fields at optical antennas [98]. Optical antennas can thus provide a controlled platform to study the fundamentals of emitters in local fields and high gradients.

Theory of the near-field driving of the antenna

The experimental results in figure 2.5 show that the antenna is only driven for an incoming polarization in the direction of the position of the antenna. This subsection uses numerical simulations to explain this observation, studies the details of the driving of the antenna by the local aperture field, and demonstrates that the antenna is indeed ideally placed at the rim of the aperture.

We calculated the local fields at an aperture with and without the antenna. The probe was modeled as a circular aperture in an infinite perfect-electrical-conducting (PEC) screen (10 nm thick), figure 2.8. The aperture diameter is 100 nm. The screen is illuminated from the back by a linearly-polarized plane wave. Despite its simplicity, this model qualitatively explains the local fields at an aperture probe [74, 75]. The antenna is modeled as a cylindrical rod of radius $R = 20$ nm with a hemispherical end. For simplicity, the antenna is, at first, taken as a perfect electric conductor. The antenna length is 100 nm, which is the first-order resonant length for this PEC antenna at the excitation wavelength of 514 nm. The electromagnetic field was calculated with the time-domain solver of CST Microwave Studio, a commercially available simulation package based on the Finite Integration Technique (FIT) [99].

We anticipate that the antenna is driven by a field component along its axis, i.e. the z direction. For the aperture without the antenna, this field component is concentrated in two lobes at the edges of the aperture in the direction of the incident/input polarization, figure 2.8a [74, 75, 89–93].

The antenna is placed next to the aperture, figure 2.8b. For an incident polarization in the direction of the antenna position, the x direction, a strongly confined field is present at the antenna apex; the antenna mode is driven effectively. The field at the antenna apex is confined within ~ 25 nm full width at half maximum, and is enhanced compared to the field of the aperture alone. For incident y polarization there is no component along the antenna; the antenna is not driven, and the aperture field remains largely unaffected. These calculated results qualitatively explain the experimental results in figure 2.5.

As the antenna position is varied, the antenna response follows the evolution of the z component of the field of the aperture without antenna, figure 2.9. The response for an antenna at the center of the aperture is weak, despite the strong x component of the aperture field at that location. These observations suggest that only the local field component along the antenna axis effectively feeds the antenna mode. As a result, the antenna is ideally positioned close to the aperture edge, justifying the fabricated probes.

The comparison of the above numerical calculations to the experimental results hinges critically on the knowledge of the antenna position in the exper-

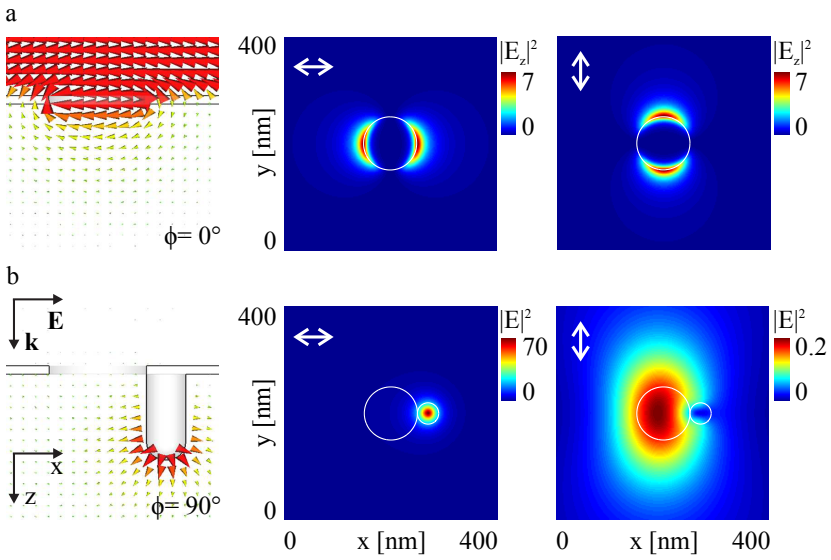

Figure 2.8: **Near-field driving of the antenna by the aperture field.** Numerical calculations for the electromagnetic fields for an aperture (a) without and (b) with the antenna. Left: time snapshots of the local field vectors in the (x, z) plane (at phase ϕ). Right: for (a) $|E_z|^2$ in a (x, y) plane 10 nm below the aperture. for (b) $|E|^2$ in a (x, y) plane 10 nm below the antenna apex. The probe is modeled as an aperture (diameter 100 nm) in an perfect electrical conducting (PEC) screen (thickness 10 nm), illuminated by a linearly-polarized plane wave ($\lambda = 514$ nm). The antenna is a PEC cylinder of 40 nm in diameter. It has a hemispherical apex, and is resonant for the excitation light (length 100 nm).

iments. Recall that this position was determined in three independent ways: from the orientation of the fluorescence patterns, from the topography, and from the far-field scattering. All methods yield the same antenna position and corroborate the idea that the antenna is only driven by the local field component along the antenna axis, i.e. by the input polarization in the direction of the antenna.

The driving of the antenna is analogous to the far-field excitation of nano-rods by a plane wave polarized along the nano-rod axis. In our case, however, the antenna is near-field driven by the local field of an aperture. Remarkably, the antenna response can be predicted from the z component of the local field without the antenna, even though the field is modified in a non-trivial way after placing the antenna.

Monopole antenna resonances

To study the antenna resonances, antennas with different length were fabricated, and scanned over single molecules (figure 2.4). Because the throughput varies strongly between fiber probes, absolute intensities cannot be compared. As a figure of merit for the field enhancement, we choose to take the fluores-

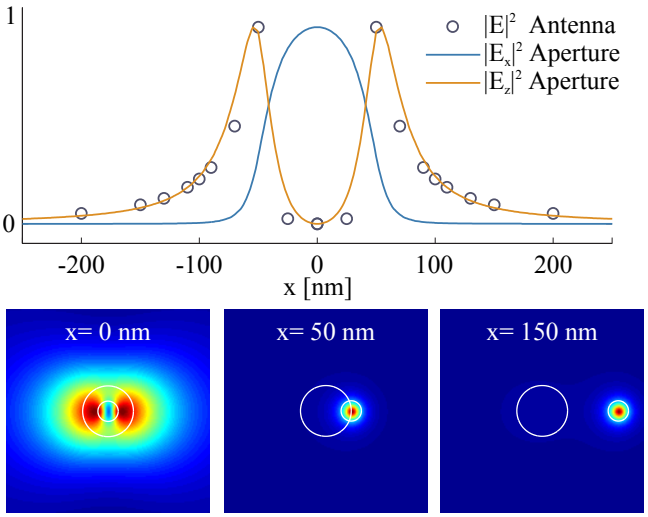

Figure 2.9: **Position dependence of the driving of the antenna** The electric field at the antenna apex, and the x and z components of the field for an aperture without antenna. The maximum of all results is set to unity. The antenna response follows the spatial distribution of the z component of the aperture field without antenna, and appears unaffected by the x component. The three insets show $|E^2|$ in the (x, y) plane 10 nm below the antenna, for three different antenna positions (0, 50 and 100 nm).

cence signal for molecules positioned at the antenna (narrow spots) relative to the signal for molecules positioned under the aperture (large spots). Averages over several of the strongest narrow spots, and independently over several of the strongest large spots (not the same molecules), were taken to partly average out any influence of the different molecular orientations and positions in the polymer. I will call the value obtained from the above procedure the antennna response[2].

Figure 2.10 shows the antenna response as a function of the antenna length. A resonance is observed. The antenna response is maximum for antennas with a length around 80 nm. The results in figure 2.10 describe the tuning of the antenna resonance to the excitation wavelength (514 nm). The experimental resonance length agrees well with the value predicted by numerical calculations that take into account the aperture field and the antenna material (aluminum with a relative permittivity of $-31.3 + 8.0i$ at 514 nm).

The expected first-order resonance length for a conventional monopole antenna is $\lambda_0/4 = 128.5$ nm, which is half the resonance length of a dipole antenna due to the mirror ground plane. The resonance of the optical antennas happens at a shorter length (~ 80 nm). The reasons for this shortening are better illustrated by figure 2.11. For a perfect electric conducting antenna of negligible thickness the first two resonant modes are expected at $\lambda_0/4$ and $3\lambda_0/4$.

[2]In the original publication [35], we named this value the antenna efficiency. This is a misnomer because an efficiency for a passive device should normally not exceed unity, and because the term antenna efficiency has a different meaning in antenna theory already.

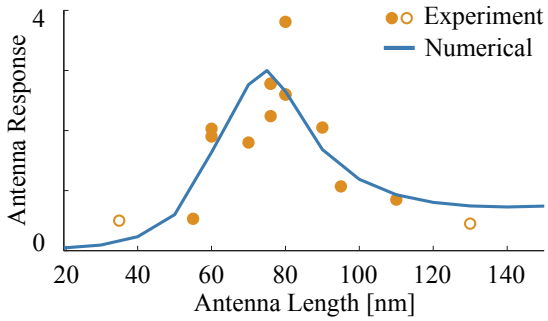

Figure 2.10: **Tuning the antenna resonance to the excitation wavelength.** The antenna response as a function of antenna length. A resonance peak around 80 nm is observed for both the experimental results and for the calculated values for aluminum antennas. The resonance is shifted to a length shorter than $\lambda_0/4$, because aluminum is not a perfect conductor at optical wavelengths. For some antennas no signature of an enhanced antenna field was observed. In those cases the noise level was used to estimate an upper limit for the antenna response. These cases are displayed as open circles. The theoretical values are taken 10 nm below the antenna apex, and are given in arbitrary units.

A thin 2 nm radius PEC antenna approaches this situation, but all resonances are slightly displaced to shorter lengths by an equal amount because the finite thickness introduces a phase shift upon reflection at the antenna ends. For the aluminum antenna, in addition to a phase shift, the surface plasmon wavelength is shorter than the free-space wavelength ($\lambda_{sp} < \lambda_0$); the spacing between the peaks is reduced. These effects will be discussed in more detail in Chapter 5, which studies the modes of optical antennas by treating them as resonators for surface plasmons.

The good agreement of the experimental antenna response with the theoretical predictions confirms the idea that the antenna is an optical version of a standard monopole antenna. This idea is further corroborated by the calculated modal fields for the first two resonant modes, figure 2.12; although the resonant length is shortened for the optical monopole the modal field are still characteristic of a monopole antenna. We performed a similar analysis for the currents, or magnetic fields, which was included in reference [100].

Conclusion

The fluorescence intensity of single molecules can be used to probe the excitation part of the molecular interaction with the modes of optical antennas. In this way, we experimentally demonstrated two key features of optical antennas, strongly confined fields and resonant modes, directly in the near field. These two properties are at the heart of the functionality of optical antennas.

Our probe-based optical antenna is the optical analog of a monopole antenna. The local field distribution, the near-field driving, and the resonances are all characteristic for monopole antennas. Here, applying the terminology

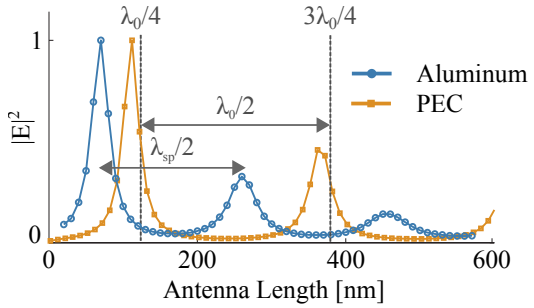

Figure 2.11: Calculated resonances for the aluminum optical antennas and for thin perfect conducting antennas. The electric field $|\mathbf{E}|$ 10 nm below the antenna apex versus the antenna length. For traditional ideal monopole antennas (infinitely thin and perfect conducting), resonances occur at lengths that satisfy $(2j-1)\lambda_0/4$, with $j = 1, 2, 3...$ The calculations for a thin, 2 nm radius, PEC antenna approach those values. For the aluminum antennas with radius 20 nm, resonances occur at shorter lengths. This shortening is a result of an additional phase shift at the antenna ends and the fact that the plasmon wavelength is shorter than λ_0.

and ideas of antenna theory provides a clear and concise description of what otherwise might be considered a complex nano-optical system.

The next chapter studies the properties of the emission process by characterizing the polarization of the emitted fluorescence. The interpretation of the data relies on the excitation field maps presented in this chapter, and is greatly simplified by the conclusion that the antenna is a monopole antenna.

Associated publications

This chapter is based on:
[35] T. H. Taminiau et al., Nano Lett. 7, 28 (2007).
[101] T. H. Taminiau et al., J. Opt. A: Pure Appl. Opt. 9, S315 (2007).
[100] T. H. Taminiau et al., IEEE Trans. Antennas Propag. 55, 3010 (2007).

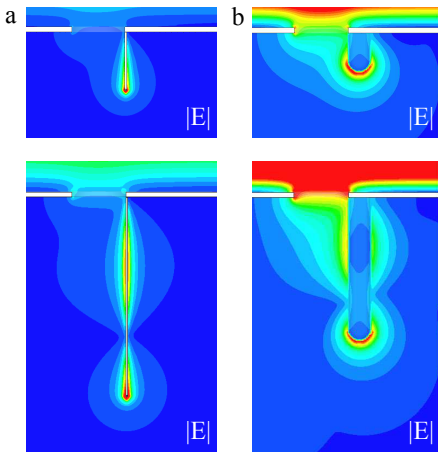

Figure 2.12: **The modal fields are characteristic for monopole antennas.** The absolute value of the electric field for the first two resonant modes for (a) a thin, 2 nm radius, PEC antenna and for (b) the aluminum antenna with a radius of 20 nm. The thin PEC antenna is equivalent to a conventional monopole antenna. Apart from the shorter resonant lengths, the mode profiles of the aluminum optical antennas have all the same characteristics as a conventional monopole antenna. The wavelength is 514 nm.

CHAPTER 3

Monopole antenna: Single-molecule emission

Antennas work both in excitation and emission. The previous chapter used the fluorescence intensity to characterize the excitation enhancement of single molecules by an optical monopole antenna. This chapter treats the control of the emission by the antenna. The key of the experiments is that the polarization of the emission provides information about the orientation of the effective dipole moment underlying that emission. By precisely positioning a single molecule close to, and far from, an optical monopole antenna we directly measure and control how the emission changes as the molecule is coupled to the antenna.

We find that if the molecule is placed at the right position and if the antenna is tuned to resonance, the angular emission of the coupled system is determined by the dipole moment of the antenna mode, regardless of the orientation of the molecular dipole. This observation provides direct insight in the role of plasmon mode: the emitter near-field couples to the antenna mode, which in turn couples to the radiation field, determining the angular emission.

The observation that the antenna determines the angular emission has several implications. First, changes in emission direction imply changes in collection efficiency, which can be beneficial, but also complicate the interpretation of intensity and ensemble measurements. Second, it is challenging to determine the position of the emitter from the emitted field alone. Third, the fact that the antenna design determines the emission provides a clear guideline for incorporating the large library of traditional antennas in nano and quantum optics. The next chapter exploits this last fact to realize highly directed emission and excitation using an optical version of the Yagi-Uda antenna.

This chapter contains four sections. Section 4.1 presents an example calculation that illustrates how an optical antenna can control the angular emission. Section 4.2 discusses the single-molecule experiments that demonstrate that the antenna determines the emission. Sections 4.3 and 4.4 discuss two consequences of that observation: changes in the collection efficiency due to the redirection of emission, and the issue of localizing the emitter by imaging.

3.1 Introduction: An example of emission control

This section presents example calculations that illustrate how the angular emission can be controlled with an optical antenna, and how changes in angular emission can be observed through changes in polarization.

Consider the case shown in figure 3.1: an emitter with a horizontal dipole moment and a vertically oriented antenna. The emission pattern of the emitter in a homogeneous medium (without antenna) is simply dipolar, figure 3.1a. If we couple the emitter to the antenna, by placing it at the point of high mode density at the antenna end, a new emission pattern is calculated. The new pattern is rotated by almost 90 degrees, and resembles the emission of a vertical dipole, which we associate with the vertical antenna, figure 3.1b. These results suggest that for the coupled system the antenna is the main radiator, and that the angular emission is determined by the antenna dipole moment.

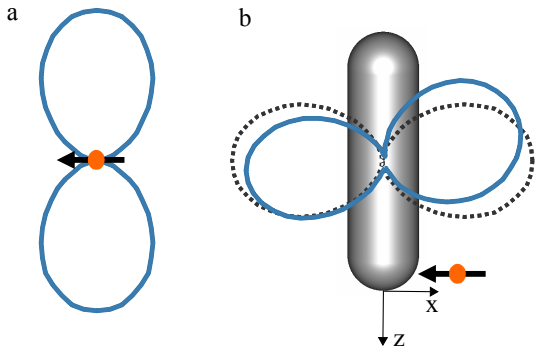

Figure 3.1: **Control of emission with optical antennas.** (a) The dipolar emission pattern of a horizontally oriented emitter. (b) The calculated emission pattern for the same emitter coupled to a vertical aluminum antenna, tuned to its dipolar resonance. The black dotted pattern is a schematic for the vertical dipole moment associated with the antenna. The angular emission of the coupled system is dominated by the antenna dipole moment.

Instead of measuring the full angular emission pattern, basic information about the orientation of the effective dipole moment of the emission can be obtained from polarization measurements [86]. For example, a horizontal (x-oriented) dipole moment emits mostly x-polarized light into the solid angle around the z-axis (which is the optical axis of the detection system in our experiments). A dipole oriented along y would result in mostly y-polarized light. A dipole oriented along the antenna axis would emit a radially polarized beam in the z-direction. In this chapter we use these differences in the polarization to study changes in the orientation of the emission dipole moment as a single molecule is coupled to an optical monopole antenna.

The modification of the angular emission of single molecules near nanostructures has been observed previously for aperture near-field microscopy probes [52, 53] and for spherical nanoparticles [10, 41]. The advantage of the optical monopole antennas studied here is that the resonant mode along the antenna axis provides a well-defined and fixed dipole moment, which allows strong control of the angular emission and a straightforward interpretation.

3.2 Experimental control of single molecule emission

The experiments to characterize the emission are similar to those discussed in chapter 2. A single molecule is scanned near a probe-based optical monopole antenna and the fluorescence is collected, figure 2.1. The quantity of interest is now, however, the change in polarization as the molecule is coupled to the antenna. This section presents the results that demonstrate that, if the molecule is placed at the right position near a resonant antenna, the antenna dipole determines the emission of coupled system, regardless of the molecular orientation.

Directing single molecule emission

Consider the experimental fluorescence map shown in figure 3.2. As in chapter 2, the fluorescence intensity shows recurring patterns consisting of a small spot and a large spot. We associate the small spots to the emission of a single molecule coupled to the antenna, and the large spots to the uncoupled emission of the same molecule when further from the antenna. The polarization of the emission is characterized by projecting the emission on two detectors with a polarizing beam splitter. This polarization is captured in the color coding: red corresponds to the detector for horizontal polarization, green for the vertical detector, and yellow corresponds to an equal projection in both channels.

Clearly, the color within individual single-molecule patterns changes with the antenna position; the angular emission is modified by coupling to the antenna. In this case the large spots tend to show a polarization along the horizontal (x) excitation polarization, i.e. red, as expected from the preferential excitation of the sub-set of molecules with a large horizontal (x) dipole moment by the residual field from the aperture [75]. The small antenna spots are mainly yellow, indicating that for the same molecules coupled to the antenna the signal on both detectors is equal; the emission is determined by the antenna dipole oriented along the optical axis, resulting in radially polarized emission and an equal signal in both polarization channels.

To quantify these observations we define a degree of (linear) polarization (DOP) as:

$$DOP = \frac{I_x - I_y}{I_x + I_y}, \tag{3.1}$$

in which I_x and I_y are the intensity counts of the detectors for x- (red/horizontal) and y- (green/vertical) polarization, respectively. The DOP provides a relative weight of the two perpendicular polarization channels.

We compare the DOP value for a molecule closely coupled to the antenna (small spots) to the value for the same molecule when it is further from the antenna (large spots). We repeat this measurement for many molecules, each with its own random orientation, and plot the results for the coupled DOP against the uncoupled DOP for each molecule, figure 3.3.

Consider the expected DOP values in the following two limiting cases. If the antenna does not affect the molecular emission then we expect both DOP values to be always equal so that one obtains the diagonal identity line, figure 3.3. However, if the antenna completely dominates the emission then the emission is radially symmetric and the coupled DOP value is always zero (equal signal

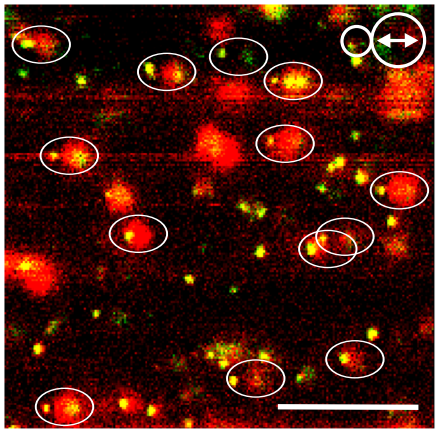

Figure 3.2: **Single molecule fluorescence.** Single molecule fluorescence map obtained by scanning an optical monopole antenna over a sample of randomly oriented and distributed individual molecules, see chapter 2 for experimental details. Scale bar: 1μm. The input polarization is horizontal, which is in the direction of the antenna position (see inset, the small circle is the antenna, the large one the aperture). Recurring patterns consisting of a small antenna spot and a large aperture spot are observed. Each such pattern originates from a single molecule. The quantity of interest is the emission polarization which is color coded: red is horizontal, green is vertical. The color changes within one individual single-molecule pattern demonstrate that the angular emission changes as the molecule is scanned near the antenna.

in both detectors), whereas the uncoupled value is still free to take any value. In that case we thus expect a horizontal line at zero.

The experimental data points deviate from the identity line. The coupled DOP values indeed tend to zero, figure 3.3. For the uncoupled molecules the DOP values are distributed over all possible DOP values, indicating molecules with a large variety of dipole orientations were studied. These results corroborate the idea that the emission of the coupled system is dominated by the antenna dipole moment. The antenna determines the angular emission regardless of the orientation of the molecular dipole moment.

This straightforward interpretation of the experiments is possible only because we observe a single molecule at the time, and because can precisely and dynamically position that molecule. By observing the same molecule close and far from the antenna a clean reference situation is established and the changes in the emission polarization as the molecule is coupled to the antenna are directly obtained.

The numerical calculations in figure 3.3 agree well with the experimental results. Figure 3.4a shows an overview of the model system used for these calculations. The calculations were done for a dipole antenna because accurate modeling of the complete monopole fiber probe is challenging. Because a monopole is half a dipole antenna with the other half replaced by the reflection in the ground plane, the angular emission of the monopole antenna can be approximated by a dipole antenna. The maximum magnitude observed

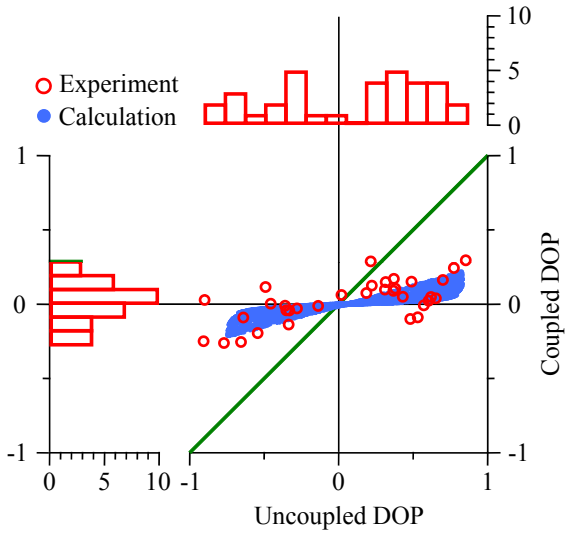

Figure 3.3: **Experimental control of angular emission.** Experimental and theoretical *DOP* values for molecules coupled to the antenna against the values for the same molecules when uncoupled. The experimental values for the 34 molecules are a compilation taken from three different antennas, all with a length close to resonant, and for a variety of different input polarizations. The theoretical values were calculated for 10^4 random dipole orientations using the model shown in figure 3.4a. The fact that the coupled *DOP* values are distributed close to 0, whereas the uncoupled values are spread out over the entire range, demonstrates that the antenna dipole moment determines the angular emission of the coupled system, regardless of the molecular dipole orientation.

for the theoretical uncoupled DOP is approximately 0.8, which is obtained for dipoles oriented along either of the polarization axis (i.e. the x- or y axis). The fact that an x-oriented dipole results in partly y-polarized light is caused by the collection through the high numerical aperture objective ($\theta_{NA} = 60°$, $NA = 1.3$) [102–104].[1]

The numerical calculations provide additional insight into the near-field coupling and the emission process, figure 3.5. The near-field coupling of the emitter to the antenna can be visualized by the local electric field at the antenna. Because the antenna response is resonant, the instantaneous local electric fields associated to the emitter and to the antenna mode can be visualized separately in time by taking two snap shots with a $\pi/2$ phase difference, figures 3.5b and 3.5c. These images show that the horizontal emitter resonantly drives the vertical dipole moment associated with the standing wave of the resonant antenna mode.

In conclusion, the combined experimental and theoretical results in this

[1]Note that the experimental DOP values do exceed 0.8. This discrepancy is likely caused by the assumption made in the calculations that all light collected by the objective falls on the detector, whereas the actual detector has a finite size, cutting a part of the cross-polarized light.

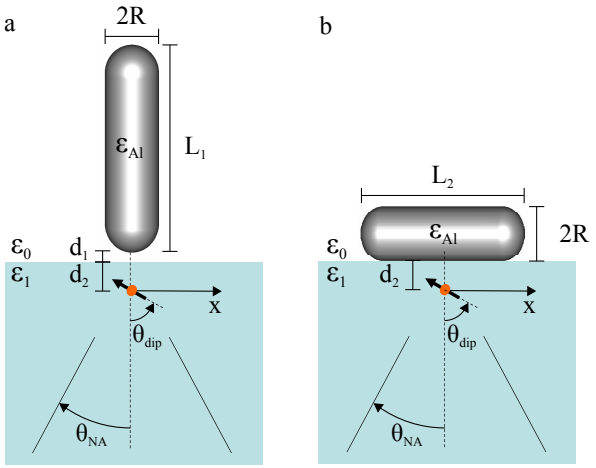

Figure 3.4: **Overview of the calculation models.** (a) Vertical antenna, which is also used as a model for the monopole antennas used in the experiments. (b) horizontal antenna. The antennas are cylinders with hemispherical ends. Parameters: wavelength $\lambda_0 = 570$ nm, $L_1 = 150$ nm, $L_2 = 130$ nm, $R = 20$ nm, $\epsilon_0 = 1$, $\epsilon_1 = 2.25$, $\epsilon_{AL} = -37.8 + 10.8i$, $d_1 = 4$ nm and $d_2 = 6$ nm.

subsection show that the angular emission of the coupled system is determined by the antenna emission. This result provides experimental corroboration for the role of the antenna in the emission process: the emitter near-field couples to the antenna plasmon mode, which in turn couples to the radiation field, determining the angular emission. The rest of this section studies the influence of the molecular position and the dependence of the coupling on the tuning of the antenna resonance.

The role of the molecular position

Due to the near-field nature of the interaction between the molecule and the antenna, the molecular position and orientation play a crucial role in the coupling. The precise scanning of single emitters employed here allows a detailed experimental study of the position dependence of the interaction.

It is illustrative to first consider the case of an x-oriented molecule, as the antenna effect on the angular emission is most prominent for an orientation perpendicular to the antenna. The theoretical far-field emission for several different positions of the emitter is shown in figure 3.5d. For the emitter far away from the antenna ($x = 500$ nm) the emission into the glass consists of two lobes, as expected for a dipole oriented parallel to a dielectric interface in the absence of the antenna [105, 106]. The emission is unperturbed. As the emitter approaches the antenna, the radiation pattern gradually changes. At $x = 20$ nm, where the coupling is maximum, the pattern resembles a cone. Such a pattern is characteristic for a dipole perpendicular to a dielectric interface (z-oriented) [105, 106], in agreement with the example in figure 3.1 and with the notion that the antenna dipole moment determines the emission.

The polarization of the emission is better visualized in the back focal plane

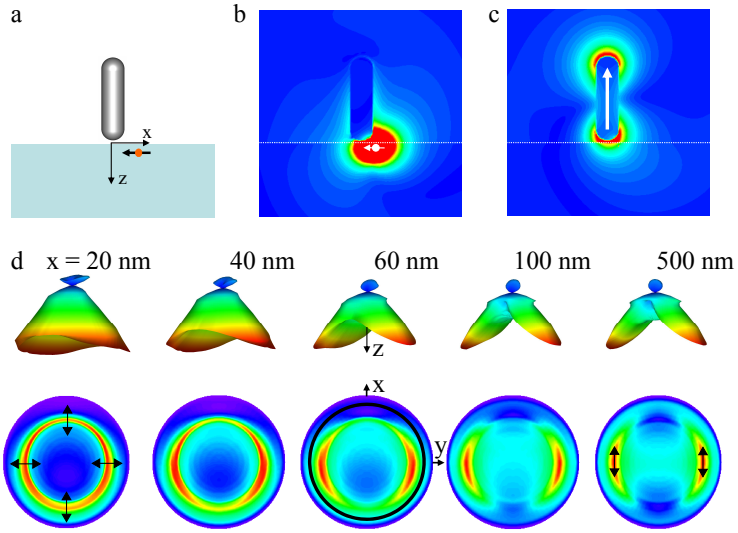

Figure 3.5: **Calculated emission for the experimental situation** (a) A horizontal emitter is scanned near a vertical antenna, details in figure 3.4a. (b)&(c) Instantaneous local electric field amplitude for $x = 20$ nm and for two different phases. Because the phase of the resonant response of the antenna lags the driving emitter field by $\pi/2$, the emitter and antenna mode fields can be visualized (approximately) separately. In (b) the dipole field is maximum, in (c) the antenna field is maximum. The arrows depict the effective dipole moments. (d) Far-field angular and back focal plane emission for different emitter positions. For the back focal plane projection an apodization factor of unity was used (whereas the standard $\cos(\theta)$ apodization factor was used for the DOP calculations). As the emitter approaches the antenna, the emission gradually changes from that characteristic for a horizontal emitter to that of the vertical dipole associated with the antenna. Red indicates high field amplitude.

of the objective, figure 3.5e. [107] For the emitter coupled to the antenna, the emission pattern is approximately radially symmetric, and the polarization approximately radial. Such an emission pattern contains equally strong x and y polarized parts, and thus give $DOP \approx 0$. The two-lobed pattern for the emitter far from the antenna is approximately linearly polarized along the emitter dipole orientation; the emission polarization will depend strongly on the emitter dipole orientation. These observations are in agreement with the experimental data of figure 3.3.

Experimentally, when a molecule is scanned near the antenna both the fluorescence intensity and the polarization change with position. Figure 3.6 shows line traces for the fluorescence intensity I and the DOP for three example molecules, each with a different orientation.

The intensity I is compared to the radiative decay rate Γ_{rad}, which was calculated for the configuration in figure 3.4a. Both parameters show qualitatively the same spatial behavior, because both the enhancement of the excitation and the emission are governed by the enhanced electric modal field at the antenna

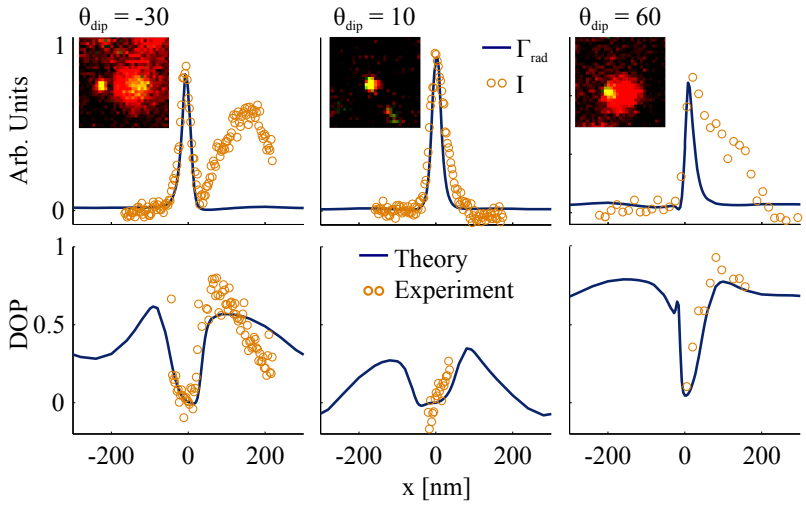

Figure 3.6: **Near-field coupling of three molecules to the antenna.** The fluorescence intensity I (experimental), radiative decay rate Γ_{rad} (calculated), and degree of polarization DOP (experimental and calculated) for three molecules with different orientations θ_{dip} when scanned along x (horizontal). The insets are the 2D fluorescence maps obtained by raster scanning the molecules under the antenna probe. The intensity I, Γ_{rad} and the DOP all vary over short distances, demonstration that coupling to the antenna is a near-field effect, both for the excitation and emission processes.

apex. Although the emission is Stokes shifted, the spatial field profile at the antenna apex is mainly determined by the radius of curvature and is fairly insensitive to wavelength changes. The calculations do not include the aperture probe, and thus give no information about the broad peaks originating from the excitation by the residual aperture field. Because the radiative decay rate Γ_{rad} provides a measure for the coupling to the antenna mode, the good agreement of the intensity curves with the radiative rate implies that the narrow intensity profiles are an indication for the coupling as well.

For the DOP the comparison to the theory is direct and quantitative. The experimental DOP values, obtained only for positions with sufficient emission intensity, agree well with the numerical calculations. For molecules far away from the antenna ($x = 200-300$ nm) the DOP value depends on the molecular orientation. As the molecules are placed closer, the DOP changes gradually in a non-trivial manner. When the coupling to the antenna is maximum, i.e. when I and Γ_{rad} are high, the DOP tends to zero, as expected for the antenna dipole moment. These changes of the DOP happen over short distances (~ 50 nm), demonstrating that the interaction is highly localized in emission as well, and that the coupling is a near-field effect.

Finally, a more complete picture can be obtained from calculations of Γ_{rad} and the DOP for emitters with a variety of different orientations near vertical and horizontal antennas, figure 3.7.

The calculations for Γ_{rad} demonstrate two implications of the near-field nature of the coupling. First, emitters of all orientations can be coupled to

the antenna modes of the vertical and horizontal antennas. Second, emitters with different orientations couple to the antenna modes at different positions. For example, a horizontal emitter ($\theta_{dip} = 90°$) does not couple to the vertical antenna mode right under the antenna apex, i.e. Γ_{rad} is minimum for $x = 0$, because the local modal field is perpendicular to the dipole. Just 20 nm to the side of the apex, however, the coupling is maximum.

In all cases the DOP tends to the value associated with the antenna dipole moment when the coupling of the emitter to the antenna is maximum. The effect is most clearly seen for emitters oriented perpendicular to the antennas. Recall that, in general, a vertical dipole moment gives $DOP = 0$, whereas a horizontal dipole moment (along the x-axis) gives a high DOP value ($\sim$ 0.8). For a horizontal emitter the DOP far away from any antenna is high, corresponding to the undisturbed emitter dipole. When the emitter is coupled to the vertical antenna, the DOP becomes low because the vertical dipole moment of the antenna determines the emission. Likewise, for a vertical dipole emitter the DOP far away from any antenna is 0, but when the emitter is coupled to the antenna, the DOP becomes high as the angular emission is now given by the horizontal dipole moment of the antenna.

In summary, the experiments and calculations in this subsection show that near-field nature of the coupling to the antenna mode implies that the interaction happens over short distances (20 nm), and that emitters of all orientations can couple to the antenna mode, but do so at different positions. Additionally these results provide further examples of the fact that the antenna dipole moment determines the emission if the emitter is coupled to the antenna by placing it at the right position.

The role of the antenna resonance

The antenna resonances play an important role in the interaction of the emitter with the antenna. Up to now all antennas considered were at resonance with the emission. This subsection studies the effect of tuning the antenna resonances, by varying the antenna length, on the coupling Γ_{rad} and the resulting angular emission.

Figure 3.8 presents calculations of the radiative decay rate Γ_{rad} and the angular directivity $D(\theta, \phi)$ as a function of the antenna length L. These calculations were done for gold antennas with different parameters, figure 3.8a, but the principles are general. The radiative decay rate Γ_{rad} reaches a maximum of 500 times the vacuum rate for the dipolar resonance at $L \approx 150$ nm, figure 3.8b.

The angular emission is dipolar for each of the four selected antenna lengths in figure 3.8c. As the resonant length is approached, the emission pattern steadily rotates from the dipolar pattern of the horizontal emitter towards the dipolar pattern of the vertical antenna dipole moment, which can be explained as follows. The angular emission is a combination of the horizontal dipole moment of the emitter, plus the transverse response of the antenna, and the vertical dipole moment of the antenna mode. As the antenna is tuned to resonance with the emission wavelength, the balance progressively shifts from the emitter dipole towards the perpendicular oriented antenna dipole, until the antenna mode dominates and fully determines the angular emission.

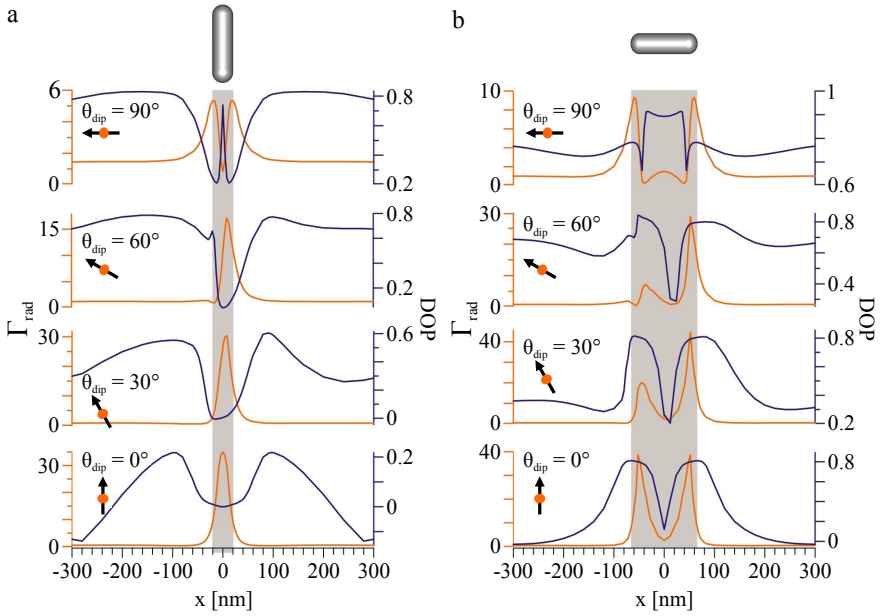

Figure 3.7: **Position dependence of the coupling and polarization** Calculated x-position dependence of the radiative transition rate Γ_{rad} and the degree of polarization DOP for (a) a vertical and (b) a horizontal antenna, and for several different emitter orientations θ_{dip}. In all cases the resulting emission can be understood from coupling and from the dipole moments of the emitter and the antenna. When uncoupled from the antenna (low Γ_{rad}) the dipole of the emitter determines the DOP, when coupled (high Γ_{rad}) the antenna dipole determines the DOP. The DOP for a vertical dipole moment is 0, for a horizontal dipole moment $DOP \approx 0.8$. Emitters with different orientations couple to the antennas at different positions, but always yield a DOP corresponding to the antenna dipole moment

Conclusion

The results in this section show that if the emitter is placed at the right position near the antenna and if the antenna is tuned to resonance, then the interaction of the emitter with radiation occurs through the antenna mode. The next sections discuss two consequences of these observation: changes in collection efficiency and challenges in determining the position of emitters near antennas.

3.3 Collection efficiency

Having established experimentally that the coupling to the antenna changes the angular emission, the question arises how this influences the actual amount of signal collected. Although the answer will depend on the specific illumination and collection configuration, some general concepts can be established. In this theoretical section I will discuss the changes in collection efficiency, and the resulting changes in detected intensity, as emitters with different orientations are coupled to vertically and horizontally oriented antennas. The results can again

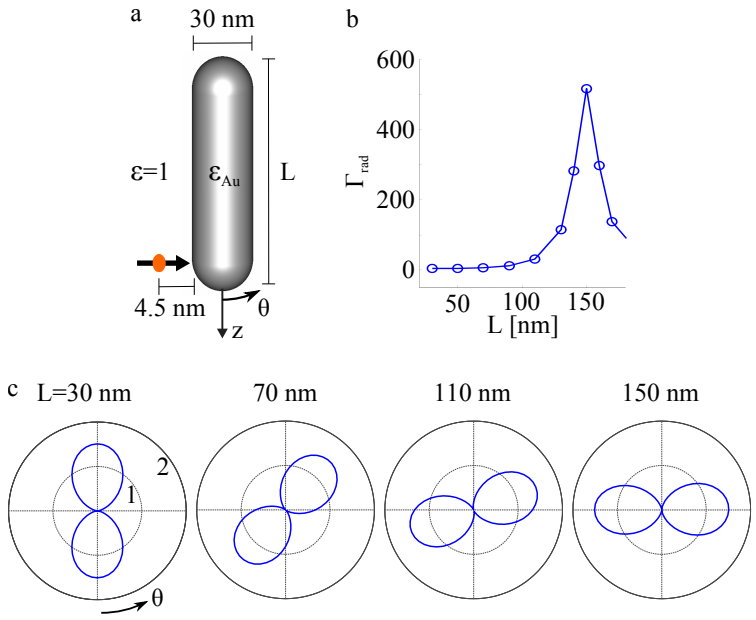

Figure 3.8: **Tuning the antenna resonance to the emission.** (a) Calculation overview. A horizontal dipole emitter coupled to a vertical dipole antenna of variable length L. Wavelength 800 nm, $\epsilon_{AU} = -26.3 + 1.85i$ (gold). (b) The radiative decay rate Γ_{rad} relative to the vacuum rate as a function of the antenna length L. The antenna is resonant with the emission wavelength for $L \approx 150$ nm. (c) The angular directivity $D(\phi, \theta)$ for different antenna length L. The dipolar emission pattern progressively rotates towards the antenna dipole moment as the antenna is tuned into resonance with the emission.

be understood in terms of the orientation of the dipole moments of the emitter and antenna, and show that strong changes in collection efficiency occur, which complicate the interpretation of intensity and ensemble measurements.

Definitions and figures of merit

The collection efficiency η_c gives the fraction of the total emission that is directed into the objective numerical aperture. We calculated η_c for the configurations of figure 3.4, and for different distances between the antenna and emitter. We consider two molecular orientations, vertical ($\theta_{mol} = 0°$) and horizontal ($\theta_{mol} = 90°$) since they show the extreme behaviors, and two numerical apertures: a low NA=0.5 ($\theta_{NA} = 20°$), and a high NA=1.3 ($\theta_{NA} = 60°$). Additionally, we define a figure of merit F for the fluorescence signal in the low excitation power regime as:

$$F = \eta_c^2 \Gamma_{rad}. \tag{3.2}$$

We justify this definition as follows. First, we assume that the excitation and emission have approximately the same wavelength and that illumination and collection use the same objective. Second, we consider the excitation and

emission separately. On the excitation side, the fluorescence intensity is proportional to the excitation rate Γ_{exc}, which generally depends on the specific illumination. In order to keep our definition general, we take the incoherent sum of the available modes, i.e. plane waves, as a measure for the excitation. The excitation is then proportional to $\eta_c\Gamma_{rad}$. On the emission side, the fluorescence intensity is proportional to the product of the quantum efficiency and the collection efficiency $\eta_q\eta_c$. The quantum efficiency η_q generally varies with position, especially very close to the antenna(< 10 nm). Here, for simplicity, we assume that the antenna is efficient, and neglect changes in η_q. The above definition of F is obtained by multiplying the excitation and emission parts.

Importantly, by not specifying phase relations, we avoid the definition of a specific illumination and the introduction of the relative position of the antenna/emitter to the optical axis of the objective as an additional spatial degree of freedom. In other words, the above definition of F gives a figure of merit for the potential fluorescence signal when the illumination is chosen wisely (whatever type of illumination that might be for the specific configuration under study).

A similar analysis could be made for other limiting cases. For example, for saturating excitation powers we get $F' = \eta_c\Gamma_{rad}$, because the excitation rate and quantum efficiency play no role. For an emitter with a near 0 intrinsic quantum efficiency and low excitation powers the symmetry between excitation and emission is restored and we find $F'' = \eta_c^2\Gamma_{rad}^2$. In general the product $\eta_c\Gamma_{rad}$, i.e. the accessible radiative states, is an important figure for an optical antenna.

Vertical antenna

Figure 3.9 shows the calculation results for a vertical antenna. The collection efficiency η_c and the figure of merit for the fluorescence F are displayed for a horizontally and a vertically oriented emitter as a function of the x-position near a vertical antenna, for both NA=0.5 and NA=1.3. Several positions are of special interest: far away from the antenna (as a reference), positions of high Γ_{rad} (where the coupling is strong) and positions of high F (high expected fluorescence signal).

The collection efficiency η_c varies with position and behaves different for the two dipole orientations. The relative variations are much larger for the low NA=0.5 than for the high NA=1.3. For NA=0.5, the most striking feature is the decrease by a factor 3 of η_c for the horizontal emitter as it approaches the antenna and Γ_{rad} increases (the dotted vertical lines indicate the maxima of Γ_{rad} from figure 3.7).

These observations are again explained by the antenna and emitter dipole moments. For a small NA, η_c is relatively low for a vertical dipole compared to a horizontal dipole, as can be seen from the values far from the antenna ($x = 300$ nm). For high NA, the two orientations are collected with a similar high efficiency. The coupling of the horizontal emitter to the vertical antenna dipole mode thus results in a decrease in collection efficiency for NA$= 0.5$, but not for NA$= 1.3$. For the vertical emitter, the coupling to the vertical antenna leaves the angular emission relatively unchanged.

The F values for both emitter orientations are shown in figure 3.9b. For NA$= 1.3$, F is strongly enhanced by the coupling to the antenna; the increase

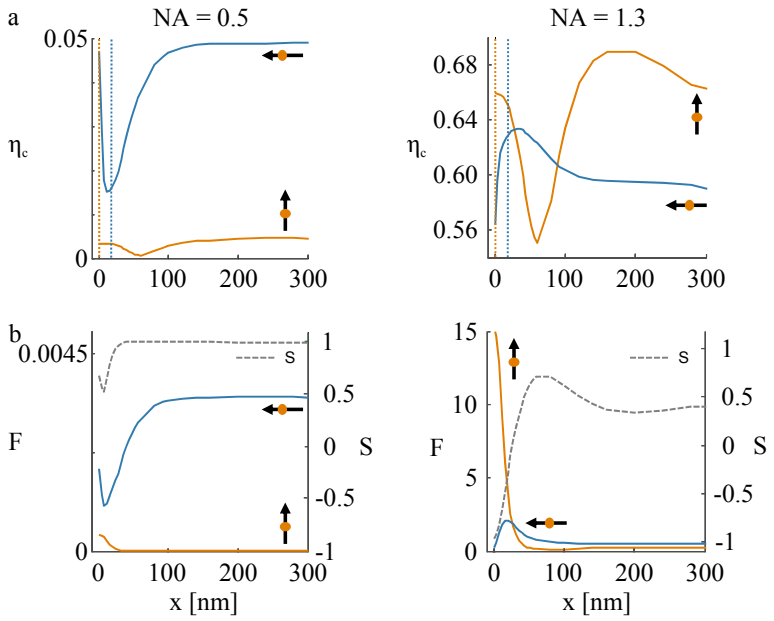

Figure 3.9: **Case of a vertical antenna.** (a) Collection efficiency η_c for a horizontal ($\theta_{dip} = 90°$) and a vertical ($\theta_{dip} = 0°$) emitter as a function of the distance x to the antenna. The vertical dotted lines indicate the maxima of Γ_{rad} in figure 3.7a, i.e. the positions of maximum coupling. (b) Figure of merit for the fluorescence F and relative weight S for horizontal and vertical emitters as a function of x. For both (a) and (b): left for NA= 0.5 and right for NA= 1.3.

of Γ_{rad} results in an increased potential fluorescence. In contrast, for a small NA, there is no significant enhancement of F compared to the emitters at x= 300 nm. The decrease in collection efficiency as the emission is channeled through the vertical antenna dipole nullifies the increase in Γ_{rad}.

Horizontal antenna

For the horizontal antenna the largest modifications of the angular emission and thus η_c happen for the vertical emitter, figure 3.10. For NA= 0.5, η_c for the vertical emitter is increased by a factor of 20 as it is coupled to the antenna. The vertical emitter couples to the horizontal antenna dipole mode, whose emission is effectively collected even with a low NA. For a horizontal emitter, the coupling to the antenna has little effect, but an abrupt jump not directly related to a clear coupling to the resonant antenna mode is seen when the emitter is moved under the antenna.

Because the horizontal antenna is effectively excited and collected for both large and small NA, the curves for F are similar in shape to Γ_{rad} (figure 3.7), and show a significant enhancement due to the antenna. The coupling is more effective for the vertical emitter, for which F is enhanced more than for the horizontal emitter.

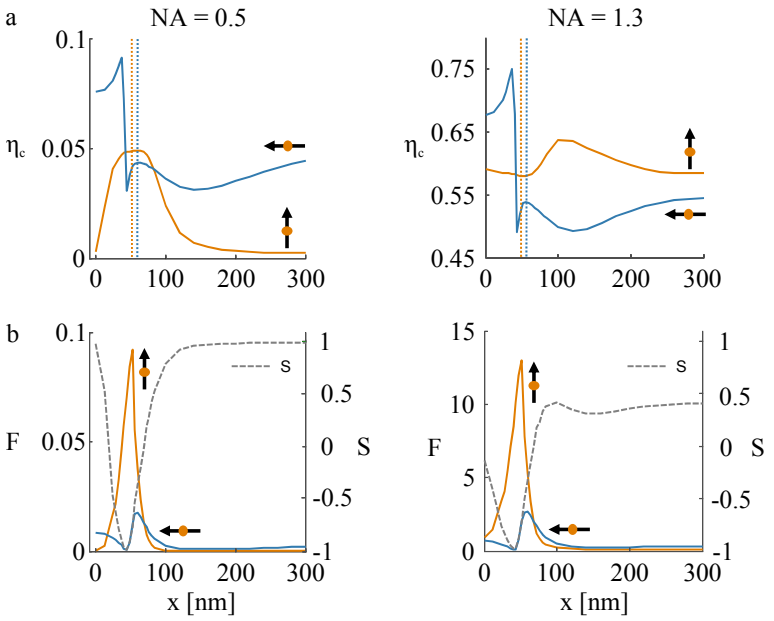

Figure 3.10: **Case of a horizontal antenna.** (a) Collection efficiency η_c for a horizontal ($\theta_{dip} = 90°$) and a vertical ($\theta_{dip} = 0°$) emitter as a function of the distance x to the antenna. The vertical dotted lines indicate the maxima of Γ_{rad} in figure 3.7b. (b) Figure of merit for the observed fluorescence F and relative weight S for horizontal and vertical emitters as a function of x. For both (a) and (b): left for NA= 0.5 and right for NA= 1.3.

Implications for ensemble measurements

In a measurement on an ensemble of emitters with different orientations, the contribution of each orientation to the total intensity differs. To quantify the relative weight of the two emitter orientations in the total fluorescence for each position, we define a parameter S:

$$S = \frac{F_x - F_z}{F_x + F_z}, \tag{3.3}$$

in which F_x and F_z are the F values for the horizontal and vertical emitters, respectively. The weight parameter S provides an estimate for which orientations are contributing most of the signal or, in other words, which orientations are actually observed. Figures 3.9b and 3.10b show that strong changes in S occur in the vicinity of the optical antennas. In an ensemble it is thus in general not straightforward to determine which subset of emitters is observed, which complicates the comparison to a reference measurement and the interpretation of the results.

As an example, consider the case of a horizontal antenna on a substrate, figures 3.4b and 3.10b. The emission far from the antenna is used as a reference measurement for the emission close to the antenna. S is mostly negative close to the antenna, indicating that vertical emitters are preferentially observed. For the reference far from the antenna S is positive and horizontal emitters

contribute most of the signal, figure 3.10b. Two different subsets of emitters are thus compared. If we are interested for example in the excited state lifetime, these two different subsets have different natural lifetimes near an interface even without antenna. As a result the interpretation of lifetime changes is not directly clear. A similar analysis applies to the vertical antenna with a high NA objective, figure 3.9b, and to other properties such as the angular emission including spectra and polarization.

For an ensemble measurement, full calculations that take into account the complete experimental conditions, i.e. including the illumination and collection, are thus required in order to quantitatively interpret any result. This is not the case for experiments on single emitters; measurements of intrinsic quantities such as the angular emission/excitation, spectrum, polarization and lifetime of a single emitter are naturally independent of the absolute fluorescence intensity, section 1.2. If in addition the emitter can be moved around controllably, as in the experiments presented in this chapter, a clear reference measurement is trivially established and changes in the emission properties are directly observed.

3.4 Localization of the emitter by imaging

Because the antenna dominates the angular emission of the coupled emitter-antenna system, any observation of the emission will reflect mostly the properties of the antenna. This section demonstrates theoretically that if we form an image of the antenna-emitter system in a microscope, we in fact "see" the antenna position, not the emitter position.

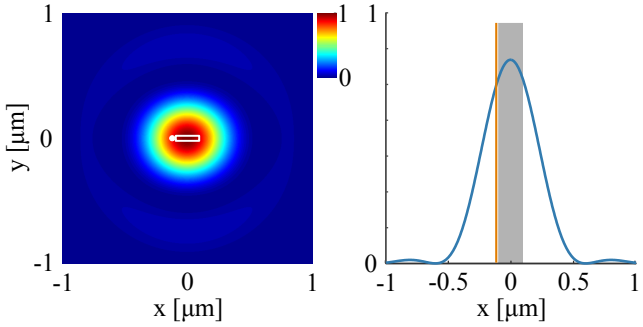

Figure 3.11: **Imaging of an antenna coupled emitter.** Calculated image (0.86 NA air objective) of an emitter placed 10 nm from the left end of a resonant gold antenna with a length of 190 nm, in vacuum. The emission wavelength is 826.6 nm. The emitter is placed on, and oriented along, the antenna axis. The image is centered (approximately) on the antenna (white rectangle in the 2D image and grey area in the cross section), not on the emitter position (white dot in the 2D image and orange line in the cross section). The x-cross section is taken for $y = 0$.

Figure 3.11 shows a calculated diffraction-limited real-space image of an emitter coupled to a resonant antenna. The image was calculated using the angular spectrum representation [84, 103, 104]. The emitter was placed at the

end of the antenna, on the antenna axis and oriented along that axis. Clearly, the image is centered on the antenna, and not on the position of the molecule. In fact, the emitter position is not easily deduced from the image.

This observation provides a challenge to recent experiments that use localization microscopy to map localized fields at nano-structures [108]. In localization microscopy the position of an emitter is determined with nanometer precision by fitting the image to the known point spread function (PSF) of the microscope in a simple or homogeneous environment [95–97]. By repeatedly observing a single emitter at the time, a sub diffraction limited image can be constructed. Near an antenna, or other particle or inhomogeneity, however, this idea cannot be simply applied, as demonstrated by figure 3.11 for which fitting of a standard PSF would yield the position of the antenna, not the emitter. In other words, if we consider the antenna part of the imaging system, the point spread function is unknown and depends non-trivially on the emitter position.

The uniqueness of the electromagnetic field ensures that the information about the emitter position is contained in the emitted field. This information is, however, hidden in the subtle details of the image. For example the profile in figure 3.11 is slightly asymmetric. Thus, a type of deconvolution could in theory be used to determine the emitter position but might require detailed a-priori knowledge of the antenna geometry and the emitter-antenna interaction that one set out to measure.

In the experiments presented in this thesis, these considerations play no direct role because the emitter is precisely and controllably scanned so that its (relative) position is independently determined. In that way spatial maps of locally enhanced fields at nano-structures can be obtained with nanometer resolution, as in figure 2.6.

Conclusion

If an emitter is placed at the right position, and if the antenna is tuned to resonance, then the antenna determines the angular emission, regardless of the emitter orientation. This result provides a direct experimental demonstration of the working mechanism of optical antennas; the emitter near-field couples to the antenna mode (enhancing emission rates), which in turn couples to radiation and determines the angular emission.

The fact that the antenna mode determines the emission properties has several implications. It implies changes in collection efficiency which complicate the interpretation of ensemble measurements. It also complicates the determination of the position of the emitter. But, maybe more importantly, it provides an opportunity and a clear guideline to design antennas to beneficially tailor the emission of single quantum emitters.

The next chapters exploit this fact. In chapter 4, I discuss the highly directional emission from a single quantum emitter by coupling to an optical Yagi-Uda antenna. Chapter 5 studies the emission of single emitters coupled to higher order antenna modes.

Associated publications

This chapter is based on:
[11] T. H. Taminiau et al., Nature Photon. 2, 237 (2008).
[109] T. H. Taminiau et al., New J. Phys. 10, 105005 (2008).

CHAPTER 4

Optical Yagi-Uda antennas

It is desirable for an antenna to have a high directivity, because this enhances the interaction with a directed set of radiation modes, and therefore facilitates effective excitation and collection. The antennas and emitters considered in the previous chapters all emit an approximately dipolar pattern with a low directivity. This chapter discusses a directional multi-element Yagi-Uda antenna.

We show by numerical calculations that the antenna enhances excitation and emission rates, due to the near-field coupling to the resonant feed element, and simultaneously strongly directs the emission, due to the passive elements surrounding the feed. We corroborate the latter prediction with experimental results.

This increased antenna directivity results in an increased enhancement of the excitation rate from the angle of high directivity, as well as the emission rate into that angle, despite the extra loss introduced by the passive elements. We use the reciprocity theorem to derive a relation between excitation and emission rates that explains the above results and gives fundamental insight in the role of the directivity in creating strong local fields and enhancing excitation rates.

The Yagi-Uda antenna increases the collection efficiency for low numerical apertures, and provides a way to further enhance excitation rates. This improved control over the interaction of light and matter shows the potential of Yagi-Uda antennas to effectively communicate light to, from, and between quantum emitters.

This chapter contains four sections. The first section introduces the concept of (optical) Yagi-Uda antennas and the specific design considered here. Section 2 shows that the emission is highly directed and can be aimed in any direction. Section 3 demonstrates that the excitation and emission rates are enhanced and relates these rates by reciprocity. Finally, section 4 summarizes our experimental realization of the theoretical predictions in this chapter.

4.1 Introduction

The Yagi-Uda antenna is a common directional radio and television antenna. A high directivity is achieved by placing several passive scatterers around an actively driven resonant feed element [110, 111]. On one side of the feed, the scatterers are slightly capacitive detuned, these are called the directors. The elements on the other side, the reflectors, are detuned inductively. The resulting interference of the scattered waves creates a beam directed towards the side of the directors.

To use this principle of directed emission in optics, it has been proposed to place an emitter in an array of properly tuned nano-particles [54, 112]. In those schemes the active feed element of the Yagi-Uda is replaced by a dipolar optical emitter. Although a directed beam was indeed predicted, one of the prime advantages of optical antennas, the strong modification of transition rates by a near-field coupling to a resonant element, is lost in such schemes.

Here we show by numerical calculations that a complete nano-optical Yagi-Uda antenna, including a resonant feed element, simultaneously enhances transition rates and achieves high directionality. In addition, I will shortly discuss our experimental realization of such a nano-optical Yagi-Uda antenna.

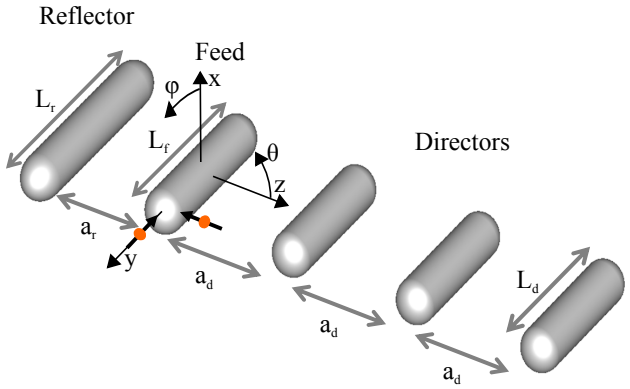

Figure 4.1: **Overview of the Yagi-Uda antenna.** For an operating wavelength of $\lambda_0 = 570$ nm and an aluminum antenna ($\epsilon_r = -38.0 + i10.9$) in free space and with elements with a radius of 20 nm, the feed element is resonant for $L_f = 160$ nm. The director length (L_d) is $0.9L_f$, the reflector length (L_r) is $1.25L_f$. The director spacing (a_d) is $\lambda_0/4$, the reflector spacing (a_r) is $\lambda_0/4.4$. Two dipole emitter orientations (y and z) and the positions where they effectively couple to the feed element are shown.

The antenna design

Figure 4.1 shows an overview of the Yagi-Uda antenna considered here. The antenna consists of 5 cylindrical elements (1 feed, 1 reflector and 3 directors) with hemispherical ends, and with a radius of 20 nm. We choose aluminum for its significant scattering cross section at the chosen wavelength (570 nm) and element radius (20 nm). The principles discussed here are, however, generally

valid. Depending on the operation wavelength other materials, such as gold or silver, give similar but quantitatively different results. In fact, the experimental demonstration discussed in section 4.4 uses gold Yagi-Uda antennas at a wavelength of 800 nm.

The length and the spacing of the antenna elements were optimized as follows. First, standard parameters for a 5-element Yagi-Uda antenna with thin elements of a perfect electrical conductor (PEC) were taken [110]. Next, the change in the dipolar resonance length of the feed element for a realistic radius (20 nm) and material (aluminum) was calculated. Then, all element lengths were scaled by the same scaling factor while keeping the spacing constant. Finally it was certified that the new parameters are indeed a (local) optimum for the directivity.

For the emission calculations, a dipolar emitter was used as a source. The emitter was coupled to the feed element by placing it at a point of high electric mode density at the one of the extremes of the feed element. Due to the near-field coupling, emitters of all orientations can couple to the feed element, but do so at different positions. The respective positions for the two orientations I will discuss here are shown in figure 4.1. For the calculations of the excitation field the antenna was illuminated by plane waves and the field at the position of the emitter was evaluated.

4.2 Enhanced directivity

In chapter 3 we found that the angular emission of an emitter coupled to an antenna mode is determined by the antenna. This section exploits that concept by showing that the angular emission of a dipole emitter coupled to the optical Yagi-Uda antenna is highly directed, and can be aimed towards an arbitrary direction. It is illustrative to distinguish two cases: an emitter oriented parallel to the feed element, and one oriented perpendicular to it.

Parallel emitter

Figure 4.2 shows the angular directivity $D(\phi, \theta)$ for a dipolar emitter oriented along the y-axis, i.e. parallel to the antenna elements. Three situations are considered: the free emitter without antenna, the emitter coupled to a dipole antenna and the emitter coupled to the Yagi-Uda antenna.

The dipole antenna is simply the feed element alone and is included as a reference situation. The radiation pattern for the emitter coupled to the dipole antenna is similar to the free emitter, figure 4.2 c and d. The maximum directivity D is slightly higher for the dipole antenna (1.7 compared to 1.5), and the emission pattern is slightly asymmetric because the symmetry is broken by the antenna.

The emission of the same emitter coupled to the Yagi-Uda is strongly directed along the $+z$-axis, figure 4.2. The maximum directivity D is 6.4, which is 3.8 times higher than for the dipole antenna, figure 4.2 c and d. For an ideal lossless PEC antenna, D is an additional factor 2 higher (not shown), in accordance with typical values for radiowave 5-element Yagi-Uda antennas [110]. The high directivity obtained shows that the Yagi-Uda concept is valid for realistic dimensions and materials in the optical domain. These results are in

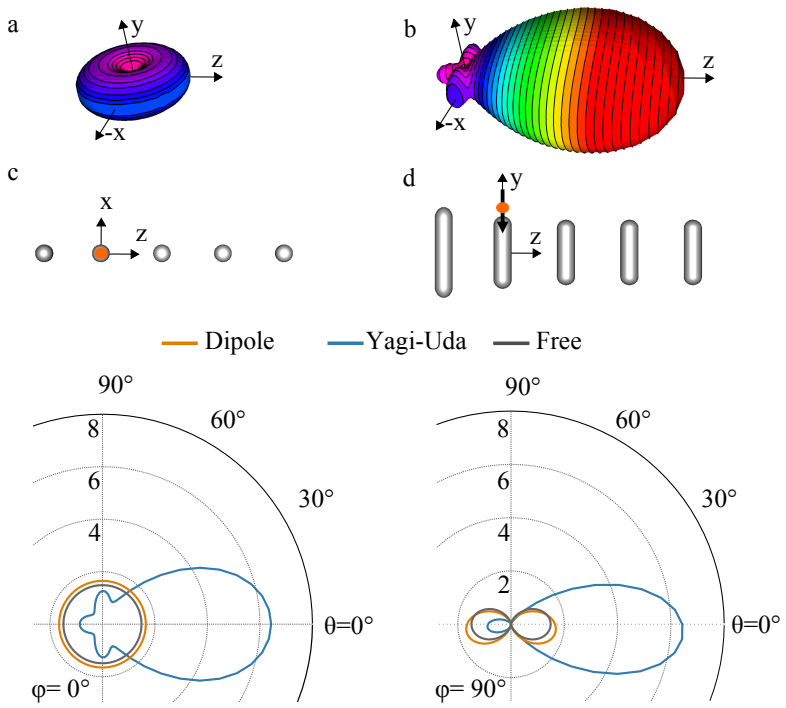

Figure 4.2: **Directional emission with an optical Yagi-Uda antenna.** Emission for a y-oriented dipolar emitter without antenna, coupled to a dipole antenna and coupled to the Yagi- Uda antenna. (a) and (b) show the three dimensional radiation patters for the free dipole emitter and the Yagi-Uda antenna respectively. (c) and (d) show the directivities $D(\phi, \theta)$ in the two major planes for all three cases. The schematics show the location of the emitter and the orientation of the emitter and Yagi-Uda antenna relative to the image plane. The distance between the emitter and the antenna element is 4 nm. The angular emission of the emitter coupled to the Yagi-Uda antenna is highly directed.

agreement with results obtained by coupled-dipole theory under a point-dipole approximation [54].

Perpendicular emitter

The near-field nature of the coupling allows any dipole orientation to be coupled to the antenna. Figure 4.3 shows the angular emission for a dipolar emitter oriented along the z-axis, i.e. perpendicular to the antenna elements, with and without Yagi-Uda antenna. Without the antenna this emitter does not emit along the along the z-axis at all. When coupled to the antenna the emission is directed mainly in the z-direction. The emission is thus both highly directed and rotated by 90° compared to the free dipole. The rotation is a result of the near-field coupling as discussed in detail in Chapter 3. The directionality is created by the surrounding passive elements. The near-field coupling to

the feed element of the Yagi-Uda antenna thus allows full control of the main direction of emission.

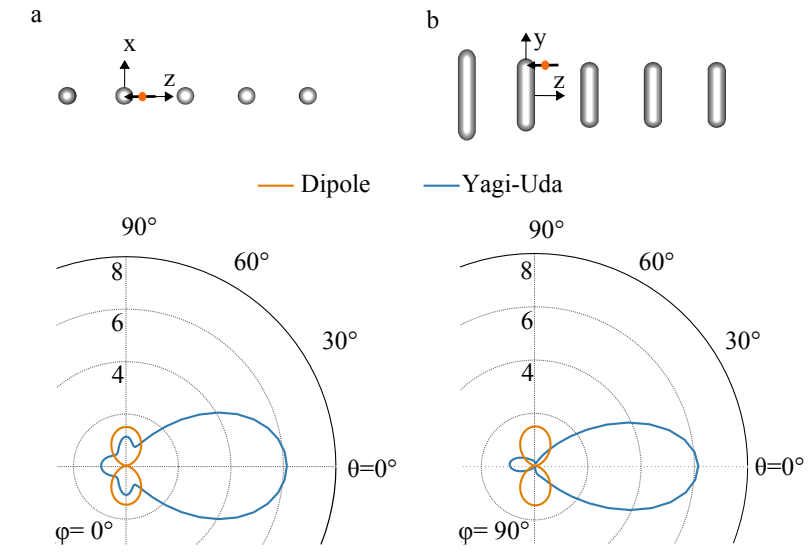

Figure 4.3: **Simultaneous rotation and direction of the emission.** Comparison of the directivity $D(\phi, \theta)$ of a z-oriented emitter with and without Yagi-Uda antenna. The schematics show the position of the emitter (3 nm from the antenna) and the orientation of the emitter and antenna relative to the image planes. The near-field coupling to the feed element rotates the emission by 90 degrees, while the passive elements direct the emission. The final emission is directed into an angle that the emitter itself does not emit into at all.

Note that the angular emission in figure 4.3 is very similar to the emission for the y-oriented emitter coupled to the Yagi-Uda (figure 4.2), as is expected because the angular emission is mainly determined by the antenna mode.

4.3 Enhanced transition rates

In addition to the increased directivity due to the passive elements, the near-field coupling to the resonant feed element enhances the emitter transition rates. This section discusses the changes of the transition rates by coupling to the Yagi-Uda antenna, and compares the results to the rate enhancements for a dipole antenna. The results show that, like a dipole antenna, the Yagi-Uda antenna enhances both excitation and emission rates. Moreover the increased directivity provides a way to further enhance the excitation rate. Although

the high directivity comes at the expense of additional losses, these losses are outweighed by the benefits of the directivity. We explain these observations by deriving a relation between the emission and excitation rates using the reciprocity theorem.

Excitation and emission rates

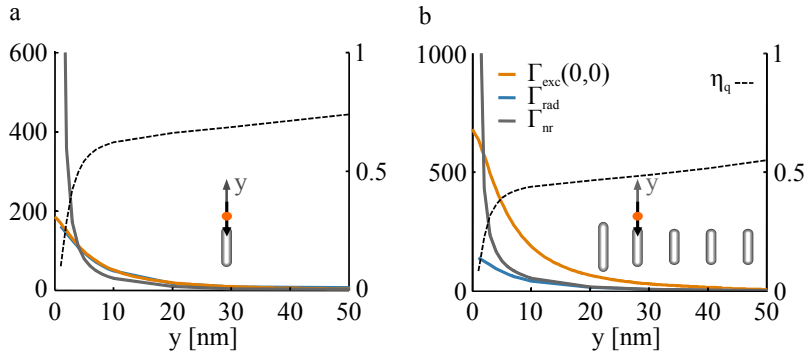

Figure 4.4: **Enhanced excitation and emission rates.** The distance dependence of the excitation $\Gamma_{exc}(0,0)$, radiative Γ_{rad}, and non-radiative Γ_{nr} rates and the quantum efficiency η_q, for a y-oriented dipole coupled to (a) a dipole antenna and to (b) a Yagi-Uda antenna. The insets show the position and orientation of the emitter relative to the antennas. The near-field coupling to the antennas enhances all rates. The high directivity of the Yagi-Uda antenna provides an additional enhancement of the excitation from the forward direction.

Figure 4.4 shows the enhancement of the transition rates for a dipole antenna and for the Yagi-Uda antenna. The radiative decay rate Γ_{rad} and the non-radiative rate Γ_{nr} are taken relative to the radiative rate for the emitter without antenna. The excitation rate $\Gamma_{exc}(0,0)$ for a y polarized plane wave traveling in the negative z direction is taken relative to the excitation rate for the emitter without antenna. This excitation direction and polarization are expected to be close to optimal for the free emitter, for the dipole antenna, and for the Yagi-Uda antenna.

For the dipole antenna, $\Gamma_{exc}(0,0)$ is enhanced up to a factor 200 for very short distances, due to the locally enhanced field. Γ_{rad} follows almost exactly the same curve as $\Gamma_{exc}(0,0)$. This similarity will be explained below using the reciprocity theorem. For Γ_{nr}, there are two types of contributions: losses of the antenna mode and losses due to the field induced directly in the metal by the dipole. The latter causes the steep increase of Γ_{nr} at short distances, which results in a strong decrease of the quantum efficiency η_q (quenching). The strong distance dependence of all rates demonstrates the local nature of the coupling to the antenna.

For the Yagi-Uda antenna the most striking result is the enhancement of $\Gamma_{exc}(0,0)$ by a factor of more than 3 compared to the reference dipole. This enhancement of the excitation rate originates from the increased directivity of the Yagi-Uda antenna in the direction under which the antenna is illuminated

($\phi = 0$, $\theta = 0$). By reciprocity the antenna works both in emission and reception; a high directivity implies an enhanced emission in a certain direction, and also an enhanced excitation from that direction.

Losses and gain

The parasitic elements introduce extra losses. These losses results in an increase of Γ_{nr} and a slight decrease of Γ_{rad}, and therefore a decrease in quantum efficiency η_q. These additional losses partly counteract the benefits of the higher directivity. To answer the question what the improvement in the actual emission of the Yagi-Uda antenna over the dipole antenna is, we consider two limiting cases: low excitation powers far from saturation, and high saturating powers.

For low powers the emission-side contribution to the detected signal is proportional to the product of the collection efficiency η_c and the quantum efficiency η_q. The high directivity of the Yagi-Uda antenna can increase the collection efficiency. If we consider the detection of plane waves, or simply a very small NA, then the collection efficiency is directly proportional to the directivity, section 1.2. The relevant figure of merit in this case is thus the product of the efficiency and the directivity, i.e. the gain G:

$$G(\phi, \theta) = \eta_q D(\phi, \theta). \tag{4.1}$$

The maximum gain for the dipole emitter without antenna is 1.5 (a directivity of 1.5 and an intrinsic quantum efficiency 1), figure 4.5. The gain for the emitter coupled to the dipole antenna is mostly lower than the gain for the emitter itself; the dipole antenna does not direct the emission much, but it does introduce losses. For the Yagi-Uda antenna, the gain is generally enhanced compared to both the emitter itself and to the dipole antenna. The enhancement of the directivity outweighs the extra losses due to the passive elements. Therefore, the Yagi-Uda antenna does not simply filter certain directions by absorption, but concentrates the emission into a directed beam.

For saturating excitation powers the detected signal is proportional to the emission rate into the detection direction. The relevant quantity is then product of the radiative decay rate Γ_{rad} and the directivity $D(\phi, \theta)$. Due to reciprocity the enhancement of this quantity is mathematically the same as the enhancement of the excitation (see also section 3.3), which is already plotted in figure 4.4. Clearly, the excitation rate in the forward direction for the Yagi-Uda is enhanced compared to the dipole antenna. Therefore, the increased directivity outweighs the small decrease in Γ_{rad} when placing the passive elements. The maximum number of photons emitted in the forward direction is thus increased by the passive elements.

Relating the excitation and emission rates by reciprocity

When placing an antenna near an emitter the excitation and emission rates are altered. The changes of both these rates are related to each other by the reciprocity theorem. The enhancement of the emission rate into a certain angle and polarization is equal to the excitation rate enhancement for illumination by a plane wave under the same angle and with the same polarization. Mathematically this statement is described as [55]:

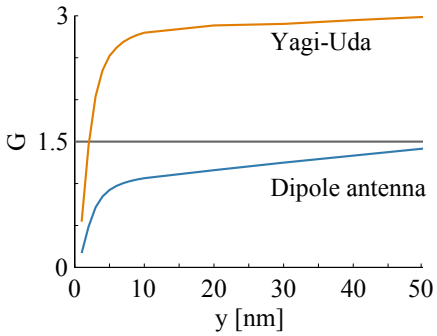

Figure 4.5: **The Yagi-Uda antenna provides increased gain.** The maximum of the angular gain G as a function of the distance of the emitter to the antenna or the antenna feed element. The gain for the dipole antenna is generally lower than the value for the emitter itself, for which $G = 1.5$. The Yagi-Uda antenna does provide a higher gain for most antenna-emitter distances. Very close to the antenna the emission is quenched and the gain diminished.

$$\frac{\Gamma_{exc}(\phi,\theta)}{\Gamma_{exc,0}} = \frac{D(\phi,\theta)}{D_0}\frac{\Gamma_{rad}}{\Gamma_{rad,0}}, \tag{4.2}$$

in which the subscript 0 marks the reference situation. This reference can be freely chosen and $\Gamma_{exc,0}$, and D_0 could be chosen to be functions of ϕ and θ. In this chapter we used a dipole in vacuum and the emission/excitation under/from the angle perpendicular to the dipole moment as a reference, i.e. $D_0 = 1.5$. Equation 4.2 assumes that the excitation and emission occur at the same wavelength, and that the excitation rate is calculated for plane-wave excitation with a polarization equal to the emission polarization. The equation can be adapted for arbitrary polarization and illumination. We have given a more general and detailed derivation, which was reproduced in reference [13].

The relation between the emission and the excitation rates in equation 4.2 gives an explanation for the results of figure 4.4. For the dipole antenna the angular emission and directivity are relatively unchanged $D(0,0)/D_0 \approx 1$ (figure 4.2), so that the enhancements of the excitation rate $\Gamma_{exc}(0,0)$ and the emission rate Γ_{rad} are nearly equal (figure 4.4a). For the Yagi-Uda antenna the directivity is strongly enhanced, so that the excitation rate is enhanced by an additional factor $D(0,0)/D_0$ compared to the emission rate (figure 4.4b).

In general, equation 4.2 shows that there are two ways to obtain high excitation rate enhancements, i.e. high electric field enhancements, for plane waves: by a high radiative decay rate or by a high directivity. A high radiative decay rate implies a high total density of radiative states, whereas a high directivity redistributes these states in angle/momentum so that they are effectively used by the excitation.

Importantly, equation 4.2 implies that the excitation and emission rate enhancements are not usually equal, even though this is often assumed [45, 113]. The enhancements are only generally equal if the angular emission does not change at all upon placement of the antenna. This is a stringent criterium that is only generally met if the system is small enough (quasistatic) so that

only dipole terms contribute to the emission, and if the system satisfies a set of symmetry requirements so that only parallel dipoles can be induced. An example of a system that satisfies these requirements is a small sphere with a dipole emitter oriented either parallel or perpendicular to the line connecting the center of the sphere with the emitter position. This example has been previously identified by Bharadwaj et al. following a different reasoning [114].

4.4 Experimental demonstration

The experimental corroboration of the theoretically predicted behavior of the Yagi-Uda antennas in the previous sections requires the realization of a nano-optical Yagi-Uda antenna and the precise placement of a quantum emitter at the end of the feed element. In a project headed by A. G. Curto, we have fabricated such antenna-emitter systems and have experimentally verified that the emission of a single emitter becomes highly directed by coupling to an optical Yagi-Uda antenna [12]. This section summarizes a few results from those experiments and demonstrates that these results corroborate the theory outlined in this chapter. I refer to A. G. Curto et al. for further details [12].

We fabricated gold optical Yagi-Uda antennas placed on a glass sample with single quantum dots (CdSeTe/ZnS, polymer coated, Invitrogen, Qdot 800 ITK) positioned at the ends of the feed elements. The fabrication process consists of two electron-beam lithography steps and a selective chemical functionalization. The antennas were created by the first electron-beam lithography step combined with the thermal evaporation of a 30 nm layer of gold and a subsequent lift-off of the resist. The second lithography step exposes only a 70×70 area of the end of the feed element to a functionalization by a self-assembled monolayer of mercapto-undecanoic acid (MUA). After activation with carbodiimide (EDC), the quantum dots were covalently bound to the MUA functionalized regions and the remaining resist was removed by a standard lift-off protocol. The resulting number of quantum dots at each antenna is typically 1-3, as determined from the observed antibunching.

Figure 4.6 shows the experimental and theoretical angular emission of a quantum dot coupled to one of the optical Yagi-Uda antennas. The measurements are images of the back focal plane of the objective (NA= 1.46) used to collect the emission through the glass sample [107]. The theoretical calculations were adapted to include the objective and the fact that the antennas are placed on the glass-air interface of the sample. Such back focal plane measurements are images of the angular emission in momentum coordinates. The outer circle in the images is given by the limit of the NA of the objective, which captures nearly the complete emission into the sample half space.

The emission of the quantum dot is split up in three spectral parts using filters. For wavelengths longer than 830 nm all the emission is concentrated in a narrow momentum range, which means that the angular emission is highly directed. This result thus demonstrates the unidirectional emission of a single quantum dot by coupling to an optical Yagi-Uda antenna.

The specific Yagi-Uda antenna in figure 4.6 is purposely detuned from the center of the quantum dot emission to a wavelength of around 840 nm. For shorter wavelengths, for which the antenna is detuned, the directional emission vanishes. And, for the shortest wavelengths the emission is even directed

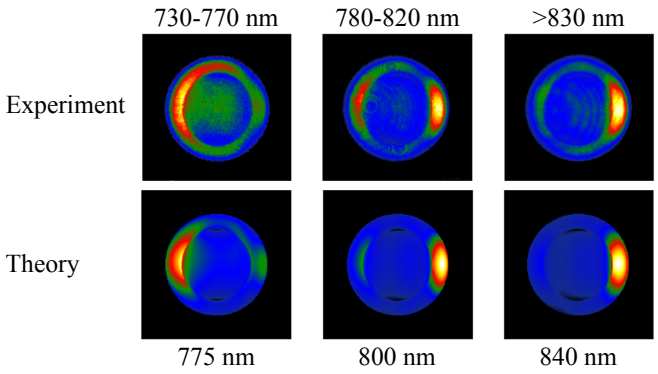

Figure 4.6: **Experimental realization of an optical Yagi Uda antenna.** Angular emission in momentum space for a single quantum dot placed at one end of the feed element of an optical Yagi-Uda antenna. The quantum dot emission spectrum (740-900 nm) is split in three parts with filters. The unidirectional quantum-dot emission, the tuning between forward and backward emission and the good agreement with the calculations corroborate the theoretical predictions made in this chapter. The experiments and calculations are taken from reference [12].

backwards. This tuning behavior is common for Yagi-Uda antennas [110, 115], giving an additional indication that these experiments indeed constitute the realization of a nano optical Yagi-Uda antenna.

The experimentally observed directional emission, the tuning behavior, and the good qualititative agreement of the experimental images with the calculated emission patterns in figure 4.6, all provide experimental corroboration of the theoretical predictions in this chapter.

Conclusion

The optical Yagi-Uda antenna brings enhancement and directionality to the nano scale. It provides a high directivity, it directs the emission in any desired direction, and it enhances both the excitation and emission rates. The increased antenna directivity results in an improved gain, and allows efficient collection of the emission with a small numerical aperture. Additionally, the enhanced directivity further enhances the local electric fields and excitation rates.

We explain this dual role of the directivity by deriving an expression that relates excitation and emission rates by reciprocity. This expression shows that the directivity plays a fundamental role in the control of the emission and absorption of single quantum emitters with optical antennas, which recently made directivity a central topic in, for example: enhanced luminescence [56, 116], local field enhancement [117, 118], surface enhanced Raman scattering (SERS) [119], and the control of emission [120], absorption and scattering [121–124].

Associated publications

[55] T. H. Taminiau et al., Optics Express 16, 10858 (2008).
[12] A. G. Curto et al., Science 329, 930 (2010).

CHAPTER 5

Nano-rod antennas as cavities

Metal nano-rods can be described as cavities for plasmons. If the wavelength of the plasmon in the cavity is known, the resonant modes can be determined. The goal of an antenna is, however, to effectively link an object with radiation. Therefore, to understand nano-rod optical antennas a description of the interaction of the modes with radiation and with a local object is required.

In this chapter, we derive an analytical model for the interaction of dipolar transitions with radiation through nanorod optical antenna modes, by treating nanorods as one-dimensional (1D) cavities. The main idea of the model is that the wavelength in the cavity is given by the waveguide modes of an infinitely-long rod, whereas the reflection coefficient at the antenna ends is determined by the radiation damping of the formed cavity mode.

The obtained analytical model accurately describes all the emission characteristics: the radiative decay rate, quantum efficiency and angular emission. We use the model to quantitatively reveal the continuous evolution of antenna modes from perfectly-conducting antenna theory to quasistatic plasmonics, i.e. from macroscopic to nanoscale antennas. In particular we give an analytical account of the gradual emergence of super-radiant, sub-radiant, and dark modes, as the antennas become increasingly more plasmonic.

The model provides a theoretical framework for nano-rod antennas. The derived results and concepts can be applied to both the emission and excitation of emitters coupled to optical antennas, as well as to scattering problems. Our description is thus valid for the interaction of nanorods with light in general, and might lead to further insights and design rules for optical antennas.

This chapter contains three sections. Section 1 considers the interaction of nano-rod antennas with radiation for the simplified case of negligible losses. Section 2 discusses the other half of the antenna problem: the interaction with a local object, in this case an electric or magnetic dipole transition. Finally, section 3 includes all the loss and source terms and studies the evolution of antenna modes as they become increasingly plasmonic.

5.1 Interaction of lossless antennas with radiation

We first consider the case of lossless nano-rod modes, i.e. we initially neglect both the dissipation and radiation losses. The solutions are then the idealized resonant modes of a cavity. The advantage of this approach is that several insights and general concepts about the interaction of the mode with radiation can be derived in a mathematically concise and straightforward way.

We show that the radiation properties of the modes can be summarized in a phase matching equation, which classifies the modes in three groups: sub-radiant modes, super-radiant modes, and modes that are neither sub- nor super-radiant. The concepts derived here help understand the results obtained for the more complete model that includes losses in section 5.3.

Plasmons on an infinite wire

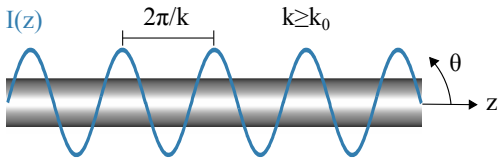

Figure 5.1: **Bound waves on a wire.** A thin infinitely long wire supports a bound plasmon polariton with a wavenumber k which is larger than the wave number in the surrounding medium k_0. We associate a sinusoidal current distribution $I(z)$ to this wave.

Consider a bound wave - a plasmon polariton - on an infinitely long straight thin wire, figure 5.1. We assume that a one-dimensional (1D) sinusoidal current distribution $I(z)$ is associated to this wave:

$$I(z) = \cos(kz), \tag{5.1}$$

in which $\mathbf{k} = k\hat{\mathbf{z}}$ is the wave vector of the plasmon polariton. Because the wave is bound, we have:

$$k \geq k_0, \tag{5.2}$$

in which k_0 is the angular wave number in the surrounding medium, see for example figure 1.4. We will find that most of the radiation properties of the antenna modes are governed by how much larger k is than k_0. To quantify this parameter we define an effective index K:

$$K = k/k_0. \tag{5.3}$$

The value of K gives a measure for how bound the mode is, or in other words how plasmonic it is. The two limiting values for K are $K = 1$, the regime of conventional antenna theory with perfect electrical conductors, and $K >> 1$, for which the mode is extremely bound and quasistatic plasmonics generally applies.

The radiated field created by a 1D current distribution is obtained from:

$$E_\theta = E_0 \int_{-\infty}^{\infty} I(z) e^{-ik_\parallel} dz, \tag{5.4}$$

in which E_0 is the field of a z-oriented unit dipole at the origin. $k_\parallel$ is the wave number parallel to the nano-rod axis, and the angle of emission θ is given by $k_\parallel = k_0 \cos(\theta)$.

In this section, we focus only on the integral expression in equation 5.4, which I will call F:

$$F(k_\parallel) = \int_{-\infty}^{\infty} I(z) e^{-ik_\parallel} dz. \tag{5.5}$$

This integral is proportional to the fourier transform of the current distribution $I(z)$, and determines all the main radiation properties of the system. For the infinitely long wire we obtain:

$$F(k_\parallel) \propto \delta(k_\parallel + k) + \delta(k_\parallel - k), \tag{5.6}$$

in which $\delta(x)$ is the Dirac delta function. Only the momentum vectors with $k_\parallel \leq k_0$ correspond propagating plane waves. Because $k > k_0$, the mode on an infinite long wire does thus not radiate at all (figure 5.3), as expected for a bound mode.

Nano-rod antennas of finite length

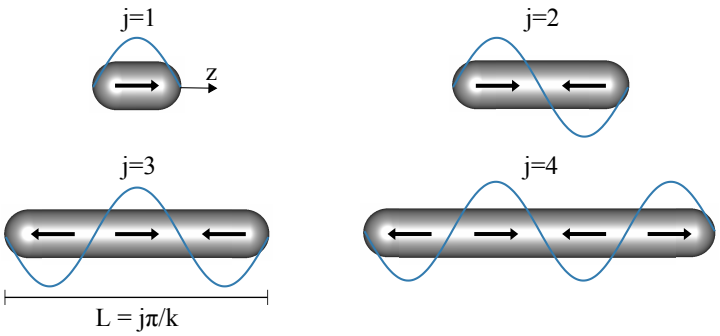

Figure 5.2: **Optical nano-rod antenna modes.** For lossless antennas solutions for $I(z)$ exist only if the length of the rod L satisfies $L = j\pi/k$, with j a positive integer. The current distribution is symmetric for $j = odd$, and antisymmetric for $j = even$.

To create a radiating antenna, a nano-rod has to be truncated. The resulting resonant antenna lengths obey $L = j\pi/k$, with j a positive integer, figure 5.2. With the origin in the center of the antenna we can write:

$$I(z) = e^{ikz} - (-1)^j e^{-ikz}, \tag{5.7}$$

for $-L/2 \leq z \leq L/2$, and $I = 0$ otherwise. The modes with $j = odd$ have symmetric current distributions, $I(z) \propto \cos(kz)$. Modes with $j = even$ have antisymmetric current distributions, $I(z) \propto \sin(kz)$. F now becomes:

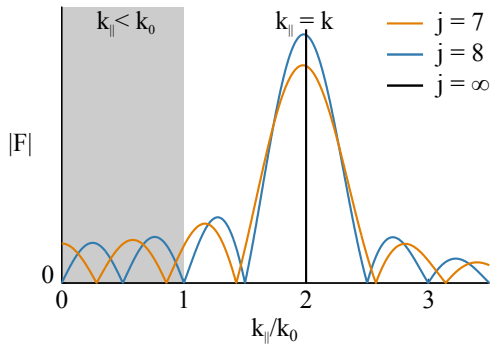

Figure 5.3: **Fourier transforms of the currents for three antennas.** The absolute value of F as a function of the parallel momentum for an infinitely long rod, a rod with $j = 7$ and a rod $j = 8$, for a plasmon wave with $k = 2k_0$. Only values for $k_\parallel$ that satisfy $k_\parallel \leq k_0$ correspond to propagating plane waves. For the infinite wire there is no radiation; the mode is bound. The radiation properties of the finite antennas are determined by the number and the positions of the subsidiary maxima within the shaded radiation zone.

$$F(k_\parallel) \propto \left(\frac{1}{k+k_\parallel} + \frac{1}{k-k_\parallel}\right)\left(e^{ik_\parallel L/2} - (-1)^j e^{-ik_\parallel L/2}\right), \tag{5.8}$$

and takes the form of a sum of cardinal sines, figure 5.3. The first term in equation 5.8 is an envelop function that is independent of j and the length of the antenna. The second term is an sinusoidal function with a period of $4\pi/L$. In the limit of a thin perfectly conducting antenna ($K = 1$), equation 5.8 converges to the standard antenna theory case (chapter 10 of reference [110]).

The number of subsidiary maxima of equation 5.8 that fall within the radiation zone ($k_\parallel \leq k_0$), and their specific positions, determine the radiation properties of the antenna. Importantly, modes with $j = odd$ always have a maximum at $k_\parallel = 0$, whereas modes with $j = even$ always have a minimum for that value. As a result modes with $j = odd$ always have at least one maximum within the radiation zone, whereas for modes with $j = even$ this is not necessarily the case.

The limiting case of very plasmonic antennas

For $K >> 1$, i.e. for very plasmonic antennas, the expressions for the emission can be further simplified. For $K >> 1$, k is much larger than the $k_\parallel$ values that correspond to radiation ($k_\parallel \leq k_0$), so that the following approximation holds (for amplitude terms):

$$k \pm k_\parallel \approx k. \tag{5.9}$$

This approximation is equivalent to approximating the cardinal sine with a sine, for values far from the central maximum. Equation 5.8 now simplifies to:

$$F(k_\parallel) \propto e^{ik_\parallel L/2} - (-1)^j e^{-ik_\parallel L/2}. \tag{5.10}$$

Equation 5.10 is just the function expected for two point dipoles at the antenna extremes. Indeed, the reverse Fourier transform of equation 5.10, yields:

$$I(z) \propto \delta(z + L/2) - (-1)^j \delta(z - L/2), \tag{5.11}$$

which describes two point dipoles placed at the antenna ends. For modes with $j = odd$ these dipoles are in phase, for modes with $j = even$ they are in anti-phase.

Therefore, in the limit of $K >> 1$ the antenna currents can be approximated by two point dipoles at the ends of the antenna. Equation 5.8 thus gives a mathematical basis for the commonly-used intuitive picture of the scattering of the plasmon at the antenna ends [26, 33, 61, 125]. This description is only strictly correct if the mode is very bound ($K >> 1$). Additionally, equation 5.10 indicates that the nano-rod is mathematically similar to the elementary double slit configuration, but with phases and amplitudes fixed by the plasmon wave.

Phasematching

The antenna emission is largely determined by those extrema of equation 5.8 that additionally satisfy $k_{\|} \leq k_0$, which for $K >> 1$ are given by a phase-matching equation:

$$k_{\|} + (m + 1/2)k_L = k. \tag{5.12}$$

This equation follows from equation 5.10, and is depicted graphically in figure 5.4. Here, $k_L = 2\pi/L$ and $m = 0, 1, 2, 3...$ give the different possible solutions to the equation. Although equation 5.12 was derived for $K >> 1$, it is a good approximation for the positions of the extrema that satisfy the radiation condition $k_{\|} \leq k_0$, even for low values of K, for example for $K = 2$ in figure 5.4.

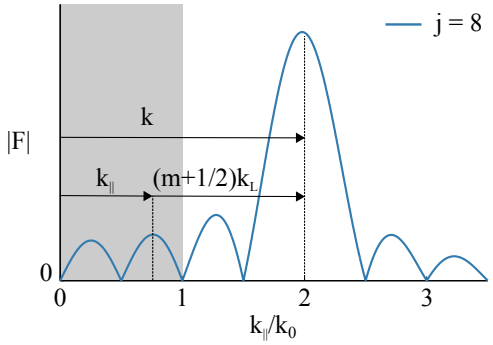

Figure 5.4: **Graphical derivation of the phasematching equation.** The values of $k_{\|}$ for the extrema of F, equation 5.8 are approximately given by the phase matching condition in equation 5.12. The solutions that additionally satisfy $k_{\|} \leq k_0$ give the angles under which the antenna emits and receives radiation effectively.

The number of possible values for m determine the nature of the mode. The values for $k_{\|}$ obtained for those solutions determine the angles θ of maximum interaction with radiation through $k_{\|} = k_0 \cos(\theta)$, i.e. the angles under which the antenna emits and receives effectively.

Sub- and super-radiant modes

Two cases are of special interest: when there are no solutions for equation 5.12 and when there is just one solution.

Only modes with $j = odd$ can result in one solution for equation 5.12. These modes have symmetric current distributions (figure 5.2). If the antenna is small the radiation from some of the current elements will interfere constructively over all angles, and energy is radiated quickly from the mode. I will call such a mode super-radiant. Such a mode is not necessarily stronger or brighter than other modes; the enhanced radiative loss is only beneficial if the total loss from the nanorod cavity is dominated by dissipative losses.

Modes with $j = even$ have anti-symmetric current distributions (figure 5.2). If the antenna is small the radiation from the different current elements cancels in all directions, and equation 5.12 yields zero solutions. The mode then radiates slowly, and I will call it sub-radiant. Note that such a mode is not necessarily weak, or "dark". The slow radiation damping of the mode is only detrimental when other faster dissipative loss channels are present.

Modes that yield two or more solutions are neither sub- nor super-radiant. In this case the antenna is long enough so that constructive or destructive interference never occurs over all angles at the same time. The criterium for a mode with $j = even$ to have at least two solutions is: $Lk_0 > \pi$, which can also be written as $j/K > 1$ or as $L > \lambda_0/2$, with λ_0 the wavelength in the surrounding medium. This condition thus depends only on the length of the antenna compared to the wave vector in the medium, as expected for a diffraction problem. For conventional (not plasmonic) antennas $K = 1$ and sub- and super-radiance play no role, as $j/K \geq 1$ for all values of j.

Angular emission and imaging

The number of solutions for equation 5.12 also determines the main characteristics of the angular emission pattern. All modes that yield zero solutions emit as quadrupoles, regardless of the actual value of j. Likewise, all modes that yield one solution emit as dipoles. Modes with 2 or more solutions emit in multi-lobed patterns with the number and angles of the lobes (approximately) determined by the solutions to equation 5.12.

The angular emission (or the angular excitation) determine the observed image when imaging nano-rods in an optical microscope [61, 126–128]. Modes with zero or one solution are thus always imaged as quadrupoles or dipoles respectively. For a mode with two or more solutions, the image depends on the NA of the objective used, as the possible momentum values are now limited by the NA: $k_{\|} \leq \frac{NA}{n} k_0$, with n the refractive index of the environment. If there are two or more solutions with a momentum within the NA the image is resolved and will resemble two spots at the antenna ends. If there are no solutions or only one solution then the image is a quadrupole or a dipole, respectively. The

condition to obtain two or more solutions within the NA is: $L > \frac{\lambda_0}{2NA}$, which not surprisingly is a statement similar to the Abbe diffraction limit.

Summary

The concepts discussed in this section are summarized in the table in figure 5.5, which classifies the possible modes of optical nanorod antennas in three groups, each with a distinct set of radiation properties.

# of solutions	Parity	Type	If $R_{nr} >> R_{rad}$	Emission	Image
0	j = even	sub-radiant	dark	quadrupole	quadrupole
1	j = odd	super-radiant	bright	dipole	dipole
2 or more	j = either	neither	normal	multiple lobes	depends on NA

Figure 5.5: **Summary of the properties of the different modes.** The modes are characterized by the number of solutions for equation 5.12 that also satisfy $k_{\|} \leq k_0$. The properties in the table are, in order: the parity of the mode for which this number of solutions can occur; the nature of the interaction with the radiation; the relative strength of the mode if the dominant loss term is dissipative (R_{nr}), i.e. if the radiation damping (R_{rad}) is small; the angular emission pattern; the result of forming a real-space image of the mode with an objective.

5.2 Interaction with local sources

The previous section demonstrates several of the properties of the interaction of nanorod modes with radiation. This section discusses the other half of the antenna problem: the interaction of the mode with a local object or source. We consider three sources: an electric dipole, and magnetic dipole and a transmission line. We show that the difference in symmetry of electric and magnetic dipoles implies that they couple to the nanorod modes at different positions. Conventional transmission lines are similar to magnetic dipoles, but the mechanism of feeding energy in the mode is different. As a result dipolar quantum emitters generally drive different modes than those commonly considered for conventional antennas.

Three types of local sources

Figure 5.6 shows the three local sources considered here: an electric dipole, a magnetic dipole and a transmission line.

Electric and magnetic dipoles differ in the symmetry of the induced waves on opposite sides of the dipole. This opposite symmetry of the emission of electric and magnetic dipoles is a general property, and can for example be used to selectively enhance the emission of either type of dipole [50, 129]. The transition rate for an electric dipole depends on the electric mode density,

whereas the rate for a magnetic dipole is proportional to the magnetic mode density.

The transmission line resembles a magnetic dipole in symmetry, but the fraction of the energy fed into the antenna is determined by impedance matching instead [130–132]. Because the design of the transmission line and the connection can be used to tailor the impedance, the coupling of such waveguides to the antenna is generally more flexible than the coupling of a dipole emitter.

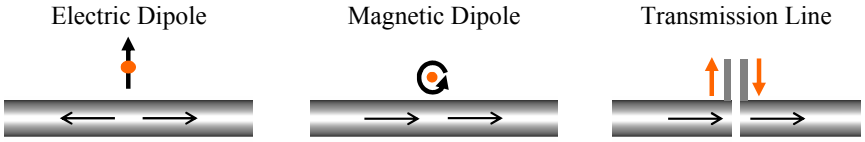

Figure 5.6: **Three different local sources.** Electric dipoles, magnetic dipoles and transmission lines and the symmetry of the induced waves on opposite sides of the source.

Coupling to nano-rod modes

Figure 5.7 shows two sets of possible 1D modes for thin rods. The modes we have considered until now, here named the optical antenna modes, differ from the conventional center-fed antenna modes, chapter 4 of reference [110], in the symmetry of the modes with $j = even$. What modes are effectively excited depends on the properties of the source and on the source position.

First consider the optical antenna modes. The electric dipoles interact strongly with the mode at positions of high electric mode density, i.e. positions with a current minimum (high input impedance). These positions are marked for the $j = 2$ mode in figure 5.7.

The magnetic dipoles couple strongly to the antenna modes at positions of maximum current, where the magnetic mode density is high (low input impedance). The magnetic mode density maxima coincide with the electric mode density minima, and vice versa, which is a direct result of the symmetry difference shown in figure 5.6.

Similar to the magnetic dipole, the transmission line can drive these modes at the positions of maximum current, i.e. at the points of low input impedance. However, in principle the transmission line can couple just as well to the mode at other positions, provided that the input impedance can be matched.

The center-fed antenna modes with $j = even$ can only be driven by the magnetic dipole or the transmission line at the center of the antennas. electric dipole transitions cannot drive modes with this symmetry. Although the magnetic dipole can theoretically drive these modes in theory, the coupling is weak because the current is minimun at the center. For any position other than the center, the magnetic dipole preferentially couples to the optical antenna mode with the opposite symmetry, because that mode is resonantly enhanced. A transmission line or waveguide can drive the center-fed mode effectively, provided that the very high input impedance - infinite for the lossless modes considered here - can be matched.

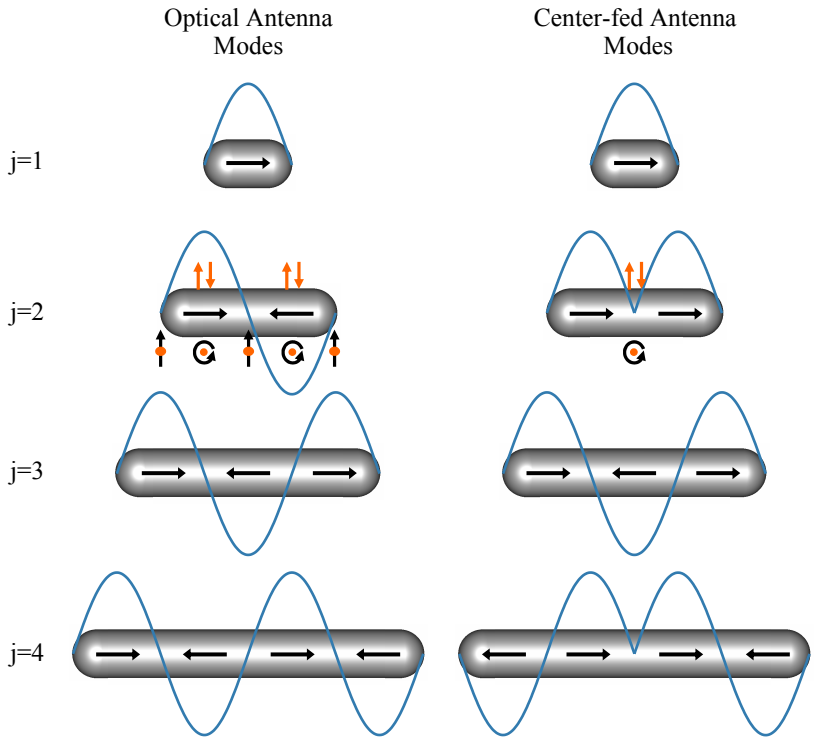

Figure 5.7: **The driving of antenna modes by the various sources** Comparison of the optical antenna modes considered in this chapter and the standard center-fed antenna modes that are usually considered for conventional antennas [110]. The difference between the two sets of modes is the symmetry of the modes with $j = even$. The symbols for the $j = 2$ mode indicate the positions of effective coupling of the three different sources to the mode. The position for the other values of j are equivalent. The center-fed modes can only be driven by the transmission line and the magnetic dipole, but the coupling of the magnetic dipole is very weak because the current minimum at the center. These center-fed modes do not play a significant role for dipolar quantum emitters coupled to optical antennas.

In summary, the dipolar transitions dominantly excite different modes than the center-fed antennas usually considered in traditional antenna theory. Because the current distributions of these modes are different, the emission properties, such as the radiation resistance and angular emission, will be different as well.

5.3 Complete model including losses

We now include dissipation and radiation losses in the simplified model of section 5.1, and combine it with the dipolar sources discussed in section 5.2.

The ohmic dissipation simply implies a complex plasmon wave vector, but the radiation loss is more complicated, and can only be treated approximately.

The challenge is that the radiation acts back on the currents, leading to a set of integro-differential equations that can only be solved numerically. We create an approximate description using the following steps. First we assume a sinusoidal current distribution, and neglect any effects of the radiation. Second we derive how this spatial current distribution radiates, i.e. we calculate the radiation resistance. Third we assume that the created radiation damps the amplitude of the mode but does not significantly alter the spatial distribution of the mode. Finally, because the wave is bound, we assume that the radiation damping is described by a reflection loss at the ends of the antenna.

The resulting model is compared to numerical calculations, and we find that the results accurately describes all the emission properties: the radiation resistance, the radiative and non-radiative decay rates and the angular emission. We study the evolution of these properties as the antennas become increasingly more bound, and in particular discuss the gradual appearance of sub-radiant, super-radiant and dark modes. The results in this section confirm the predictions from the simplified model in section 5.1.

The cavity model

Consider an elongated antenna of physical length L_p with a central section, of constant cross-sectional shape and size, that supports a charge density wave with complex wave vector $\mathbf{k} = k\hat{\mathbf{z}}$:

$$k = k' + ik''. \tag{5.13}$$

The wave is reflected with a reflection coefficient r at both the antenna ends, which form a resonator that we model as a two-mirror cavity of length L, figure 5.8. The model developed applies to any cross-sectional shape, provided that k can be determined.

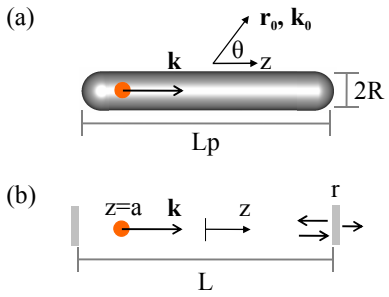

Figure 5.8: **Overview and definitions of the cavity model** (a) The antenna (total length L_p) is a rod of constant cross-sectional shape and size that supports a charge-density wave (wave vector $\mathbf{k}$). Although the ideas derived here are general, we study gold cylindrical antennas with radius R and hemispherical ends, as a concrete example to compare to numerical calculations. (b) We model the antenna as a 1D cavity with length L and amplitude reflection coefficient r. The antenna is driven by an electric or magnetic dipole at position $z = a$.

Resonant modes are expected for physical antenna lengths that are shifted from the multiples of π/k' by a constant value [15, 32, 35]. When modeling the

antenna as a cavity, this displacement can be introduced by a positive phase shift upon reflection [27, 29, 32] or by an extended cavity length [15, 130, 133]. The two corrections give the same resonant length, but are otherwise not equivalent. Here, we choose to set an extended length $L = L_p + L_c$ and a real-valued reflection coefficient r.

Current distribution

To derive the resultant current distribution $I(z, a)$ we again assume a one-dimensional (1D) sinusoidal distribution and do not distinguish between conduction and displacement currents. A superposition in complex notation for time-harmonic waves gives, for $-L/2 \leq z < a$,

$$I(z,a) = \frac{I_0(e^{ika} \pm re^{ikL}e^{-ika})}{1 - r^2e^{2ikL}}(re^{ikL}e^{ikz} - e^{-ikz}), \tag{5.14}$$

and, for $a < z \leq L/2$,

$$I(z,a) = \frac{I_0(re^{ikL}e^{ika} \pm e^{-ika})}{1 - r^2e^{2ikL}}(e^{ikz} - re^{ikL}e^{-ikz}). \tag{5.15}$$

The initial amplitude of the induced wave, I_0, depends on the type of dipole (electric or magnetic), its oscillator strength, and the three-dimensional (3D) configuration and modal fields [38, 133]. Its value is not specified here, and, because all the calculated rates are taken relative to other antenna lengths, none of the presented results depend on it.

The + signs in equation 5.14 and equation 5.15 are for electric dipoles, and the − signs for magnetic dipoles; electric and magnetic dipoles couple effectively to the antenna modes at different positions, a result of the symmetry argument in figure 5.6. The magnetic mode density maxima coincide with the electric mode density minima, similar as for the lossless modes in figure 5.7.

The radiated field

The far field observed at r_0 is again given by equation 5.4:

$$E_\theta = E_0 \int_{-L/2}^{L/2} I(z,a)e^{-ik_\parallel z}dz, \tag{5.16}$$

in which $E_0 = i\eta_0 k_0 e^{ik_0 r_0} \sin\theta/(4\pi r_0)$ is the field of a z-oriented point dipole at the origin, and $k_\parallel = k_0 \cos\theta$ is the parallel component of the wave vector k_0 in the surrounding medium of impedance η_0. The other components of the electric field are zero. After evaluating the integral, equation 5.16 gives:

$$E_\theta = \frac{iI_0E_0}{1 - r^2e^{2ikL}}\Big(A\Big[\frac{re^{ikL}e^{-i(k_\parallel - k)z}}{k_\parallel - k} - \frac{e^{-i(k_\parallel + k)z}}{k_\parallel + k}\Big]_{-L/2}^{a}$$
$$+B\Big[\frac{e^{-i(k_\parallel - k)z}}{k_\parallel - k} - \frac{re^{ikL}e^{-i(k_\parallel + k)z}}{k_\parallel + k}\Big]_{a}^{L/2}\Big), \tag{5.17}$$

in which $A = e^{ika} \pm re^{ikL}e^{-ika}$ and $B = re^{ikL}e^{ika} \pm e^{-ika}$ contain the dependence on the dipole position.

The angular emission in equation 5.17 gives a complete description of the interaction of the antenna with a dipole and with radiation. The equation describes the emission of the dipole through the antenna mode and, by reciprocity (chapter 4), its excitation by radiation. Indeed, by setting $r = 1$, which is equivalent to neglecting radiation damping, the results for the excitation of nano-rods from Fabry-Pérot models [30, 133] can be derived from equation 5.17.

Next, we use the derived model to account for the radiation damping, study the main characteristics of optical antennas in a set of concrete examples, and compare the results to numerical simulations. We show in particular how the antenna characteristics evolve as the modes become increasingly more bound for increasing K, equation 5.3.

Concrete case: cylindrical gold rods

As a concrete case we choose cylindrical gold antennas with hemispherical ends, figure 5.8a. The advantage of cylinders is that semi-analytical waveguide solutions exist [37, 38, 134]. We study three radii, $R = 20, 10$ and 5 nm, which lead to three different values for K for the TM_0 modes [15, 38], see for example figure 1.4. The antenna length L is varied for a constant wavelength. As a source, we choose an electric dipole at the antenna end, because it effectively excites all relevant resonant modes (see figure 5.7). The dipole source in the 1D model is placed at the end of the extended cavity length: $a = -L/2$.

Radiation damping

We first neglect the effect of the radiation damping on the current distribution by setting $r = 1$, and study the radiation damping by means of the radiation resistance, which we define as [130]:

$$R_{rad} \equiv 2P/I_{max}^2. \tag{5.18}$$

P is the total emitted power obtained by integrating the emitted far field given by equation 5.17, and I_{max} is the maximum of $|I(z)|$, equations 5.14 and 5.15. The radiation resistance gives the radiation damping per unit amplitude in the resonator; it is independent of the total amplitude and is a characteristic of the spatial distribution of the mode. After studying the radiation resistance, we will account for the effect of the radiation damping on the amplitude of the mode by relating the reflection coefficient r to the radiation resistance.

The evolution of the radiation resistance with increasingly bound modes is illustrated in figure 5.9, which shows R_{rad} as a function of L for the three optical antennas, together with the limiting cases of $K = 1$ (thin perfectly-conducting antenna), and large K (quasistatic limit). We make the following three initial observations. First, the radiation resistance for the modes excited by electric dipoles at $a = -L/2$ differ from the results for transmission-line center-fed antenna modes [110], because the modes excited have different symmetry for even values of j, figure 5.7. Magnetic dipoles at $a = 0$ do reproduce the results for center-fed perfectly-conducting [110] ($K = 1$) and carbon nano-tube [131] ($K = 100$) antennas. Second, unlike for $K = 1$, the radiation resistance for optical antennas does not increase with increasing length; the waves are bound.

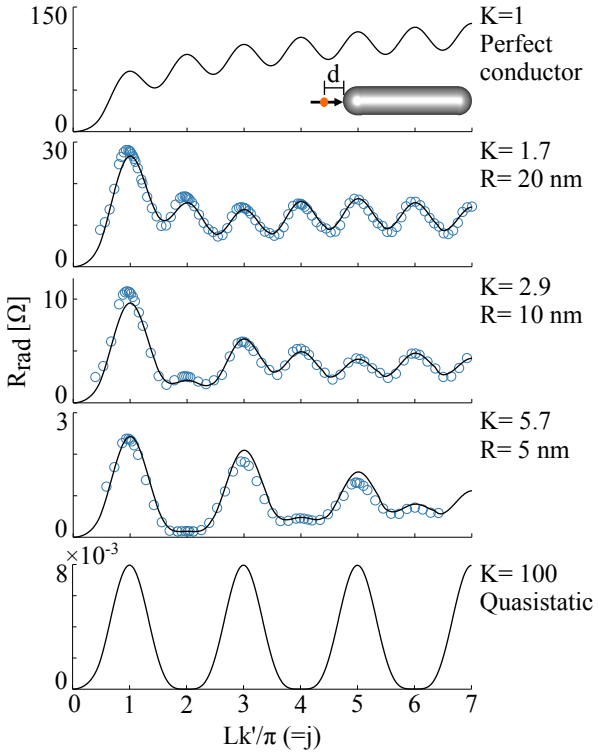

Figure 5.9: **The radiation resistance.** Evolution of the radiation resistance $R_{rad}(L)$ for increasingly bound antennas, i.e. increasing K. The optical antennas ($K = 1.7, 2.9$ and 5.7) are intermediate cases between the limits of perfect electrical conductors ($K = 1$) and quasistatics ($K = 100 >> 1$). Resonant modes occur if $Lk'/\pi = j$, with j a positive integer. Lines: 1D model. Circles: 3D Numerical calculations for cylindrical gold antennas in vacuum, figure 5.8. **Parameters:** $\lambda_0 = 826.6$ nm. *3D Numerical*: $\varepsilon_{au} = -29 + 2.0i$. Electric dipole at $d = (5, 2.5, 1.25)$ nm for $R = (20, 10, 5)$ nm respectively (see inset). *1D model*: Electric dipole at $a = -L/2$ and $r = 1$. For $K = 1$ and $K = 100$, $k'' = 0$. For $R = 20, 10$ and 5 nm: $k/k_0 = 1.7{+}0.045i, 2.9{+}0.11i$ and $5.7{+}0.23i$, and $L_c = 54, 26$ and 12 nm.

Third, the radiation resistance decreases with increasingly bound modes, i.e. increasing K.

Sub- and super-radiance

Modes with $j = odd$ and $j = even$ evolve differently with increasing K. The radiation resistance of even modes diminishes with increasing K. As discussed in section 5.1, these modes have anti-symmetric current distributions, no net dipole moment and become sub-radiant if $j/K < 1$; opposite-oriented current elements cancel and the radiation resistance tends to zero. Odd modes behave oppositely, and evolve into super-radiant modes with high radiation resistance.

For example, for $R = 20$ nm and $K = 1.7$, the $j = 1$ mode gives $j/K < 1$

and is expected to be super-radiant. Indeed, the radiation resistance of this mode is increased compared to the other modes, which are neither sub- nor super-radiant. For higher K the antennas are relatively smaller and more modes become sub- or super-radiant. For $K = 5.7$, $j/K < 1$ for $j = 1..5$, so that the $j = 1, 3, 5$ modes are super-radiant and have an increased radiation resistance, and the $j = 2, 4$ modes are sub-radiant with a diminished radiation resistance. For $K = 100$ all lower order odd modes are super-radiant, all even modes sub-radiant.

Reflection coefficient

Because of super- and sub-radiance, the radiation damping is different for the different modes. Clearly, the radiation resistance depends on the antenna length L. A nanorod is therefore *not* a simple Fabry-Pérot cavity. Because the wave is bound, the radiation damping is most naturally taken into account through the reflection coefficient r, which means that the reflection coefficient r is a function of the antenna length L. This surprising conclusion implies that the reflection coefficient is not locally determined by the properties of the antenna termination. Because the light radiated from both antenna ends interferes, the reflection depends on the distance between the ends and the relative phase of the scattered waves. If this interference is destructive, less light is scattered (sub-radiance), and thus more light must be reflected back into the nano-rod cavity.

We relate r to the radiation resistance:

$$r(L) = \frac{Z - R_{rad}/2}{Z + R_{rad}/2}, \tag{5.19}$$

in which Z is the real part of the antenna wave impedance, and is determined from the waveguide solutions (i.e. considering an infinitely long rod) as:

$$Z = 2 \int \mathbf{S} \cdot d\mathbf{A} / | \int \mathbf{J} \cdot d\mathbf{A}|^2, \tag{5.20}$$

in which $\mathbf{S}$ is the time-averaged Poynting vector, $\mathbf{J}$ is the current density, $d\mathbf{A}$ is oriented along the rod axis, and both integrals are over an infinite plane perpendicular to the nano rod axis. r approaches unity for large K (small radius R).

Equation 5.19 takes the form of an impedance matching equation, and was obtained by equating the reflection loss in the cavity model with the radiation by the antenna. It relies on three arguments. First, all radiative loss is due to reflection, because the plasmon wave is bound. Second, the dissipation is small so that I_{max} is an approximate measure for the currents at all positions. Third, equation 5.19 introduces small deviations of r from unity. These small changes can strongly affect the amplitude of the current distribution if the dominant damping is radiative, but they do not significantly affect the spatial distribution, so that the calculation of R_{rad} with $r = 1$ remains accurate. For the antennas considered here the minimum value obtained for r is 0.79, which occurs for the $j = 1$ mode of the $R = 20$ antenna for which R_{rad} is high.

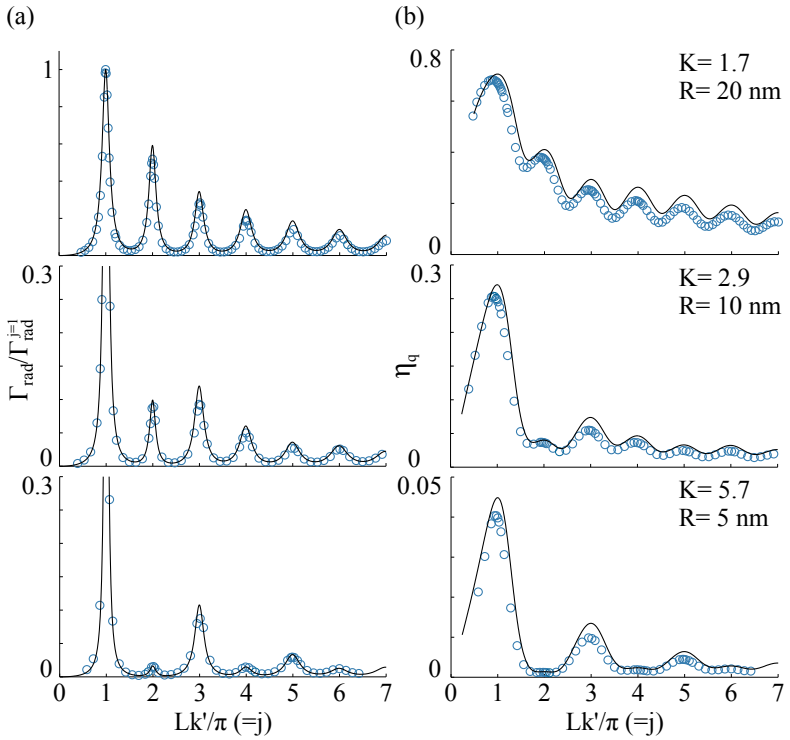

Figure 5.10: **Radiative transition rates and quantum efficiency** (a) The radiative transition rate Γ_{rad} relative to the rate for $j = 1$ and (b) the quantum efficiency η_q for the three optical antennas. All parameters as in 5.9, but r from 5.19 with $Z = 130.4, 219.4$ and $414.8\ \Omega$.

Rates and efficiencies

With the radiation damping taken into account, the radiative transition rate Γ_{rad} ($\propto P$) and the quantum efficiency η_q can be compared quantitatively between the different resonant modes, figure 5.10. The quantum efficiency η_q is given by the balance between radiative and dissipative (Γ_{nr}) rates: $\eta_q = \Gamma_{rad}/(\Gamma_{rad} + \Gamma_{nr})$. Here, the intrinsic efficiency of the dipole emitter is taken as unity. The constant non-resonant dissipation due to the proximity of the dipole to the metal is not included in the model and is subtracted from the numerical results. Therefore, η_q is the antenna efficiency and sets an upper limit to the efficiency of emission through the antenna modes.

The results for Γ_{rad} and η_q agree well with the numerical results, figure 5.10. Without taking the radiation damping into account, no such agreement is obtained [36].

For increasing K, higher order modes are in general weaker compared to the $j = 1$ mode, 5.10a. Γ_{rad} decays quicker with increasing L for higher K, as a result of the lower R_{rad} (figure 5.9). As the mode becomes more bound, the dissipative losses (k'', per unit length) gain in importance compared to the radiative losses (r, per reflection or round trip). This shift in the prevalent loss mechanism additionally implies a decrease in efficiency η_q with increasing

K, figure 5.10b. Clearly, an efficient antenna should not be too plasmonic and should in general operate away from the quasistatic small-particle plasmon resonance.

Dark modes

Although for $R = 20$ all modes are pronounced in figure 5.10a, even modes disappear with increasing K. These modes result in relatively low values for Γ_{rad} and thus do not radiate effectively under any angle. By reciprocity, a low Γ_{rad} also implies low field enhancements under far-field illumination [55]. These modes interact weakly with radiation, and can be called dark modes [135].

Such dark modes combine sub-radiance, i.e. an antisymmetric current distribution ($j = even$) and a small antenna length ($j/K < 1$), with a significant dissipative loss that dominates the radiative loss. Under these conditions a reduced radiation resistance results in a low Γ_{rad}, as the slower radiation is not compensated by a higher quality factor, because the quality factor was limited by the dissipative loss already.

The low efficiencies η_q for the antennas with large K confirm that the dissipation is, in that case, the dominant loss mechanism. The efficiency of the sub-radiant even modes becomes particularly low, and approaches zero, which explains why those modes become dark. The analytical model presented here thus gives a quantitative description for the gradual emergence of dark modes as antennas become increasingly plasmonic.

The local currents and fields are still resonantly enhanced (equations 5.14 and 5.15). As a result large-K sub-radiant modes with low radiation damping, and consequently narrow line-widths, can be advantageous in applications where efficient conversion into a photon is not required, or even unwanted. Examples are sensors [136] and spasers [137].

Angular emission

The angular emission is given by equation 5.17. Unlike previous 0D models [138], our model gives the emission patterns of higher order modes in good agreement with numerical calculations, figure 5.11. The maxima of these emission patterns are approximately given by the solutions for the phase matching equation 5.12. The discrepancies between the maxima and the solutions to equation 5.12 are due to the amplitude envelope functions in equation 5.17.

Higher order modes can give multi-lobed patterns with an odd or even amount of maxima for modes with odd or even j respectively. The patterns are obviously different from standard antenna theory ($K = 1$) [110, 133], which always yields j lobes, whereas the optical antennas result in j or less lobes. Modes with $j = even$ do not interact with radiation perpendicular to the antenna axis, as expected by their symmetry. The asymmetry in the patterns is caused by the radiative and dissipative losses, in conjunction with the position of the dipole source at one of the ends of the antenna.

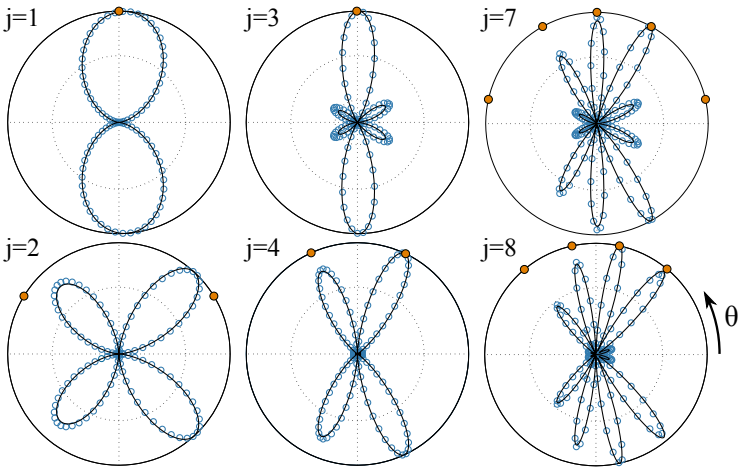

Figure 5.11: **Angular emission patterns.** The angular (θ) emitted power for modes j of the optical antenna with $R = 20$ nm ($K = 1.7$), all other parameters as in figure 5.10. 1D analytical model: line. 3D numerical calculations: circles (blue). Phase matching, equation 5.12: dots (orange).

Limiting behavior for $K >> 1$

In the limit of very plasmonic modes, $K >> 1$, the equations simplify and we can derive the limiting behavior and scaling laws for several quantities.

In the quasistatic limit ($K >> 1$), the plasmon wavelength becomes proportional to the antenna radius, so that $K \propto 1/R$ [38]. Equation 5.17 yields the scaling law $R_{rad} \propto 1/K^2$, which therefore also implies $R_{rad} \propto R^2$. The radiation resistance thus drops quickly with decreasing radius, as observed in figure 5.9. Since $Z \propto K$ [38], we thus also find that r quickly converges to unity for large K, equation 5.19.

Furthermore, if one requires the resonances to depend only on the shape (or aspect ratio) of the antenna not on its absolute dimensions, then one must have $L_c \propto R$, or equivalently the reflection phase must be a constant, which gives a compelling argument supporting previous postulates [15], and unexpected calculation results [33, 139].

For $K >> 1$ we also have $k_\parallel \pm k \approx \pm k$ (see also section 5.1), and the θ dependence of the denominator terms in equation 5.17 can be neglected. The emission is then a sum of three dipole terms: $E_0 e^{ik_\parallel L/2}$, $E_0 e^{-ik_\parallel L/2}$ and $E_0 e^{-ik_\parallel a}$, with the latter contribution negligible for strong modes. In this limit, the emission is thus described by two dipoles at the antenna ends, consistent with the results derived in section 5.1.

Limits of the model

The analytical results agree well with numerical calculations (figure 5.9, figure 5.10 and figure 5.11). Only two fitting parameters were used: k' and L_c. All other parameters were obtained from the semi-analytical waveguide solutions.

The fitted values for k' differ by approximately 5% from the waveguide solutions, which is within the expected error margin of the numerical calculations. The fitted values for L_c are close to the previously postulated $2R$ [15], and follow the trends from previous calculations [33, 139], as well as the scaling laws derived here.

For the specific configuration considered here, no good agreement is obtained if a phase shift, or an integration over only Lp, is used. The emission is, in this case, better described by an additional length. However, a complete description of the $3D$ vector field at the ends is an open problem despite recent progress [33, 139, 140]. A precise study of the problem is likely out of reach of the approximate $1D$ model presented here.

Conclusion

To conclude, the analytical model presented here accurately describes the interaction of dipolar emitters with radiation through nano-rod modes. The antenna properties are primarily governed by a single parameter $K = k'/k_0$ that describes how plasmonic the antenna modes are, and can be summarized in a phase-matching equation. The model includes radiation damping, and is not limited to the quasistatic approximation, which is crucial because quasistatic antennas are usually inefficient antennas.

Although here we focused on the evolution of the emission properties for increasingly bound waves, particularly the gradual emergence of sub-radiant, super-radiant and dark modes, the model applies to all interactions with any spatio-temporal beam and is equally valid for field enhancement and scattering problems. The results are thus widely applicable and might lead to further insights and design rules for optical antennas, nano-rod spasers [137], and generally for coupling light in/from nano-rods [25, 26, 32, 33, 125, 141].

Associated publications

[36] T. H. Taminiau et al., Nano Lett. 11, 1020 (2011).

Conclusion

The results presented in this thesis show that optical antennas provide a new way to link single emitters to light. By carefully designing the antenna, and its coupling to the emitter, both the absorption and emission properties of the emitter can be tailored in a variety of ways. The absolute emission and excitation rates can be enhanced and the angular, polarization, spectral, and spatial dependence of the interaction can be controlled. The combination of these effects can be used to improve the interaction of nanoscale matter with light, making optical antennas a powerful tool.

Although the study of nano-particles goes back a long way, and their optical properties are quite well understood, the description of such systems in the context of optical antennas sheds a new light on the locally enhanced fields at such particles. This description provides several new insights, convenient design rules, and ways to intuitively understand otherwise complex systems and problems in nano-optics.

Many of these new insights are the result of experiments with precisely designed antennas and a controlled coupling to (single) quantum emitters. It will be interesting to see if the next generation of antennas and experiments can improve the control and interaction strength to the point where new regimes can be systematically explored. Two examples are the strong coupling between a single emitter and plasmons or the breakdown of selection rules in strongly confined fields.

Finally, optical antennas theoretically promise controlled rate enhancements by three orders of magnitude. Such numbers have not yet been realized experimentally. If such enhancements can be obtained, optical antennas might play a vital role in optical quantum information processing, where the amount of photons detected is often a key obstacle. If not, then surely the mechanism that prevents this is worthwhile studying in itself.

Bibliography

[1] E. H. Synge, "A suggested model for extending microscopic resolution into the ultra-microscopic region," *Phil. Mag.*, vol. 6, pp. 356–362, 1928.

[2] J. Wessel, "Surface-enhanced optical microscopy," *J. Opt. Soc. Am. B*, vol. 2, no. 9, pp. 1538–1541, 1985.

[3] D. W. Pohl, W. Denk, and M. Lanz, "Optical stethoscopy: Image recording with resolution lambda/20," *Appl. Phys. Lett.*, vol. 44, no. 7, pp. 651–653, 1984.

[4] M. Kerker, D.-S. Wang, and H. Chew, "Surface enhanced raman scattering (sers) by molecules adsorbed at spherical particles," *Appl. Opt.*, vol. 19, no. 24, pp. 4159–4174, 1980.

[5] D. S. Wang and M. Kerker, "Enhanced raman scattering by molecules adsorbed at the surface of colloidal spheroids," *Phys. Rev. B*, vol. 24, no. 4, p. 1777, 1981.

[6] U. Kreibig and M. Vollmer, *Optical Properties of Metal Clusters*. Springer, 1995.

[7] D. W. Pohl, "Near-field optics seen as an antenna problem," *Near-field Optics, Principles and Applications*, 2000.

[8] K. B. Crozier, A. Sundaramurthy, G. S. Kino, and C. F. Quate, "Optical antennas: Resonators for local field enhancement," *J. Appl. Phys.*, vol. 94, no. 7, pp. 4632–4642, 2003.

[9] P. Muhlschlegel, H. J. Eisler, O. J. F. Martin, B. Hecht, and D. W. Pohl, "Resonant optical antennas," *Science*, vol. 308, no. 5728, pp. 1607–1609, 2005.

[10] S. Kuhn, U. Hakanson, L. Rogobete, and V. Sandoghdar, "Enhancement of single-molecule fluorescence using a gold nanoparticle as an optical nanoantenna," *Phys. Rev. Lett.*, vol. 97, no. 1, p. 017402, 2006.

[11] T. H. Taminiau, F. D. Stefani, F. B. Segerink, and N. F. van Hulst, "Optical antennas direct single-molecule emission," *Nature Photon.*, vol. 2, no. 4, pp. 234–237, 2008.

[12] A. G. Curto, G. Volpe, T. H. Taminiau, M. P. Kreuzer, R. Quidant, and N. F. van Hulst, "Unidirectional emission of a quantum dot coupled to a nanoantenna," *Science*, vol. 329, no. 5994, pp. 930–933, 2010.

[13] P. Bharadwaj, B. Deutsch, and L. Novotny, "Optical antennas," *Adv. Opt. Photon.*, vol. 1, no. 3, pp. 438–483, 2009.

[14] J.-J. Greffet, M. Laroche, and F. Marquier, "Impedance of a nanoantenna and a single quantum emitter," *Phys. Rev. Lett.*, vol. 105, no. 11, p. 117701, 2010.

[15] L. Novotny, "Effective wavelength scaling for optical antennas," *Phys. Rev. Lett.*, vol. 98, no. 26, p. 266802, 2007.

[16] J. A. Schuller, E. S. Barnard, W. Cai, Y. C. Jun, J. S. White, and M. L. Brongersma, "Plasmonics for extreme light concentration and manipulation," *Nature Mater.*, vol. 9, no. 3, pp. 193–204, 2010.

[17] L. Novotny and N. van Hulst, "Antennas for light," *Nature Photon.*, vol. 5, no. 2, pp. 83–90, 2011.

[18] P. Biagioni, J.-S. Huang, and B. Hecht, "Nanoantennas for visible and infrared radiation," *arXiv:1103.1568v1*, 2011.

[19] T. H. Taminiau, "10th international conference on near-field optics, nanophotonics and related techniques," 2008.

[20] K. J. Vahala, "Optical microcavities," *Nature*, vol. 424, no. 6950, pp. 839–846, 2003.

[21] J.-J. Greffet, "Nanoantennas for light emission," *Science*, vol. 308, no. 5728, pp. 1561–1563, 2005.

[22] M. Ringler, A. Schwemer, M. Wunderlich, A. Nichtl, K. Kurzinger, T. A. Klar, and J. Feldmann, "Shaping emission spectra of fluorescent molecules with single plasmonic nanoresonators," *Phys. Rev. Lett.*, vol. 100, no. 20, pp. 203002–4, 2008.

[23] S. Asano and G. Yamamoto, "Light scattering by a spheroidal particle," *Appl. Opt.*, vol. 14, no. 1, pp. 29–49, 1975.

[24] G. W. Bryant, F. J. GarciadeAbajo, and J. Aizpurua, "Mapping the plasmon resonances of metallic nanoantennas," *Nano Lett.*, vol. 8, no. 2, pp. 631–636, 2008.

[25] G. Schider, J. R. Krenn, A. Hohenau, H. Ditlbacher, A. Leitner, F. R. Aussenegg, W. L. Schaich, I. Puscasu, B. Monacelli, and G. Boreman, "Plasmon dispersion relation of au and ag nanowires," *Phys. Rev. B*, vol. 68, no. 15, p. 155427, 2003.

[26] H. Ditlbacher, A. Hohenau, D. Wagner, U. Kreibig, M. Rogers, F. Hofer, F. R. Aussenegg, and J. R. Krenn, "Silver nanowires as surface plasmon resonators," *Phys. Rev. Lett.*, vol. 95, no. 25, pp. 257403–4, 2005.

[27] G. Della Valle, T. Sondergaard, and S. I. Bozhevolnyi, "Plasmon-polariton nano-stripresonators: from visible to infra-red," *Opt. Express*, vol. 16, pp. 6867–6876, 2008.

[28] S. I. Bozhevolnyi and T. Sondergaard, "General properties of slow-plasmon resonant nanostructures: nano-antennas and resonators," *Opt. Express*, vol. 15, no. 17, pp. 10869–10877, 2007.

[29] E. S. Barnard, J. S. White, A. Chandran, and M. L. Brongersma, "Spectral properties of plasmonic resonator antennas," *Opt. Express*, vol. 16, pp. 16529–16537, 2008.

[30] L. Douillard, F. Charra, Z. Korczak, R. Bachelot, S. Kostcheev, G. Lerondel, P.-M. Adam, and P. Royer, "Short range plasmon resonators probed by photoemission electron microscopy," *Nano Lett.*, vol. 8, no. 3, pp. 935–940, 2008.

[31] E. J. R. Vesseur, R. deWaele, M. Kuttge, and A. Polman, "Direct observation of plasmonic modes in au nanowires using high-resolution cathodoluminescence spectroscopy," *Nano Lett.*, vol. 7, no. 9, pp. 2843–2846, 2007.

[32] J. Dorfmuller, R. Vogelgesang, R. T. Weitz, C. Rockstuhl, C. Etrich, T. Pertsch, F. Lederer, and K. Kern, "Fabry-perot resonances in one-dimensional plasmonic nanostructures," *Nano Lett.*, vol. 9, no. 6, pp. 2372–2377, 2009.

[33] R. Kolesov, B. Grotz, G. Balasubramanian, R. J. Stohr, A. A. L. Nicolet, P. R. Hemmer, F. Jelezko, and J. Wrachtrup, "Wave-particle duality of single surface plasmon polaritons," *Nature Phys.*, vol. 5, no. 7, pp. 470–474, 2009.

[34] Z. Li, F. Hao, Y. Huang, Y. Fang, P. Nordlander, and H. Xu, "Directional light emission from propagating surface plasmons of silver nanowires," *Nano Lett.*, vol. 9, no. 12, pp. 4383–4386, 2009.

[35] T. H. Taminiau, R. J. Moerland, F. B. Segerink, L. Kuipers, and N. F. van Hulst, "Lambda/4 resonance of an optical monopole antenna probed by single molecule fluorescence," *Nano Lett.*, vol. 7, no. 1, pp. 28–33, 2007.

[36] T. H. Taminiau, F. D. Stefani, and N. F. van Hulst, "Optical nanorod antennas modeled as cavities for dipolar emitters: Evolution of sub- and super-radiant modes," *Nano Lett.*, vol. 11, no. 3, pp. 1020–1024, 2011.

[37] C. F. Bohren and D. R. Huffman, *Absorption and scattering of light by small particles*. John Wiley and Sons, Inc., 1983.

[38] D. E. Chang, A. S. Sorensen, P. R. Hemmer, and M. D. Lukin, "Strong coupling of single emitters to surface plasmons," *Phys. Rev. B*, vol. 76, no. 3, pp. 035420–26, 2007.

[39] P. Anger, P. Bharadwaj, and L. Novotny, "Enhancement and quenching of single-molecule fluorescence," *Phys. Rev. Lett.*, vol. 96, no. 11, p. 113002, 2006.

[40] F. Tam, G. P. Goodrich, B. R. Johnson, and N. J. Halas, "Plasmonic enhancement of molecular fluorescence," *Nano Lett.*, vol. 7, no. 2, pp. 496–501, 2007.

[41] S. Kuhn, G. Mori, M. Agio, and V. Sandoghdar, "Modification of single molecule fluorescence close to a nanostructure: radiation pattern, spontaneous emission and quenching," *Mol. Phys.*, vol. 106, no. 7, p. 893, 2008.

[42] A. Kinkhabwala, Z. Yu, S. Fan, Y. Avlasevich, K. Mullen, and W. E. Moerner, "Large single-molecule fluorescence enhancements produced by a bowtie nanoantenna," *Nature Photon.*, vol. 3, no. 11, pp. 654–657, 2009.

[43] O. L. Muskens, V. Giannini, J. A. Sanchez-Gil, and J. GomezRivas, "Strong enhancement of the radiative decay rate of emitters by single plasmonic nanoantennas," *Nano Lett.*, vol. 7, no. 9, pp. 2871–2875, 2007.

[44] L. Rogobete, F. Kaminski, M. Agio, and V. Sandoghdar, "Design of plasmonic nanoantennae for enhancing spontaneous emission," *Opt. Lett.*, vol. 32, no. 12, pp. 1623–1625, 2007.

[45] J. N. Farahani, D. W. Pohl, H. J. Eisler, and B. Hecht, "Single quantum dot coupled to a scanning optical antenna: A tunable superemitter," *Phys. Rev. Lett.*, vol. 95, no. 1, p. 017402, 2005.

[46] A. Mohammadi, V. Sandoghdar, and M. Agio, "Gold nanorods and nanospheroids for enhancing spontaneous emission," *New J. Phys.*, vol. 10, p. 105015, 2008.

[47] R. Esteban, T. V. Teperik, and J. J. Greffet, "Optical patch antennas for single photon emission using surface plasmon resonances," *Phys. Rev. Lett.*, vol. 104, no. 2, p. 026802, 2010.

[48] R. Carminati, J. J. Greffet, C. Henkel, and J. M. Vigoureux, "Radiative and non-radiative decay of a single molecule close to a metallic nanoparticle," *Optics Communications*, vol. 261, no. 2, pp. 368–375, 2006.

[49] J. S. Biteen, N. S. Lewis, H. A. Atwater, H. Mertens, and A. Polman, "Spectral tuning of plasmon-enhanced silicon quantum dot luminescence," *Appl. Phys. Lett.*, vol. 88, no. 13, pp. 131109–3, 2006.

[50] S. Karaveli and R. Zia, "Spectral tuning by selective enhancement of electric and magnetic dipole emission," *Phys. Rev. Lett.*, vol. 106, no. 19, p. 193004, 2011.

[51] H. Mertens, J. S. Biteen, H. A. Atwater, and A. Polman, "Polarization-selective plasmon-enhanced silicon quantum-dot luminescence," *Nano Lett.*, vol. 6, no. 11, pp. 2622–2625, 2006.

[52] R. J. Moerland, T. H. Taminiau, L. Novotny, N. F. vanHulst, and L. Kuipers, "Reversible polarization control of single photon emission," *Nano Lett.*, vol. 8, no. 2, pp. 606–610, 2008.

[53] H. Gersen, M. F. Garca-Paraj, L. Novotny, J. A. Veerman, L. Kuipers, and N. F. van Hulst, "Influencing the angular emission of a single molecule," *Phys. Rev. Lett.*, vol. 85, no. 25, p. 5312, 2000.

[54] H. F. Hofmann, T. Kosako, and Y. Kadoya, "Design parameters for a nano-optical yagi-uda antenna," *New J. Phys.*, vol. 9, no. 7, pp. 217–217, 2007.

[55] T. H. Taminiau, F. D. Stefani, and N. F. van Hulst, "Enhanced directional excitation and emission of single emitters by a nano-optical yagi-uda antenna," *Opt. Express*, vol. 16, no. 14, pp. 10858–10866, 2008.

[56] H. Aouani, O. Mahboub, N. Bonod, E. Devaux, E. Popov, H. Rigneault, T. W. Ebbesen, and J. Wenger, "Bright unidirectional fluorescence emission of molecules in a nanoaperture with plasmonic corrugations," *Nano Lett.*, vol. 11, p. 637644, 2011.

[57] W. Min, S. Lu, S. Chong, R. Roy, G. R. Holtom, and X. S. Xie, "Imaging chromophores with undetectable fluorescence by stimulated emission microscopy," *Nature*, vol. 461, no. 7267, pp. 1105–1109, 2009.

[58] M. Righini, P. Ghenuche, S. Cherukulappurath, V. Myroshnychenko, F. J. Garcia de Abajo, and R. Quidant, "Nano-optical trapping of rayleigh particles and escherichia coli bacteria with resonant optical antennas," *Nano Lett.*, vol. 9, no. 10, pp. 3387–3391, 2009.

[59] J. A. Schuller, T. Taubner, and M. L. Brongersma, "Optical antenna thermal emitters," *Nature Photon.*, vol. 3, no. 11, pp. 658–661, 2009.

[60] P. J. Schuck, D. P. Fromm, A. Sundaramurthy, G. S. Kino, and W. E. Moerner, "Improving the mismatch between light and nanoscale objects with gold bowtie nanoantennas," *Phys. Rev. Lett.*, vol. 94, no. 1, p. 017402, 2005.

[61] P. Ghenuche, S. Cherukulappurath, T. H. Taminiau, N. F. van Hulst, and R. Quidant, "Spectroscopic mode mapping of resonant plasmon nanoantennas," *Phys. Rev. Lett.*, vol. 101, no. 11, pp. 116805–4, 2008.

[62] A. Bouhelier, M. Beversluis, A. Hartschuh, and L. Novotny, "Near-field second-harmonic generation induced by local field enhancement," *Phys. Rev. Lett.*, vol. 90, no. 1, p. 013903, 2003.

[63] M. Danckwerts and L. Novotny, "Optical frequency mixing at coupled gold nanoparticles," *Phys. Rev. Lett.*, vol. 98, no. 2, p. 026104, 2007.

[64] S. Kim, J. Jin, Y.-J. Kim, I.-Y. Park, Y. Kim, and S.-W. Kim, "High-harmonic generation by resonant plasmon field enhancement," *Nature*, vol. 453, no. 7196, pp. 757–760, 2008.

[65] R. Esteban, M. Laroche, and J. J. Greffet, "Influence of metallic nanoparticles on upconversion processes," *J. Appl. Phys.*, vol. 105, no. 3, pp. 033107–10, 2009.

[66] S. Nie and S. R. Emory, "Probing single molecules and single nanoparticles by surface-enhanced raman scattering," *Science*, vol. 275, no. 5303, pp. 1102–1106, 1997.

[67] R. M. Stckle, Y. D. Suh, V. Deckert, and R. Zenobi, "Nanoscale chemical analysis by tip-enhanced raman spectroscopy," *Chem. Phys. Lett.*, vol. 318, no. 1-3, pp. 131–136, 2000.

[68] L. G. Cancado, A. Hartschuh, and L. Novotny, "Tip-enhanced raman spectroscopy of carbon nanotubes," *J Raman Spectrosc.*, vol. 40, no. 10, pp. 1420–1426, 2009.

[69] W. E. Moerner, "A dozen years of single-molecule spectroscopy in physics, chemistry, and biophysics," *The Journal of Physical Chemistry B*, vol. 106, no. 5, pp. 910–927, 2002.

[70] D. Brinks, F. D. Stefani, F. Kulzer, R. Hildner, T. H. Taminiau, Y. Avlasevich, K. Mullen, and N. F. van Hulst, "Visualizing and controlling vibrational wave packets of single molecules," *Nature*, vol. 465, no. 7300, pp. 905–908, 2010.

[71] B. Lounis and M. Orrit, "Single-photon sources," *Rep. Prog. Phys.*, vol. 68, no. 5, p. 1129, 2005.

[72] L. Tang, S. E. Kocabas, S. Latif, A. K. Okyay, D.-S. Ly-Gagnon, K. C. Saraswat, and D. A. B. Miller, "Nanometre-scale germanium photodetector enhanced by a near-infrared dipole antenna," *Nature Photon.*, vol. 2, no. 4, pp. 226–229, 2008.

[73] H. A. Atwater and A. Polman, "Plasmonics for improved photovoltaic devices," *Nature Mater.*, vol. 9, no. 3, pp. 205–213, 2010.

[74] E. Betzig and R. J. Chichester, "Single molecules observed by near-field scanning optical microscopy," *Science*, vol. 262, no. 5138, pp. 1422–1425, 1993.

[75] J. A. Veerman, M. Garcia Parajo, L. Kuipers, and N. F. van Hulst, "Single molecule mapping of the optical field distribution of probes for near-field microscopy," *J. Microsc.*, vol. 194, no. 2-3, pp. 477–482, 1999.

[76] H. G. Frey, F. Keilmann, A. Kriele, and R. Guckenberger, "Enhancing the resolution of scanning near-field optical microscopy by a metal tip grown on an aperture probe," *Appl. Phys. Lett.*, vol. 81, no. 26, pp. 5030–5032, 2002.

[77] H. G. Frey, S. Witt, K. Felderer, and R. Guckenberger, "High-resolution imaging of single fluorescent molecules with the optical near-field of a metal tip," *Phys. Rev. Lett.*, vol. 93, no. 20, p. 200801, 2004.

[78] J. M. Gerton, L. A. Wade, G. A. Lessard, Z. Ma, and S. R. Quake, "Tip-enhanced fluorescence microscopy at 10 nanometer resolution," *Phys. Rev. Lett.*, vol. 93, no. 18, p. 180801, 2004.

[79] Z. Ma, J. M. Gerton, L. A. Wade, and S. R. Quake, "Fluorescence near-field microscopy of dna at sub-10 nm resolution," *Phys. Rev. Lett.*, vol. 97, no. 26, p. 260801, 2006.

[80] T. S. van Zanten, M. J. Lopez-Bosque, and M. F. Garcia-Parajo, "Imaging individual proteins and nanodomains on intact cell membranes with a probe-based optical antenna," *Small*, vol. 6, no. 2, pp. 270–275, 2010.

[81] C. Hoppener and L. Novotny, "Imaging of membrane proteins using antenna-based optical microscopy," *Nanotechnology*, vol. 19, no. 38, p. 384012, 2008.

[82] B. Sick, B. Hecht, and L. Novotny, "Orientational imaging of single molecules by annular illumination," *Phys. Rev. Lett.*, vol. 85, no. 21, p. 4482, 2000.

[83] L. Novotny, M. R. Beversluis, K. S. Youngworth, and T. G. Brown, "Longitudinal field modes probed by single molecules," *Phys. Rev. Lett.*, vol. 86, no. 23, p. 5251, 2001.

[84] L. Novotny and B. Hecht, *Principles of nano-optics*. Cambridge: Cambridge University Press, 1st ed., 2006.

[85] A. G. T. Ruiter, J. A. Veerman, K. O. van der Werf, and N. F. van Hulst, "Dynamic behavior of tuning fork shear-force feedback," *Appl. Phys. Lett.*, vol. 71, no. 1, pp. 28–30, 1997.

[86] A. G. T. Ruiter, J. A. Veerman, M. F. Garcia-Parajo, and N. F. van Hulst, "Single molecule rotational and translational diffusion observed by near-field scanning optical microscopy," *J. Phys. Chem. A*, vol. 101, no. 40, pp. 7318–7323, 1997.

[87] J. A. Veerman, A. M. Otter, L. Kuipers, and N. F. van Hulst, "High definition aperture probes for near-field optical microscopy fabricated by focused ion beam milling," *Appl. Phys. Lett.*, vol. 72, no. 24, pp. 3115–3117, 1998.

[88] U. Durig, D. W. Pohl, and F. Rohner, "Near-field optical-scanning microscopy," *J. Appl. Phys.*, vol. 59, no. 10, pp. 3318–3327, 1986.

[89] A. Naber, D. Molenda, U. C. Fischer, H. J. Maas, C. Hppener, N. Lu, and H. Fuchs, "Enhanced light confinement in a near-field optical probe with a triangular aperture," *Phys. Rev. Lett.*, vol. 89, no. 21, p. 210801, 2002.

[90] D. Molenda, G. Colas des Francs, U. C. Fischer, N. Rau, and A. Naber, "High-resolution mapping of the optical near-field components at a triangular nano-aperture," *Opt. Express*, vol. 13, no. 26, pp. 10688–10696, 2005.

[91] C. J. Bouwkamp, "On bethe's theory of diffraction by small holes," *Phillips Res. Rep.*, vol. 5, p. 321, 1950.

[92] C. J. Bouwkamp, "On the diffraction of electromagnetic waves by small circular disks and holes," *Phillips Res. Rep.*, vol. 5, p. 401, 1950.

[93] O. J. F. Martin and M. Paulus, "Influence of metal roughness on the near-field generated by an aperture/apertureless probe," *J. Microsc.*, vol. 205, no. 2, pp. 147–152, 2002.

[94] B. Hecht, H. Bielefeldt, Y. Inouye, D. W. Pohl, and L. Novotny, "Facts and artifacts in near-field optical microscopy," *J. Appl. Phys.*, vol. 81, no. 6, pp. 2492–2498, 1997.

[95] E. Betzig, G. H. Patterson, R. Sougrat, O. W. Lindwasser, S. Olenych, J. S. Bonifacino, M. W. Davidson, J. Lippincott-Schwartz, and H. F. Hess, "Imaging intracellular fluorescent proteins at nanometer resolution," *Science*, vol. 313, no. 5793, pp. 1642–1645, 2006.

[96] M. J. Rust, M. Bates, and X. Zhuang, "Sub-diffraction-limit imaging by stochastic optical reconstruction microscopy (storm)," *Nat. Methods*, vol. 3, no. 10, pp. 793–796, 2006.

[97] S. W. Hell, "Far-field optical nanoscopy," *Science*, vol. 316, no. 5828, pp. 1153–1158, 2007.

[98] M. L. Andersen, S. Stobbe, A. S. Sorensen, and P. Lodahl, "Strongly modified plasmon-matter interaction with mesoscopic quantum emitters," *Nature Phys.*, vol. advance online publication, 2011.

[99] T. Weiland, "Discretization method for solution of maxwells equations for 6-component fields," *Electron. Commun. AEU*, vol. 31, pp. 116–120, 1977.

[100] T. H. Taminiau, F. B. Segerink, and N. F. van Hulst, "A monopole antenna at optical frequencies: Single-molecule near-field measurements," *IEEE Trans. Antennas Propag.*, vol. 55, no. 11, pp. 3010–3017, 2007.

[101] T. H. Taminiau, F. B. Segerink, R. J. Moerland, L. Kuipers, and N. F. van Hulst, "Near-field driving of a optical monopole antenna," *J. Opt. A: Pure Appl. Opt*, vol. 9, no. 9, pp. S315–S321, 2007.

[102] D. Axelrod, "Carbocyanine dye orientation in red cell membrane studied by microscopic fluorescence polarization," *Biophys. J.*, vol. 26, no. 3, pp. 557–573, 1979.

[103] B. Richards and E. Wolf, "Electromagnetic diffraction in optical systems ii: structure of the image field in an aplanatic system.," *Proc. Roy. Soc. London A*, vol. 253, no. 1274, pp. 358–379, 1959.

[104] E. Wolf, "Electromagnetic diffraction in optical systems i: an integral representation of the image field," *Proc. Roy. Soc. London A*, vol. 253, no. 1274, pp. 349–357, 1959.

[105] R. R. Chance, A. Prock, and R. Silbey, "Molecular fluorescence and energy transfer near interfaces," *Adv. Chem. Phys.*, vol. 37, p. 1, 1978.

[106] W. Lukosz, "Light-emission by magnetic and electric dipoles close to a plane dielectric interface. iii. radiation patterns of dipoles with arbitrary orientation.," *J. Opt. Soc. Am.*, vol. 69, pp. 1495–1503, 1979.

[107] M. A. Lieb, J. M. Zavislan, and L. Novotny, "Single-molecule orientations determined by direct emission pattern imaging," *J. Opt. Soc. Am. B*, vol. 21, no. 6, pp. 1210–1215, 2004.

[108] H. Cang, A. Labno, C. Lu, X. Yin, M. Liu, C. Gladden, Y. Liu, and X. Zhang, "Probing the electromagnetic field of a 15-nanometre hotspot by single molecule imaging," *Nature*, vol. 469, no. 7330, pp. 385–388, 2011.

[109] T. H. Taminiau, F. D. Stefani, and N. F. v. Hulst, "Single emitters coupled to plasmonic nano-antennas: angular emission and collection efficiency," *New J. Phys.*, vol. 10, no. 10, p. 105005, 2008.

[110] C. A. Balanis, *Antenna Theory: Analyses and Design*. Hoboken, New Jersey: John Wiley and Sons, Inc., 3rd ed. ed., 2005.

[111] H. Yagi, "Beam transmission of ultra short waves," *Proc. IRE*, vol. 16, pp. 715–741, 1928.

[112] J. Li, A. Salandrino, and N. Engheta, "Shaping light beams in the nanometer scale: A yagi-uda nanoantenna in the optical domain," *Phys. Rev. B*, vol. 76, no. 24, pp. 245403–7, 2007.

[113] Y. Wang, T. Yang, M. T. Tuominen, and M. Achermann, "Radiative rate enhancements in ensembles of hybrid metal-semiconductor nanostructures," *Phys. Rev. Lett.*, vol. 102, no. 16, p. 163001, 2009.

[114] P. Bharadwaj and L. Novotny, "Spectral dependence of single molecule fluorescence," *Opt. Express*, vol. 15, no. 21, pp. 14266–14274, 2007.

[115] A. F. Koenderink, "Plasmon nanoparticle array waveguides for single photon and single plasmon sources," *Nano Lett.*, vol. 9, no. 12, pp. 4228–4233, 2009.

[116] Y. C. Jun, K. C. Y. Huang, and M. L. Brongersma, "Plasmonic beaming and active control over fluorescent emission," *Nat. Commun.*, vol. 2, p. 283, 2011.

[117] J. Dorfmuller, D. Dregely, M. Esslinger, W. Khunsin, R. Vogelgesang, K. Kern, and H. Giessen, "Near-field dynamics of optical yagi-uda nanoantennas," *Nano Lett.*, vol. 11, p. 28192824, 2011.

[118] S. V. Boriskina and L. Dal Negro, "Multiple-wavelength plasmonic nanoantennas," *Opt. Lett.*, vol. 35, no. 4, pp. 538–540, 2010.

[119] A. Ahmed and R. Gordon, "Directivity enhanced raman spectroscopy using nanoantennas," *Nano Lett.*, vol. 11, no. 4, pp. 1800–1803, 2011.

[120] J. Li, A. Salandrino, and N. Engheta, "Optical spectrometer at the nanoscale using optical yagi-uda nanoantennas," *Phys. Rev. B*, vol. 79, no. 19, p. 195104, 2009.

[121] T. Kosako, Y. Kadoya, and H. F. Hofmann, "Directional control of light by a nano-optical yagi-uda antenna," *Nature Photon.*, vol. 4, no. 5, pp. 312–315, 2010.

[122] D. Dregely, R. Taubert, J. Dorfmuller, R. Vogelgesang, K. Kern, and H. Giessen, "3d optical yagi-uda nanoantenna array," *Nat. Commun.*, vol. 2, p. 267, 2011.

[123] T. Shegai, V. D. Miljkovic, K. Bao, H. Xu, P. Nordlander, P. Johansson, and M. Kall, "Unidirectional broadband light emission from supported plasmonic nanowires," *Nano Lett.*, vol. 11, no. 2, pp. 706–711, 2011.

[124] X.-X. Liu and A. Alu, "Subwavelength leaky-wave optical nanoantennas: Directive radiation from linear arrays of plasmonic nanoparticles," *Phys. Rev. B*, vol. 82, no. 14, p. 144305, 2010.

[125] A. V. Akimov, A. Mukherjee, C. L. Yu, D. E. Chang, A. S. Zibrov, P. R. Hemmer, H. Park, and M. D. Lukin, "Generation of single optical plasmons in metallic nanowires coupled to quantum dots," *Nature*, vol. 450, no. 7168, pp. 402–406, 2007.

[126] G. Volpe, S. Cherukulappurath, R. Juanola Parramon, G. Molina-Terriza, and R. Quidant, "Controlling the optical near field of nanoantennas with spatial phase-shaped beams," *Nano Lett.*, vol. 9, no. 10, pp. 3608–3611, 2009.

[127] J.-S. Huang, J. Kern, P. Geisler, P. Weinmann, M. Kamp, A. Forchel, P. Biagioni, and B. Hecht, "Mode imaging and selection in strongly coupled nanoantennas," *Nano Lett.*, vol. 10, no. 6, pp. 2105–2110, 2010.

[128] A. McLeod, A. Weber-Bargioni, Z. Zhang, S. Dhuey, B. Harteneck, J. B. Neaton, S. Cabrini, and P. J. Schuck, "Nonperturbative visualization of nanoscale plasmonic field distributions via photon localization microscopy," *Phys. Rev. Lett.*, vol. 106, no. 3, p. 037402, 2010.

[129] S. Karaveli and R. Zia, "Strong enhancement of magnetic dipole emission in a multilevel electronic system," *Opt. Lett.*, vol. 35, no. 20, pp. 3318–3320, 2010.

[130] A. Alu and N. Engheta, "Input impedance, nanocircuit loading, and radiation tuning of optical nanoantennas," *Phys. Rev. Lett.*, vol. 101, no. 4, pp. 043901–4, 2008.

[131] P. J. Burke, L. Shengdong, and Y. Zhen, "Quantitative theory of nanowire and nanotube antenna performance," *IEEE Trans. Nanotech.*, vol. 5, no. 4, pp. 314–334, 2006.

[132] A. Alu and N. Engheta, "Tuning the scattering response of optical nanoantennas with nanocircuit loads," *Nature Photon.*, vol. 2, no. 5, pp. 307–310, 2008.

[133] J. Dorfmuller, R. Vogelgesang, W. Khunsin, C. Rockstuhl, C. Etrich, and K. Kern, "Plasmonic nanowire antennas: Experiment, simulation, and theory," *Nano Lett.*, vol. 10, no. 9, pp. 3596–3603, 2010.

[134] J. Jackson, *Classical Electrodynamics*. New York: Wiley, 2nd ed. ed., 1975.

[135] M. Liu, T.-W. Lee, S. K. Gray, P. Guyot-Sionnest, and M. Pelton, "Excitation of dark plasmons in metal nanoparticles by a localized emitter," *Phys. Rev. Lett.*, vol. 102, no. 10, p. 107401, 2009.

[136] F. Hao, Y. Sonnefraud, P. V. Dorpe, S. A. Maier, N. J. Halas, and P. Nordlander, "Symmetry breaking in plasmonic nanocavities: Subradiant lspr sensing and a tunable fano resonance," *Nano Lett.*, vol. 8, no. 11, pp. 3983–3988, 2008.

[137] D. J. Bergman and M. I. Stockman, "Surface plasmon amplification by stimulated emission of radiation: Quantum generation of coherent surface plasmons in nanosystems," *Phys. Rev. Lett.*, vol. 90, no. 2, p. 027402, 2003.

[138] E. R. Encina and E. A. Coronado, "Plasmonic nanoantennas: Angular scattering properties of multipole resonances in noble metal nanorods," *J. Phys. Chem. C*, vol. 112, no. 26, pp. 9586–9594, 2008.

[139] R. Gordon, "Reflection of cylindrical surface waves," *Opt. Express*, vol. 17, no. 21, pp. 18621–18629, 2009.

[140] S. B. Hasan, C. Rockstuhl, R. Vogelgesang, and F. Lederer, "Relating localized nanoparticle resonances to an associated antenna problem," *arXiv*, p. 1010.2972v1, 2010.

[141] A. L. Falk, F. H. L. Koppens, C. L. Yu, K. Kang, N. de Leon Snapp, A. V. Akimov, M.-H. Jo, M. D. Lukin, and H. Park, "Near-field electrical detection of optical plasmons and single-plasmon sources," *Nat Phys*, vol. 5, no. 7, pp. 475–479, 2009.